POLITECNICO
MILANO 1863

SCUOLA DI INGEGNERIA INDUSTRIALE
E DELL'INFORMAZIONE

Energy targeting for heat recovery from carbon capture processes using hybrid absorption heat pumps

TESI DI LAUREA MAGISTRALE IN
ENERGY ENGINEERING
INGEGNERIA ENERGETICA

Author: **Gianluca Abrami**

Student ID: 943578
Advisor, Politecnico di Milano: Tommaso Toppi
Advisor, Chalmers University of Technology: Simon Harvey
Co-Advisor, Chalmers University of Technology: Max Biermann
Academic Year: 2020-2021

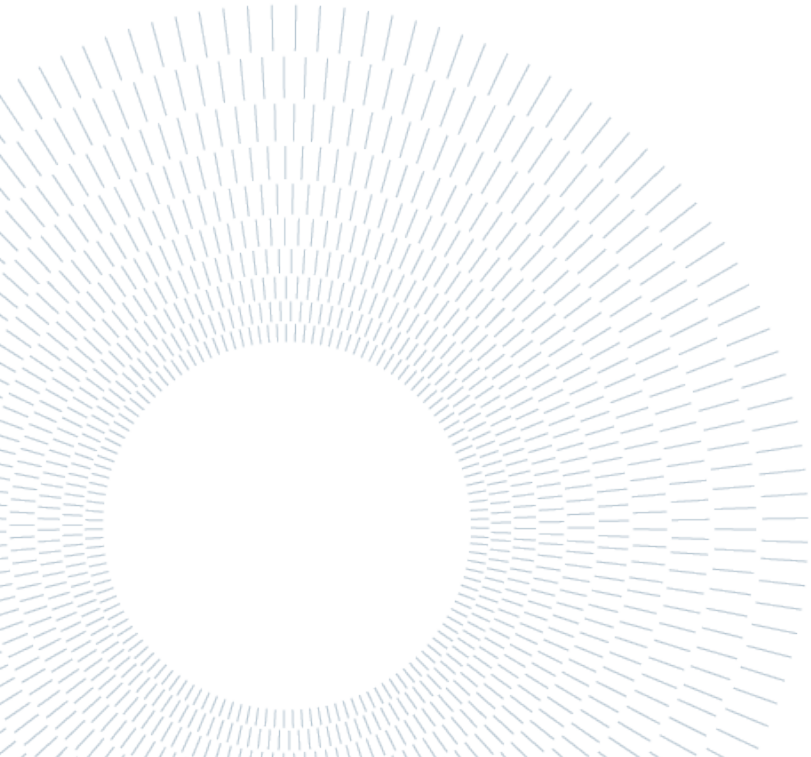

CHALMERS
UNIVERSITY OF TECHNOLOGY

A substantial part of this master thesis was developed as part of an Eramsus Programme agreement between Politecnico di Milano and Chalmers University of Technology.

I have been a guest student at Chalmers University of Technology from September 2021 to March 2022. In this period of time, I had the opportunity to attend the course "Industrial energy systems", held by Professor Simon Harvey, who kindly accepted to supervise my thesis work while I was abroad. This course was fundamental for the writing of this thesis, providing me with knowledge that I am sure will be useful for my future.

Abstract

District heating has been identified as a key solution to decarbonize the heating sector and to reach the limit of 1.5 °C temperature rise by 2050, imposed by the Paris agreement. A Waste-to-Energy plant represents an important source for district heating, especially in cold countries such as in Scandinavia. This technology, however, is far from being carbon free, because of the fossil CO_2 content of the flue gases. Waste-to-Energy plants can be retrofitted with carbon capture technology, significantly reducing the carbon emissions. Carbon capture has a considerable heat demand, which could be satisfied by steam bled from the turbine of the Waste-to-Energy plant, resulting in a loss in the original district heating supply. At the same time, residual heat could be recovered from the carbon capture plant, in order to compensate for the loss associated with carbon capture integration. In this context, heat pumps could further increase the amount of heat recovery, exploiting lower temperature residual heat.

This thesis evaluated waste heat recovery solutions from a possible future carbon capture unit implemented to capture CO_2 from the flue gases from boiler number 7 of the Sävenäs plant, a Waste-to-Energy plant located in Gothenburg (Sweden). Process integration methods and tools have been used to evaluate residual heat recovery (including direct heat recovery and heat pumps) with a view to minimize the loss of district heat delivery. Two different heat pumps have been compared, a hybrid absorption-compression device and a more common vapor compression heat pump. The results indicated that the implementation of CCS to boiler nr. 7 determines a loss of 37.7 % in district heating supply (compared to the reference case). Direct heat recovery to district heating water could partially compensate this loss, while with the implementation of a heat pump, the loss could be completely recovered and the district heating supply could be even increased by 9.9 % compared to the original system.

A comparison between the two heat pumps revealed that the hybrid compression device performs better both from technical and economic point of view.

Key-words: waste heat recovery; district heating; heat pumps; pinch analysis; absorption cycle

Abstract in italiano

Un impianto Waste-to-Energy (termovalorizzatore) costituisce un'importante fonte per il teleriscaldamento, soprattutto nei paesi freddi come la Scandinavia. Questa tecnologia, tuttavia, è lontana dall'essere carbon-free, a causa del contenuto di CO_2 fossile dei gas di scarico. Un impianto di cattura e stoccaggio della CO_2 (CCS) può essere implementato in un termovalorizzatore, riducendo significativamente le emissioni di anidride carbonica. Tale impianto, tuttavia, è caratterizzato da una notevole domanda energetica; nel caso in cui quest'ultima dovesse essere soddisfatta da vapore prelevato dalla turbina del termovalorizzatore, si determinerebbe una perdita nella rete di teleriscaldamento. Allo stesso tempo, tuttavia, il calore residuo derivante dall'impianto CCS potrebbe essere recuperato, integrando anche una pompa di calore, al fine di compensare tale perdita.

Lo scopo di questa tesi è stato quello di valutare soluzioni di recupero del calore residuo (inteso come recupero diretto + pompa di calore) da un possibile futuro impianto CCS implementato nella caldaia numero 7 dell'impianto Waste-to-Energy "Sävenäs", situato a Göteborg (Svezia), al fine di ridurre al minimo la perdita sulla rete di teleriscaldamento. La metodologia ha combinato l'approccio teorico della "pinch analysis" e software di modellazione numerica per confrontare due diverse tipologie di pompe di calore: un dispositivo ibrido ad assorbimento-compressione e una comune pompa di calore a compressione di vapore. I risultati hanno indicato che la domanda di calore dell'impianto CCS dimensionato sulla caldaia nr. 7 è pari a 12.3 MW; ciò determina una perdita di capacità sulla rete di teleriscaldamento del 37.7% rispetto al sistema originale. Il recupero diretto del calore può provvedere solo parzialmente questa perdita, mentre l'implementazione di una pompa di calore non solo può totalmente compensarla; ma anche aumentare la capacità del teleriscaldamento del 9.9% rispetto al sistema originale.

Un confronto tra le due pompe di calore ha evidenziato come il modello ibrido sia vantaggioso sia da un punto di vista tecnico che economico.

Parole chiave: recupero del calore residuo; teleriscaldamento; pompe di calore; cicli ad assorbimento; pinch analysis.

Acknowledgments

Giunto alla fine di questo tortuoso ma affascinante percorso chiamato Politecnico, mi sembra doveroso ringraziare le persone con le quali ho condiviso questi incredibili anni e che hanno, anche solo in parte, contribuito al raggiungimento di questo importante obiettivo.

La prima persona che vorrei ringraziare è il mio supervisore Prof. Tommaso Toppi, che mi guidato per l'intera durata di questo progetto, stimolando sempre di più il mio interesse e la mia curiosità verso tematiche di cui ero appena a conoscenza. Inoltre, gli sono grato per avermi supportato nella mia decisione di partecipare al programma Erasmus.

In the context of my stay at Chalmers University of Technology, I would really like to thank my advisor Professor Simon Harvey, who helped me in all the difficult situations since the beginning of this thesis. If I came back from Sweden with a much wider range of knowledge and insights, I owe it to him.
Another person I would like to express gratitude to is my Co-Advisor Max Biermann, who is one of the nicest and most helpful persons I have met during my stay.
A special thank you to Jennie Rodin and Anders Stand from Göteborg Energi for the guidance and the interesting meetings we had.
I wish to extend my thanks to all the people I met during my Erasmus in Gothenburg, with whom I shared memories that I will never forget. To all the people from "Phadder Group 8" and "How Ya Doin'": you really contributed to make this experience the best of my life so far.

Vorrei poi ringraziare tutti gli amici conosciuti al Politecnico in questi anni, con i quali ho condiviso interminabili pomeriggi (e notti) di studio, oltre a numerose avventure al di fuori dell'ambiente universitario. Tra tutti, meritano una citazione Ronaldo e Giacomo: senza di voi, probabilmente, la laurea sarebbe ancora un miraggio.

Un ringraziamento a tutti gli amici di una vita che mi hanno supportato (e sopportato) in questi anni: Giorgio, Alessandro e tutta la SurfOnStreet, spero rimarrete parte della mia vita per molto tempo ancora.

Ringrazio Giacomo, Davide e Giacomo, i coinquilini storici di Porta Romana 46: ricordo sempre con grande piacere, e un po' di nostalgia, tutte le avventure trascorse in quel magnifico appartamento.

L'ultimo ringraziamento, il più importante, va alla mia famiglia, a cui dedico questo traguardo. Devo, infatti, ringraziare mia mamma e mio papà per essere diventato ciò che sono oggi. Gli sarò sempre grato per l'educazione e per le possibilità che mi hanno fornito.

Contents

1 Introduction

According to the analysis of the heating sector performed by the International Energy Agency (IEA) [1], heat is the "world´s largest energy use, accounting for almost half of global energy consumption in 2021, significantly more than electricity and transport". Buildings are responsible for a large share of heat consumption (46%), consuming energy for space and water heating. [1].

Figure 1-1 illustrates the contribution of different heat supply sources in the global buildings sector (excluding traditional biomass fuel use in developing countries [2])

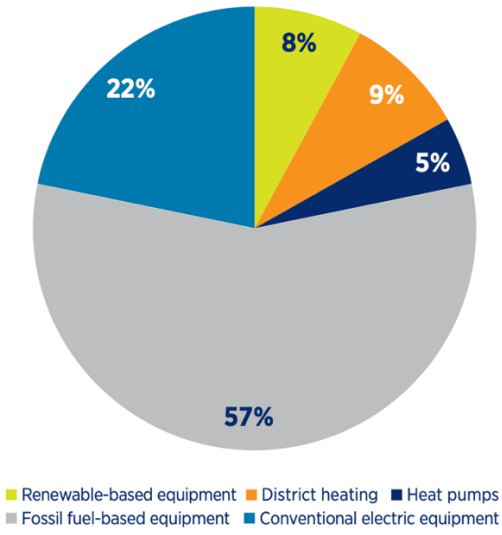

Figure 1-1: Global shares of heat supply sources in buildings in 2019, excluding traditional biomass fuel use [2]

Fossil fuel technologies (indicated in grey in Figure 1-1) account for 57 % of heat supply [2]. These technologies are typically single fossil fuel-based boilers, sized for the individual building. The main drawback of these systems is that they deliver thermodynamically valuable energy (around 1200-1500 °C) to heat buildings which request much lower temperature (~ 20 °C), with an efficiency of 75 % [3]. Thus such systems are characterized by poor performance, together with a considerable environmental impact, since they contribute to CO_2 emissions generation and thus to the greenhouse effect [1].

Nowadays, the reduction of environmental impact has indeed become a priority. This is evidenced by the fact that more and more countries have pledged to reduce fossil fuel emissions over the coming decades, with the objective of limiting the global temperature increase to 1.5 °C by 2050 [4]. This scenario envisages the radical change of the heating sector: IEA pointed out that the share of clean energy technologies in this field must increase significantly in the next decades [4].

Among the different opportunities to reach this target, low carbon district heating is considered a fundamental solution [5].

1.1. District heating

District heating is an energy service located in urban areas that consists in the distribution of hot water by means of insulated pipes, intended for heating buildings and the production of domestic hot water [3]. Its ultimate purpose, according to [6], is "to use local fuel or heat resources that would otherwise be wasted, in order to satisfy local customer demands for heating"

District heat originates from different energy sources, such as waste-to-energy plants, cogeneration plants, residual heat from industries or even low temperature renewable heat sources, including geothermal heat [7]. A key advantage of district heating networks is that it can be supplied by different sources, which would be unsuitable in stand-alone systems.

The first generation of district heating, developed in 1877 in Lockport by an American engineer [8], was characterized by a high temperature supply, due to the high thermal losses associated with this system. The high temperature requirements and the lack of knowledge about energy technologies limited the sources of such a system, which relied solely on coal [8].

The constant evolution of energy systems allowed for the reduction of district heating supply temperature over time, with the possibility of including different sources, such as renewables or residual heat.

Figure 1-2 represents the evolution of district heating system, from the first to the fourth generation, the latest technological achievement.

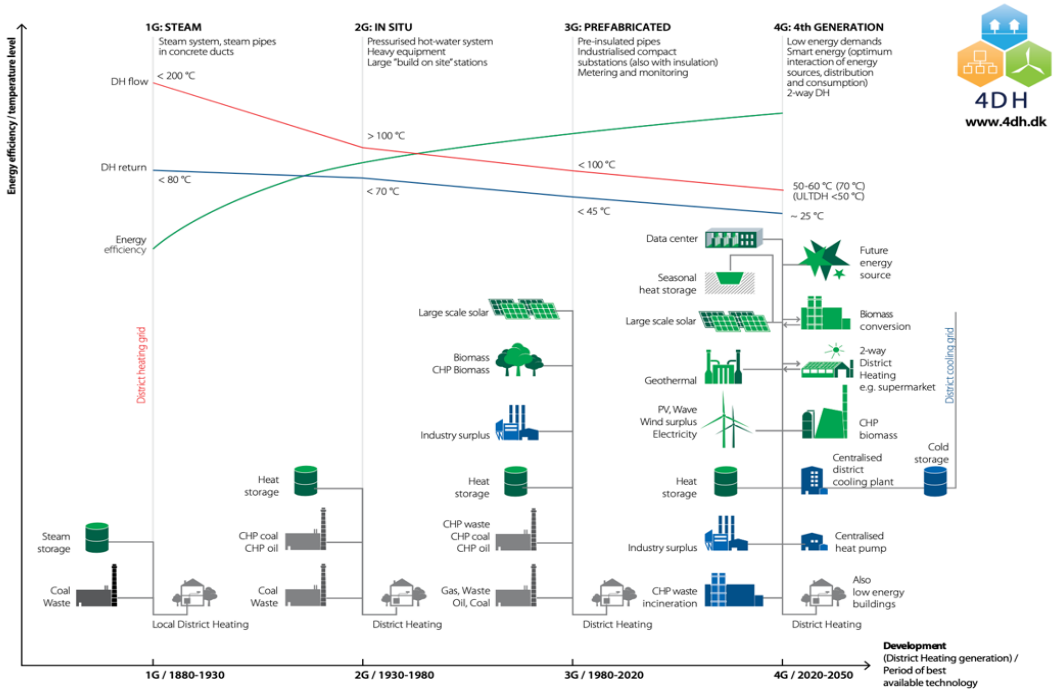

Figure 1-2: Evolution of district energy heat supply systems from first to fourth generation: the decreasing of supply temperature (red line) allows for the inclusion of different energy sources, working at lower temperatures. (note: blue line represents district cooling, not treated in this thesis) [2]

Despite the technological improvements achieved, around 90% of global district heat production today still relies on fossil fuels [5], which limits the potential of this system to contribute to future sustainable energy systems.

IRENA emphasized the importance of including different fossil fuel free energy sources to meet the demand for district heating. These are indicated as solar thermal energy, geothermal sources, bioenergy and residual heat from industrial processes [2].

1.1.1. Waste-to-energy plants (WtE) for District Heating supply

Waste that cannot be reused or recycled often ends up in landfills and could eventually be combusted in a waste-to-energy plant in order to generate electricity and thermal energy, in the form of steam or water.

One of the most common configurations of such plant uses a steam boiler together with a steam turbine [9], as represented in Figure 1-3.

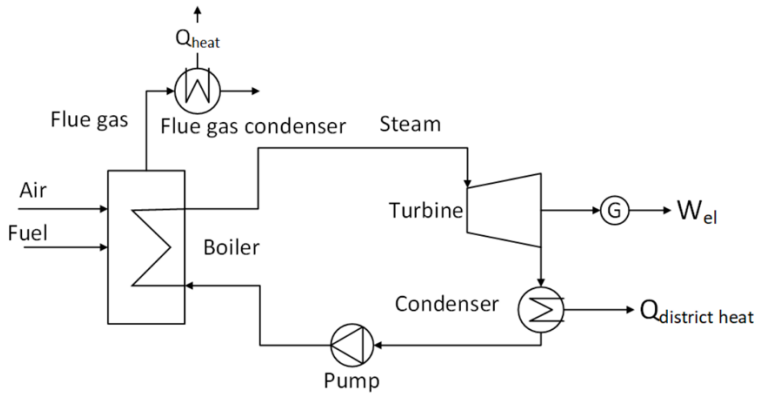

Figure 1-3: Combined heat and power plant based on a steam cycle [10]

The boiler is fueled with municipal and industrial solid waste (indicated as fuel in Figure 1-3) and generates high pressure steam, which is then fed into the turbine, linked to a generator for electricity production. The outgoing steam from the turbine is fed to the condenser, where its condensation heat is recovered and delivered to the district heating network [9]; this is indicated by $Q_{district\ heat}$ in Figure 1-3. A pump is used to recirculate the condensate to the boiler.

Many such plants are also equipped with a flue gas condenser unit for additional recovery of heat that can be supplied to the district heating network.

In cold countries, such as in Scandinavia, these plants are primarily used to provide district heat rather than electricity, due to high heating demand typical of these latitudes [11]. Although a WtE plant is designed to reduce the emissions of air pollutants, such as sulfur oxides, nitrogen oxides and particulates, this technology is far from being carbon free since a considerable amount of fossil CO_2 is emitted in the atmosphere as a consequence of waste burning. A study considering only the European Union countries revealed that in 2017 over 40 Mt of fossil CO_2 was released by Waste-to-Energy plants [12].

A possible solution to this issue is the adoption of post combustion carbon capture and storage (CCS) technology. Existent WtE plant could be retrofitted and the CO_2 content of the flue gases could be significantly decreased before they are emitted into the atmosphere.

The downside to such a configuration is that the CCS plant is an energy intensive process, characterized by a considerable heat demand, which could be supplied by steam bleeds from the turbine of the WtE plant thus resulting in a loss in the district heating supply.

At the same time a CCS plant is characterized by residual heat availability, which could be recovered in order to compensate for this loss.

All these aspects will be clarified in section 2.2 and 4.1.2.

1.1.2. Residual heat recovery for district heat supply

Residual heat from industrial processes is defined as "all the heat flows resulting from any industrial process that cannot be recovered for the process itself but can be reutilized for other purposes"[2] and is of particular interest for district heating. The reason behind that is mainly related to the abundance of residual heat, since it is basically present in all processes that rely upon energy conversion.

The main sources of residual heat include industrial facilities, data centers, supermarkets, sewage and wastewater treatment plants. A study performed by the EU showed that approximately 340 TWh per year could be recovered from such sources, which corresponds to more than 10 % of total EU´s total energy demand [13]. The same study also estimated that this amount of residual heat could cover 25 % of current district heat supply [13].

However, without the appropriate equipment, residual heat cannot be recovered and is discharged to the environment. This is because residual heat temperature levels (abundant in the range 30 – 100 °C [14]) are too low to allow direct usage in district heating systems.

In this context, heat pumps are considered to be a solution: these devices, in fact, could broaden the range of heat sources included in district heating systems, allowing lower temperatures to be exploited.

Among the different heat pump technologies, the hybrid absorption compression heat pump (HACHP), working with the zeotropic mixture ammonia-water is a relevant technology for residual heat recovery application. In a HACHP unit, the conventional isothermal condensation/evaporation of vapor compression heat pumps (VCHP) is replaced by non-isothermal absorption/desorption of a binary working fluid. The temperature glide exhibited by these processes can be matched to that of the heat source/sink, resulting in an increased efficiency, due to the reduction of entropy generation caused by heat transfer over a finite temperature difference [15]; this makes the HACHP a suitable candidate in district heating supply and residual heat recovery, as these processes often require large sink/source temperature glides [16].

One of the main challenges in heat pump integration is related to their appropriate placement in a heat recovery process, since these are normally constituted by many hot and cold streams, which are interacting together and with external utilities. Therefore, identifying the connection of the heat pump with the process streams is

a complicated task, which may leads to non-optimized integration and thus poor energy performances [17].

Pinch analysis, which is defined as an "energy integration methodology"[18], allows to identify the minimum energy requirement of a process, in terms of heat that must be delivered by heat sources, as well as heat that must be cooled/evacuated (i.e. residual heat). Also, pinch analysis helps engineer in the practical heat exchanging network design [19] and therefore plays a significant role in the development of an efficient heat recovery system [17].

1.2. Aim and scope

The purpose of this project is to investigate waste heat recovery possibilities from a carbon capture and storage (CCS) plant that is currently under investigation by Renova, a waste management company located in the city of Gothenburg (Sweden).

The CCS plant would be eventually installed at their waste-fueled combined heat and power plant in Sävenäs, located just outside Gothenburg.

The work carried out in this thesis started from the considerations investigated in another master's thesis project that was also focusing on carbon capture and storage possibilities on the same plant.[20]

Two different carbon capture technologies were investigated, namely monoethanolamide (MEA) and chilled ammonia process (CAP), concluding that, in both cases, there were possibilities for heat recovery implementation, both in the form of direct heat recovery and heat pumping. This, however, was estimated based on simplified assumptions, leaving a detailed investigation as future work.

Even though the Sävenäs WtE plant includes four different furnaces, the investigation carried out in [20] focused on furnace nr 7 , since this represents the state-of-the-art. In order to further investigate the considerations discussed in [20] and due to data availability, it was decided, together with Renova, to focus on the same process.

Therefore, in the context of this thesis, process integration methods and tools were used to establish targets for maximum heat recovery from a CO_2 capture plant designed for capture of CO_2 from the flue gas stream from furnace nr 7.

The targeted application for the recovered heat is district heating, in order to compensate for the loss that would occur if the heat needed to drive the reboiler is supplied by steam bled from the turbine.

The heat pump selected for the application is a hybrid absorption compression device, due to its advantages related to residual heat recovery applications: a consistent methodology was defined, exploiting process integration methods and modeling software together to identify opportunities for usage of this device.

To demonstrate the advantage of this solution, a comparison with a standard vapor compression heat pump was performed.

2 Background

2.1. Renova waste-to-energy (WtE) plant

Renova is a waste management company located in Gothenburg, Sweden.

Waste is collected and processed in their WtE combined heat and power plant in Sävenäs, located just outside the city of Gothenburg, considered to be a highly efficient plant [21].

The plant has the permit to receive *550 000* tons of waste each year, which derives from households and business activities. Part of the waste is recycled, while the remaining is burned in four furnaces in order to produce electrical and thermal energy: electricity is delivered to the grid, while thermal energy is used to supply the district heating network of Gothenburg. [22]

In 2020 the electricity production was 276 GWh, while district heat delivery was equal to 1538 GWh.[10] The production covers around 5 % of electricity demand and 30 % of district heat of the city. [22]

2.2. Carbon capture and storage (CCS)

The purpose of CCS technology is to capture CO_2 from flue gas streams and other process streams containing CO_2, avoiding its emission in the atmosphere. CCS has been identified in many studies as being a key technology for achieving the limits imposed by the Paris Agreement (i.e. limit global warming to well below 2 °C) [23]. As pointed out by International Energy Agency, the momentum is growing for CCS and, after some years of declining, new plants will most probably be built in the coming years [24].

The overall process can be divided in three steps, namely CO_2 capture, transportation and storage. Focusing on the capture technology, three different systems are identified, depending on the combustion process of flue gases: pre-combustion, oxyfuel-combustion and post-combustion. Here, only the latter will be treated, since it is the preferred option for retrofitting existing power plants, which is the case for the Sävenäs plant [25]. Pre-combustion and oxyfuel, instead, are both

implemented before the combustion, hence the retrofitting process would be much harder to implement [26]. Also, post-combustion is considered a mature technology (commercial), whereas pre-combustion and oxyfuel have only reached demonstration scale technology readiness.[27]

2.2.1. Post combustion capture technology

Among the different post-combustion capture processes, the most common technology implemented to-date involves chemical absorption using amine solvents. The solvent 30% aqueous monoethanolamine (MEA) is a widely used benchmark given that it is particularly suited to low CO_2 partial pressure [27]. Moreover, MEA-based capture has been demonstrated in a number of large-scale demonstration plants and is thus considered a well-proven technology [28].

Figure 2-1 illustrates a simplified amine-based capture process.

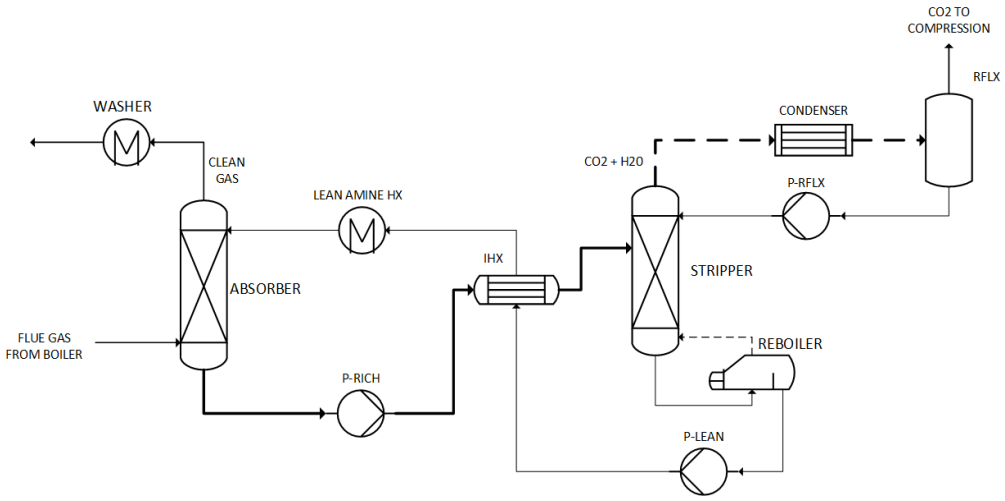

Figure 2-1: Capture section of a CCS plant, based on amine; adapted from [29]

Flue gas enters the absorber at the bottom, creating a counter current flow with a lean solution of MEA that is fed at the top of the column. In this way, CO_2 contained in the flue gases is absorbed by the amine solution in a reversible reaction.

The cleaned gases are collected at the top of the absorber and pass through the washer, where water vapor and volatile MEA are condensed, so to be recirculated to the solvent loop.

The CO_2-rich amine solution, instead, is collected at the bottom of the absorber and flows through an internal heat exchanger, where it is pre-heated by heat exchanging with the hot lean solution leaving the reboiler, and finally enters the desorber (stripper), where the CO_2 is stripped from the rich solvent by increasing the temperature to ~120 °C (temperature-swing absorption) due to external heat supply

in the reboiler. The released CO_2 is collected at the top of the desorber. The water in the CO_2-rich top gas exiting the desorber is condensed and the water is sent back to the desorber.

At the bottom of the desorber the lean solution is collected, a part of it is circulated through the reboiler, before it is sent back to the absorber. Before re-entering in the absorber, the lean solution temperature is decreased to a suitable operating temperature (~40 – 50 °C) through a cooler.

2.2.2. CO_2 conditioning

Report [29] revealed that, considering Sweden, the most efficient way of transporting CO_2 to the final permanent storage location is by ship. To be feasible, the gas must be compressed and liquefied, so to lower its density and the cost for transportation [27]. The Northern Lights project, which is currently developing an "open and flexible infrastructure" to transport and store CO_2 for European industries, indicated a pressure of 15 bar and a temperature of – 25 °C as suitable transport condition for CO_2 [30].

A commercial liquefaction processes that could achieve these conditions is presented in Figure 2-2.

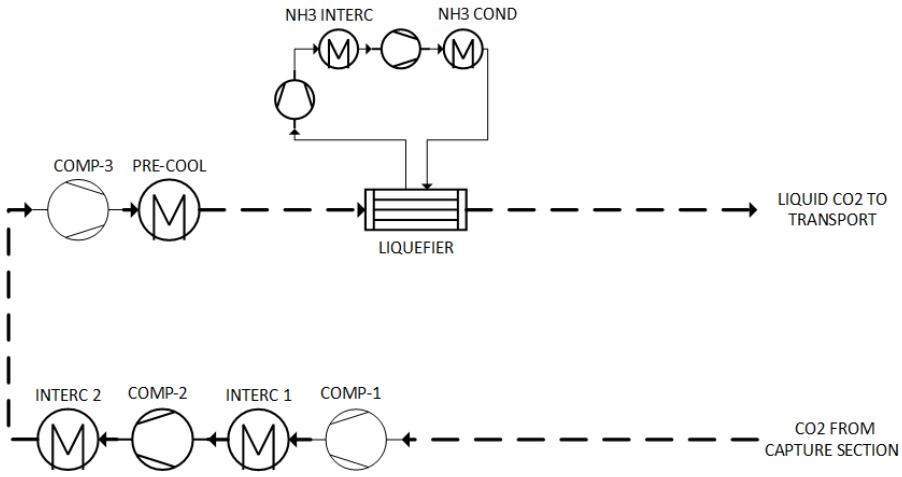

Figure 2-2: Conditioning section of a CCS plant, adapted from [31]

The process includes three compressor stages, with intercooling to lower the temperature of CO_2, and a knockout drum (not represented in the figure above), to remove condensed water.

High pressure CO_2 is then precooled and finally enters in the liquefier, that is powered by an ammonia refrigeration cycle. At this point, CO_2 will be flashed and

its impurities removed (flash not represented in Figure 2-2), so that the stream will be condensed and ready to be stored and transported.

It is worth noting that the ammonia refrigeration cycle is also a two-stage vapor compression cycle, with an intercooler and heat exchanger, used to condensate the refrigerant.

2.3. Energy targeting: pinch analysis

Energy analysis of a general industrial process is a complex task to perform, especially because these systems are normally composed of different units, which are linked together by material flows, energy transfer and they are all working together during the operation of the plant. This is the reason why these processes are seldom fully optimized from an energetic point of view. Energy savings and higher efficiency can be achieved by implementing systematic analysis tools.

One of these techniques is called "pinch analysis": it can be defined as a method to minimize energy consumption of industrial process through the calculation of feasible energy targets; this is true both for grassroot design, but also for retrofitting. Pinch analysis provides engineers with a better view of the system and it can help understanding how to optimize it from an energetic point of view, therefore achieving savings in thermal energy and thereby in fuel and money.

Pinch analysis methodology was developed during the 1980s by Bodo Linnhoff, a chemical engineer and academic at the University of Manchester in the UK. Key concepts for pinch analysis were carried out in his MSc dissertation and in his PhD thesis; starting from 1978 he published different papers regarding this topic which were thereafter compiled in the *IchemE User Guide on process integration for the efficient use of energy*, of 1982. This is considered the reference book when dealing with this topic and it formed the backbone of the revised versions that are used today.

The main advantage of pinch analysis is that it is based on easy considerations which can be translated in a graphical representation, allowing then a straightforward approach to the problem.

This technique can be summarized in a serious of steps, as illustrated by Linnhoff [32]:

- Data extraction: this has to do with the gathering of all the data that are necessary in order to proceed with the analysis. Normally, these can be in the form of general layout of the system, streams temperature and thermal capacity.

- Utility targeting: it is the first step of pinch analysis and it is used to compute information regarding minimum energy requirements, minimum number of heat exchangers, as well as some first indications about costs.
- Process modifications, in case retrofit is considered
- Design of the heat exchanging network, as conceived in the previous steps
- Optimization: pinch analysis is just a theoretical way of proceeding, facing real life constrain, the process has to be modified and optimization of the system can be achieved

2.3.1. Pinch analysis basics

Pinch analysis defines a stream as "any flow which requires to be heated or cooled but does not change in composition"[32]. These can be in the form of hot streams, i.e a stream that needs to be cooled from the supply to the target temperature, and a cold stream, i.e. a stream that needs to be heated from supply to target temperature. Each of the streams is completely characterized when mass flow rate, specific heat capacity, temperatures and heat duty are defined.

Hot and cold streams may exchange heat between each other through internal heat exchangers. The purpose is to reach the target temperature for each of the streams.

This, however, is not always possible due to capacities or temperature constraints.

For example, a cold stream may have a heating duty which is higher than the cooling needs of the hot stream. In this case, a so called "hot utility" is introduced, which is able to provide the additional heating effect required by the cold stream.

Vice versa, a hot utility provides heat to a cold stream that is not internally heated by a hot stream.

These concepts are showed in a simple example, Figure 2-3.

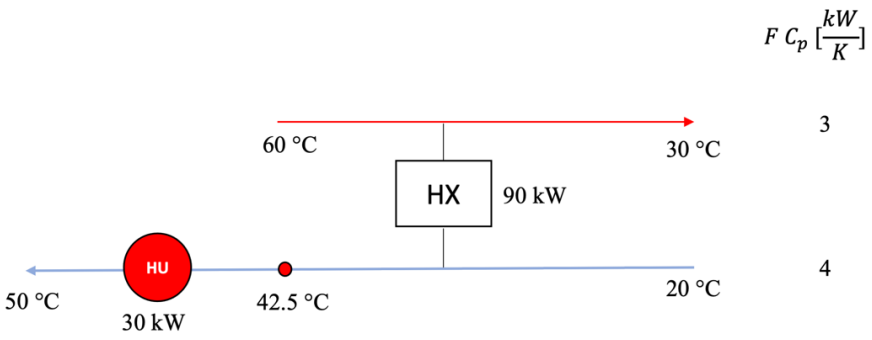

Figure 2-3: Hot and cold stream exchanging heat through internal heat exchanging HX: the remaining duty of the cold stream must be provided by a hot utility (HU)

In this example, two streams are present. The hot stream needs to be cooled from 60 °C to 30 °C, while the cold stream needs to be heated from 20 °C to 50 °C.

Their thermal capacity FC_p is defined and represented on the right in Figure 2-3. Heat duty can be found through equation (2-1).

$$\dot{Q} = FC_p * \Delta T \tag{2-1}$$

The cooling duty of the hot stream is completely satisfied by internal heat exchanging, equal to *90 kW*.

The cold stream, instead, requires *120 kW* to be completely heated from its starting temperature to the target one. Hence, a hot utility equal to *30 kW* is needed: the cold stream will first be heated by heat recovered from the hot stream through HX and will reach the target temperature by additional heat provided by the hot utility.

The most important concept of pinch analysis is the minimum temperature approach (ΔT_{min}), which corresponds to the minimum temperature difference that is acceptable in a heat exchanger between a hot stream and a cold stream. It is normally set considering economical and technical analysis: a higher value of ΔT_{min} coincides with higher driving forces, and thus lower heat exchanging area. However, this also correspond to lower internal heat recovery, because of temperature constraint, with a consequence increase in hot and cold utility needs

On the other hand, lowering ΔT_{min} allows for higher internal heat recovery, but requires larger heat exchanging area: a tradeoff must be found between operational and capital costs

2.3.2. Composite curve

Normally, an industrial process is characterized by different hot and cold streams that are interacting together. To handle multiple streams, composite curves are constructed; this is done separately for hot and cold streams.

The hot composite curve shows the total heat content of all the hot streams in the indicated temperature range; this gives an indication of the overall heat availability of the system, and thus reveals the cooling needs of the process.

The cold composite curve, instead, gathers all the cold streams at their relative temperature interval, so to demonstrate the total heat demand that is required by the process.

Hot and cold composite curve are then represented together in a temperature – heat diagram, in a way that guarantees the minimum temperature approach between the

two lines. The temperature where the two lines are as close as possible is called the *pinch point*: the temperature difference in this point is equal to ΔT_{min}.

The composite curves graph also reveals the eventual needs and entity of both hot and cold utility.

To provide a straightforward comprehension of the topic, an example is proposed, involving two hot and two cold streams.

In Figure 2-4, the hot composite stream is built: in each temperature interval, the thermal capacity of the existing streams is summed together.

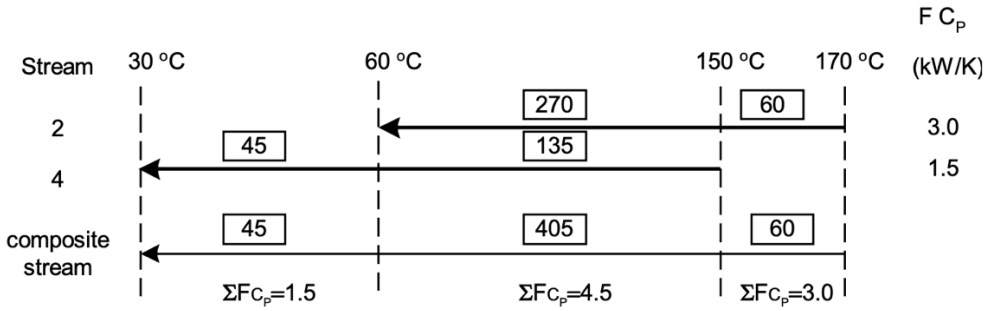

Figure 2-4: Hot composite stream generation (the text in the box represents the the heat content in each temperature interval)[33]

Repeating the same procedure for the cold streams, the cold composite stream is found (Figure 2-5):

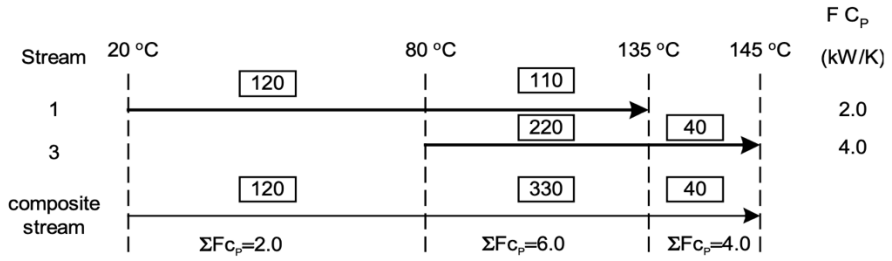

Figure 2-5: Generation of cold composite stream (the text in the box represents the the heat content in each temperature interval) [33]

For a given value of minimum temperature approach, the hot and cold composite curves can be represented together in the temperature – heat diagram, in which the pinch point is clearly represented as the closest approach between the two curves. In this case, the selected value of ΔT_{min} is equal to 10 °C

Hot and cold utility duties are also represented on the same curve (Figure 2-6).

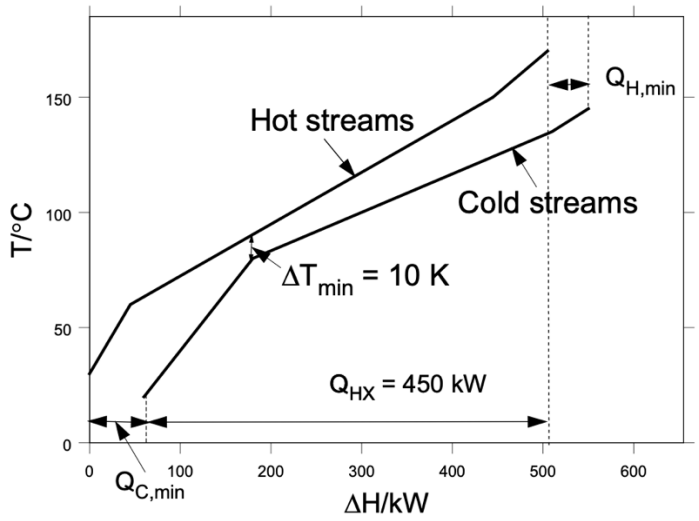

Figure 2-6: Hot and cold composite curves represented together, $\Delta T_{min} = 10\ °C$ [33]

2.3.3. Problem table and grand composite curve

The Problem Table is an algorithm developed as a support to pinch analysis, which is able to automatically find the pinch point and external utilities duty, as well as defining the grand composite curve, an essential tool necessary for heat recovery investigation.

This is done for a given value of ΔT_{MIN}.

The algorithm starts by shifting the temperature of the hot streams by $-\frac{\Delta T_{MIN}}{2}$, while the one of the cold streams by $+\frac{\Delta T_{MIN}}{2}$. In this way, the temperature difference at the pinch point will be exactly equal to zero; of course, the shifted temperature of a stream does not correspond to the real one. It is simply a mathematical way to guarantee a minimum temperature approach equal to ΔT_{MIN}.

The same streams introduced in the section before are here represented at their shifted temperature in Figure 2-7.

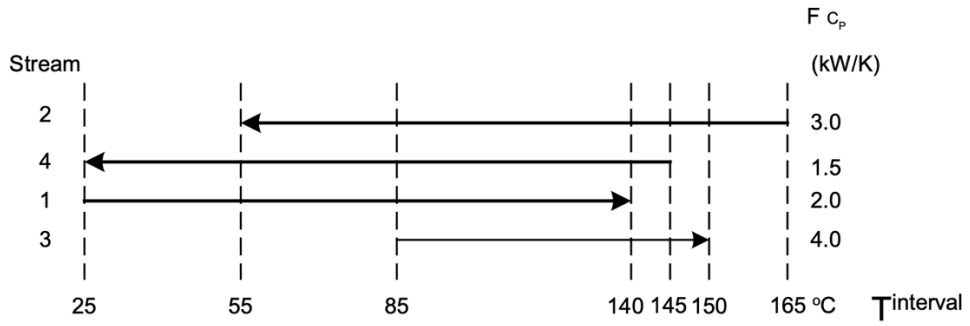

Figure 2-7: Hot and cold streams represented at their shifted temperature [33]

Hot and cold streams together define the "background process".

In each interval of shifted temperature, the overall amount of heat exchanged between hot and cold streams is computed:

$$Q_{inteval} = \sum ((F\ CP)_{hot} - (F\ CP)_{cold}) * \Delta T_{shifted,i} \quad (2\text{-}2)$$

Hot streams provide a heat surplus, while cold streams a heat deficit. Hence, in each interval information regarding whether the background process "requests" heat or cooling are available.

This is equivalent to represent a heat cascade of the process; normally, a negative value is found in this heat cascade. However, this would mean that heat is flowing from a lower temperature to a higher one, and it is against the second principle of thermodynamic.

Eventually, the minimum negative value of the heat cascade is identified and summed to the heat cascade, so to obtain the feasible heat cascade of the process. This is graphically represented in Figure 2-8.

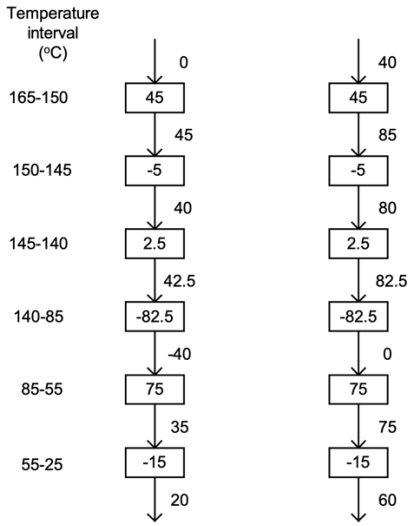

Figure 2-8: Unfeasible heat cascade (left image): the value inside the box correspond to the heat exchanged in each temperature interval, while the one just outside represented the heat cascade. On the right, the feasible heat cascade [33]

The minimum value of the heat cascade is equal to *-40 kW*, hence this will be summed so to obtain the feasible process on the right. It is crucial to understand that if more heat is added to the heat cascade (i.e. more than *40 kW)* additional hot utility is added, which would be cascaded through the process, eventually ending up as additional cold utility.

Hence, *40 kW* is the amount of heat that guarantees minimum hot and cold utility requirements, optimizing the cascading process.

Representing the feasible heat cascade, together with the shifted temperatures interval, gives what is indicated as the grand composite curve (GCC), Figure 2-9.

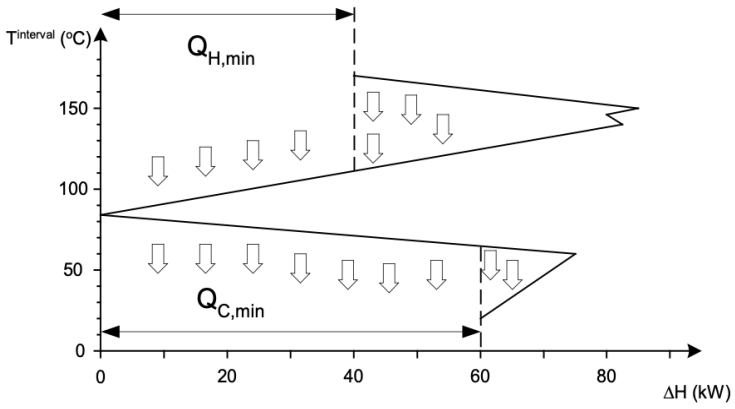

Figure 2-9: Grand composite curve of the considered streams [33]

The grand composite curve clearly divides the streams in two regions, above and below the pinch point.

Above the pinch, the hot streams transfer all their heat to the cold streams, leaving a hot utility necessary to reach the targets. This region is then a net heat sink and cold utility is not needed.

Conversely, below the pinch point a heat surplus is represented, hence this region could be seen as a heat source. Hot utility is not required below the pinch point.

From Figure 2-9 is possible to notice two regions in which the grand composite curve folds back on itself: these regions are known as *pockets* and here the process "takes care of itself", in the sense that the heat demand can be completely satisfied though interval to interval heat transfer.

It is now possible to state the three golden rules of pinch analysis:

- Do not transfer heat across the pinch
- Do not use cold utilities above the pinch
- Do not use hot utilities below the pinch

In this way, the minimum requirements for both hot and cold utility are achieved, providing the best theoretical way of building a heat exchanging network.

Lastly, the GCC is useful when dealing with utility integration since it provides a graphical tool to make initials considerations: for the purpose of this thesis, the curve was used to evaluate the integration of heat pump.

3 High temperature heat pumps

Heat pumps are machines capable of extracting and transferring thermal energy from low to high temperature level. Recalling the second law of thermodynamics, this is not a spontaneous process (i.e. a process "that occurs naturally under certain conditions"[34]) and energy is required for it to be viable. This could be in the form of mechanical work (often supplied by an electricity-driven motor) or thermal energy.

Figure 3-1 provides a schematic representation of a heat pump working with electrical energy.

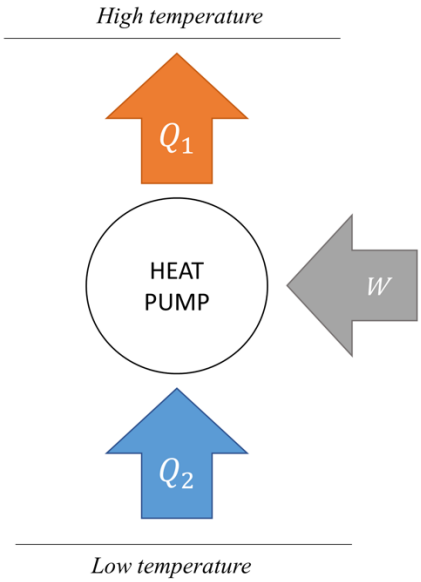

Figure 3-1: Schematic representation of a heat pump working with electrical energy: heat (Q_2) is extracted from low temperature and discharged at high temperature (Q_1), exploiting electrical work (W)

Heat pumps can be divided in two major families: the open systems and the closed ones. The former is composed of mechanical and thermal vapor recompression heat pumps (MVR and TVR in Figure 3-2); the latter includes compression heat pumps, the most common type of this technology, and the sorption systems.

This is presented in Figure 3-2

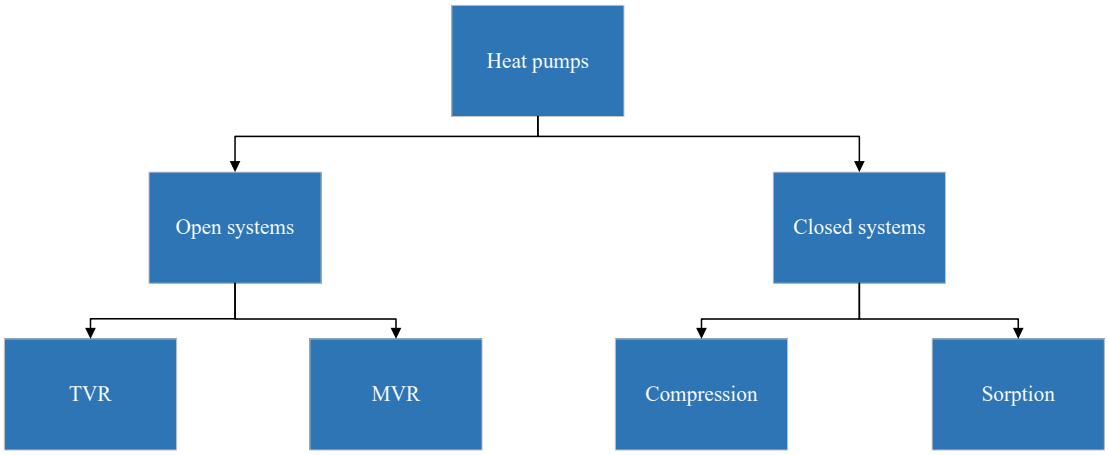

Figure 3-2: Heat pump classification, adapted from [35]

Having to deal with residual heat recovery, the focus of this thesis is on closed cycles, as this is the most used technology, available in a variety of sizes and applications [35].

An additional classification for heat pumps takes into account their operating temperature, as proposed by proposed by Pereux and Bobelin [36]

They identified very high temperature heat pump (VHTHP), high temperature heat pumps (HTHP) and common heat pumps (HP). This distinction is based on the temperature of the heat source and of the heat sink, as presented in Figure 3-3

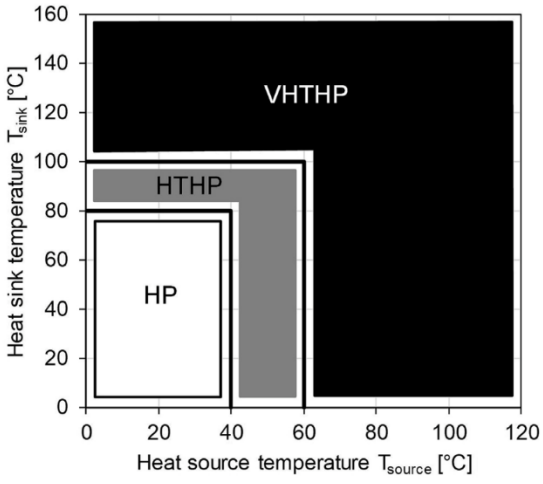

Figure 3-3: Heat pump classification based on temperature levels [37]

A common heat pump (HP, Figure 3-3) is not suitable to for residual heat recovery in most industrial applications, due to limitation in the supply temperature that could be reached (maximum 80 °C)

High temperature heat pumps (including both HTHP and VHTHP), on the other hand, are designed to provide a solution when higher temperature are needed; it was found that at least 20 high temperature heat pumps are present on the market, with the capacity to deliver heat at temperatures of at least 90 °C [38].

The use of high temperature heat pumps is of interest for heat recovery applications in industrial processes since they could provide an alternative to fossil fuel technologies. The replacement of such technologies with a heat pump working with an environmentally friendly fluid becomes a solution to climate change mitigation and may improve the energy efficiency of the overall process [39].

3.1. HTHP challenges: the compressor

Closed cycles heat pumps are a well-known technology, since they have been used for a long time in different sectors. The basic cycle could be extended to higher temperatures; however, several challenges, mainly related to the design of the compressor, have to be overcome.

These complications are a consequence of constant high pressure and temperatures, that are outside the common operating range of a standard compressor. The main difficulties were highlighted by [40] and they can be summarized in the following points:

- Mechanical failures and wear which determine a lower efficiency or the failure of operation
- Degradation of the oil that is used for the lubrication of the mechanical part of the compressor.
- Cooling requirements for the compressor's electric motor

The compressor must have a high efficiency, otherwise the performance of the whole cycle will be penalized, resulting in a low coefficient of performance (COP) and thus high electrical consumption [41]. Therefore, the design of this component represents a critical step in the building of a high temperature heat pump: this is achieved through new design or, more often, through modifications of existing topologies. In this case, the main changes that are adopted have to do with thermal management of the system, to account for heat distribution across compressor´s body [42]. Also, modification to oil separation systems are often required in order to guarantee a proper lubrication of the device [39]

3.1.1. Compressor classification

Compressors can be divided in open systems, where the electric motor is separated from the rest of the components, and hermetic/semi hermetic, in which the motor is directly integrated in the machine. The first system is easier to cool down (i.e with ambient air) and more reliable, however it is characterized by higher mechanical losses. On the other hand, in hermetic and semi-hermetic topologies the motor is cooled by the refrigerant itself, which affects the thermodynamic cycle of the heat pump. The efficiency is normally higher, but the maintenance is more complicated. Compressors used in high temperature heat pumps normally belong to this second category.

Depending on the working principle, two categories are identifiable: positive displacement or dynamic compressors (Figure 3-4).

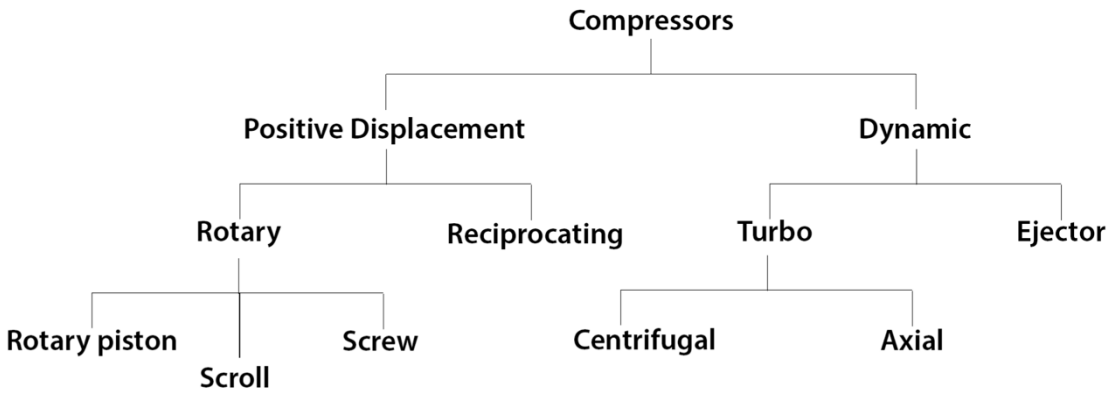

Figure 3-4: Compressor classification [43]

In positive displacement devices, the compressor works by decreasing the volume of the refrigerant itself. This is achieved through different configurations: in rotary compressor, as the name suggests, pressure increases through a rotary motion that is impressed by a piston, scroll or a screw; in reciprocating compressors, instead, the fluid is delivered to high pressure thanks to the alternating movement of a piston.

In the dynamic type, the pressure increases through a continuous exchange of angular momentum between the rotating part and the refrigerant. Turbo compressors are part of this category.

Even though it is not possible to provide a general criteria for the selection of a compressor, since this is highly dependent on working conditions, state of the art of high temperature heat pumps often use piston or screw compressors: these, in fact,

are found to be more reliable, while guaranteeing higher efficiencies in the typical sizes required for HP applications [44]

3.2. HTHP challenges: the refrigerant

The selection of the refrigerant is a key element in the design of a high temperature heat pump; it must guarantee high efficiency, while having compatible thermodynamic properties with temperatures and pressure required. The optimal design of a heat pump will be achieved through a combination of proper fluid and compressor.

Historically, industrial heat pumps have used chlorinated hydrocarbons (CFC), such as R114 due to their high condensation temperature [45]. However, these are characterized by high ozone depletion potential (ODP), hence they were replaced by fluorinated hydrocarbons (HFC) in the nineties. These refrigerants are still common nowadays, but they have a high global warming potential (GWP). Therefore, after the restrictions on greenhouse gases emissions introduced by the Kyoto protocol of 1997, these refrigerants will be slowly phased out in the future and replaced by new categories [46].

The main criteria that are taken into account when evaluating the performance of a refrigerant are the following:

- Critical temperature: a gap of 10 to 15 K should be granted between condensation and critical temperature to avoid supercritical operation of the heat pump.
- The higher pressure reached by refrigerant during heat pump's operation provides an indication about the material efforts of the equipment, and should not be too high (a reasonable value is 25 bar [38], although in some devices this limit is overcome with appropriate solutions)
- Vapor pressure at ambient temperature higher 1 atm: to avoid leakages during downtime period of the heat pump
- Thermal stability of the oil – refrigerant mixture at high temperature: this is critical, since it provides the lubricant effect to mechanical part of the compressor to ensure correct operation
- Safety: non-toxic and non-flammable refrigerant are preferred
- Environmental compatibility: desirable characteristics are zero ODP and low GWP (< 10) [38]
- Performance parameters: these are normally characterized in terms of COP and volumetric heating capacity (VHC, generated heat capacity per volume

of processed refrigerant [$\frac{J}{m^3}$]), which gives an idea about the dimension of the compressor

- Economy: measured in terms of prices and availability

3.2.1. HFO (hydrofluoroolefins)

The latest generation of refrigerants is composed by the hydrofluoroolefins (HFO). These have very low GWP and ODP as well as enabling high efficiencies. R1234yf and R1234ze(E) are currently in use, as they are considered the perfect replacement for R134a, since their critical pressure and temperature are comparable.

Their main thermodynamic properties are reported in Table 3-1

The only concern about R1234yf is related to its flammability, however this refrigerant has a pressure–temperature curve that is almost identical to that of R134a, which means that it is suitable in the same field of application.

R1234ze(E), instead, exhibits a similar phase profile, but it is characterized by a slightly lower vapor pressure. The pressure–temperature curve of these refrigerants, compared to that of R134, is shown in Figure 3-5

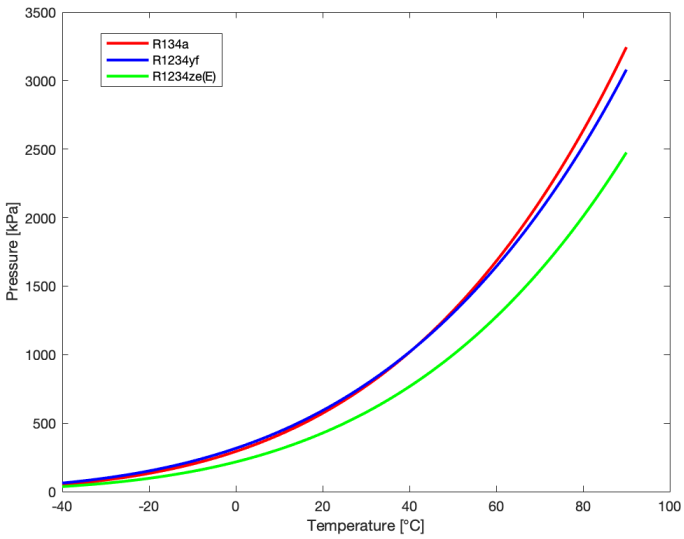

Figure 3-5: Pressure temperature curve of R1234yf and R1234ze(E) compared to that of R134a

The main advantage of R1234ze(E) is its higher critical temperature, which extends the range of working conditions. Also, this working fluid typically leads to high COP and VHC values, resulting in smaller compressor size [47].

Table 3-1: Main thermodynamic properties of R1234yf and R1234ze(E) compared to R134a

Refrigerant	T_C [°C]	$P_C[bar]$	GWP	ODP
R134a	101.1	40.6	1300	0
R1234yf	94.7	33.8	0	<1
R1234ze(E)	109.4	36.4	0	<1

If higher temperatures are required, the most attractive fluids are R1336mzz(Z) and R1234ze(Z). These would replace fluorinated hydrocarbons such as R245fa and R365mfc.

The most cited in the literature is R1336mzz(Z), characterized by high critical temperature of 171.3 °C at a pressure of 29 bar, which is relatively low. As Figure 3-6 shows , its vapor pressure is lower than that of R245fa and this allows to supply heat by condensing at a temperature of 160 °C, while not overcoming the theoretical limit of 25 bar pressure [48]

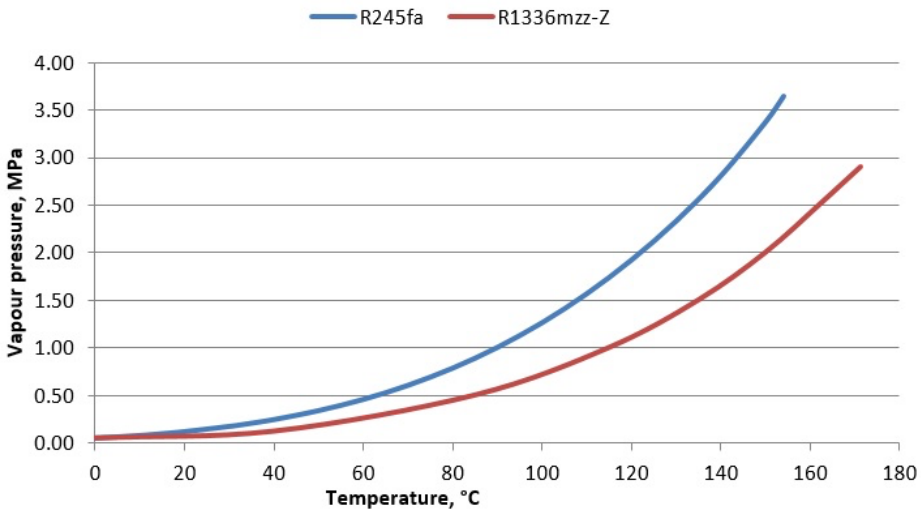

Figure 3-6: Pressure temperature curve of R1336mzz(Z) compared to that of R245fa[48]

It has demonstrated high COP in several studies and it exhibited a similar interaction with materials to that of R245fa [49].

The main concern about this refrigerant is that the volumetric heating capacity is lower than the one of other alternatives (resulting in a larger compressor [50]) and the fact that its vapor pressure at ambient temperature is lower than 1.013 bar, which may result in leakage during heat pump downtime period [51].

R1234ze(Z) is an isomer of R1234ze(E) and, due to its higher critical temperature, is suitable for high temperature applications. Even though its volumetric capacity is lower than R1234ze(E), it has demonstrated higher COP values and should be further investigated, due to limited amount of information available in literature [52].

Their main thermodynamic properties are reported in Table 3-2.

Table 3-2: Main thermodynamic properties of R1336mzz(Z) and R1234ze(Z) compared to R245fa

Refrigerant	T_C [°C]	P_C[bar]	GWP	ODP
R245fa	154	36.5	858	0
R1336mzz(Z)	171.3	29	0	2
R1234ze(Z)	150.1	35.3	0	<1

Another consideration that normally arises is related to the shape of the *T–s* curve of these refrigerants: R1336mzz(Z) has a two-phase region that is shifted towards the right, compared to that of other refrigerants (example (c) in Figure 3-7). The consequence is that an additional degree of superheating is required at the compressor inlet, to avoid "wet compression". This may result in modifications to the basic vapor compression cycle [49].

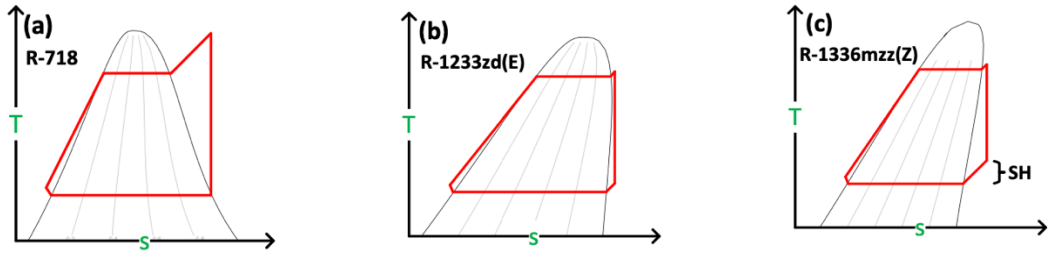

Figure 3-7: Comparison between wet (a), isentropic (b) and dry (c) refrigerants

3.2.2. HCFO (Hydrochlorofluoroolefins)

Hydrochlorofluoroolefins is another promising category of refrigerants. These are characterized by a low content of chlorine, which implies an ODP that is close to zero, and excellent thermodynamic properties, such as high critical temperature and non-toxicity/flammability.

The most cited one is R1233zd(E), which requires a low superheating degree, as this is identified as an isentropic fluid (case (b) Figure 3-7), and has a decent volumetric heat capacity as well as COP values. As for R1336mzz(Z), a low vapor pressure is shown at ambient temperature (1.079 bar) [51].

However, it is a relatively new refrigerant and further studies are necessary to demonstrate its efficiency. Some of its properties are reported in Table 3-3.

Table 3-3: Main thermodynamic properties of R1233zd(E)

Refrigerant	$T_C[°C]$	$P_C[°bar]$	**GWP**	**ODP**
R1233zd(E)	166.5	36.2	1	0.00034

3.2.3. Natural fluids and hydrocarbons

Among the different natural fluids, the most promising choice for high temperature heat pumps is ammonia: this, in fact, is widely used in industrial heat pumps, but limited to heat supply temperatures of around 90 °C due to the high compressor's discharge pressure when higher temperatures are required, as shown in Figure 3-8 where the ammonia vapor pressure is compared to the one of R245fa. Moreover, at high pressure ratios, the temperature of ammonia at the compressor outlet is very high, causing additional issues when designing the compressor.

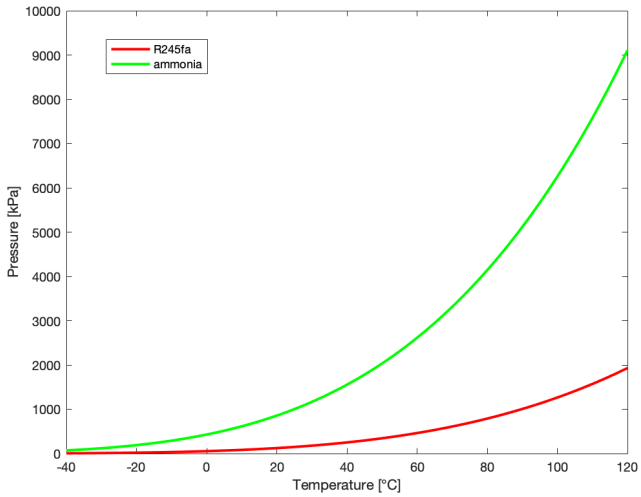

Figure 3-8: Pressure-temperature curve of ammonia compared to that of R245fa

Considering, for example, a temperature of 120 °C, the ammonia vapor pressure is higher than 90 bar, making it impossible to be implemented in real configurations.

Other problems are the toxicity and flammability, although this can be handled, especially in industrial applications.

Another possibility than has been explored is related to hydrocarbons, with a special focus on n-Butane (R600) and pentane (R601). The latter was demonstrated to have the highest COP for applications up to 125 °C among several refrigerants but showed a low VHC.

R600, instead, has a slightly lower COP, while requiring lower compressor sizes and is considered one of the most promising alternatives in the short-term period.

Both hydrocarbons have low GWP and ODP, but they are flammable.

Main thermodynamic properties of these fluids are reported in Table 3-4

Table 3-4: Main thermodynamic properties of ammonia, R600 and R601

Refrigerant	$T_C[°C]$	$P_C[°bar]$	**GWP**	**ODP**
Ammonia	132.3	113.3	0	0
R600	152	38	4	2
R601	196.6	33.7	5	<1

As for R1336mzz(Z), also these fluids have the necessity of a superheating degree, which is due to the shape of their T-s curve.

3.3. Vapor compression heat pumps

Vapor compression heat pumps are closed systems, as illustrated in Figure 3-2. The basic topology is unvaried for high and low temperature application, and it consists of four main components: compressor, evaporator, condenser and expansion valve. These are shown in Figure 3-9, together with the temperature – entropy plot and the the pressure – enthalpy plot of the relevant cycle.

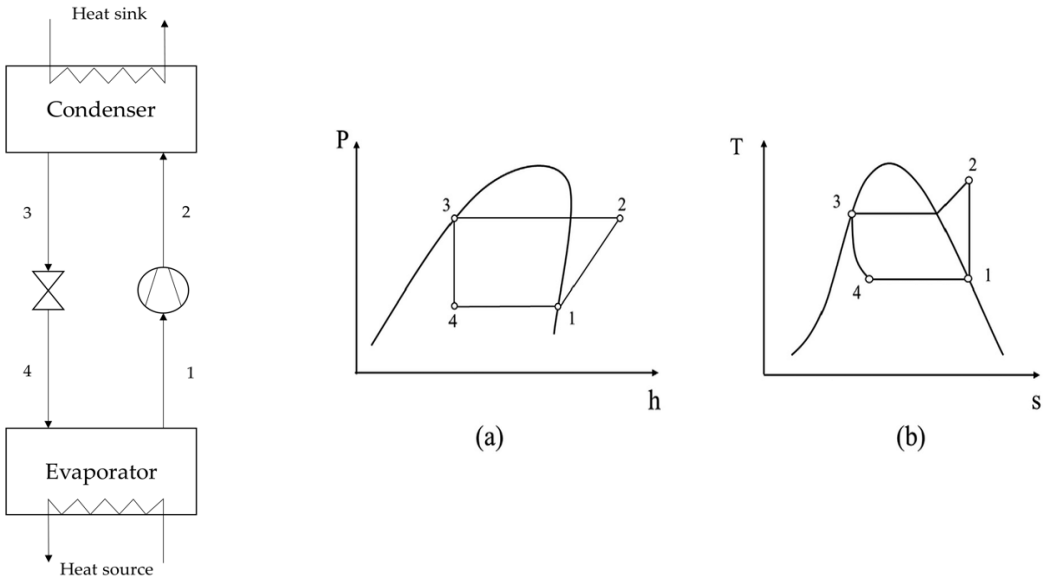

Figure 3-9: Heat pump basic cycle topology (left) and thermodynamic stages in the T-s and p-h diagrams (right) [53]

The working fluid of heat pumps is circulated through the compressor, which is used to create the pressure difference between the low and the high-pressure level, also associated to low and high temperature of the cycle. The mechanical work required by the compressor, specific to the mass flow rate of the refrigerant, is computed in equation (3-1)

$$W_{comp} = h_2 - h_1 \tag{3-1}$$

At low pressure, the refrigerant is in the vapor–liquid state and it flows through the evaporator, where it absorbs energy from the external heat source, performing phase transition and exiting in the vapor state, ideally saturated. As a consequence, the external source is cooled. The specific heat exchanged in the evaporation is derived as

$$Q_{eva} = h_1 - h_4 \tag{3-2}$$

The fluid is then compressed at high pressure, becoming superheated vapor.

The refrigerant vapor at high temperature and high pressure is fed in the condenser; as the sink temperature is lower than the refrigerant, heat flows from the refrigerant fluid to the external heat sink, causing the condensation of the working fluid. This normally exits the condenser in the saturated liquid state (or subcooled).

The specific heat of condensation processes is computed in equation (3-3)

$$Q_{cond} = h_2 - h_3 \tag{3-3}$$

The last component is the expansion valve, where the refrigerant is laminated to the low- pressure level. At this point, the cycle starts again.

One of the most important parameters that is considered when evaluating the performance of a heat pump is the coefficient of performance (*COP*). This is defined as the ratio of the useful effect to the energy input. In the case of a heating application, the *COP* can be computed as:

$$COP = \frac{W_{comp}}{Q_{cond}} \tag{3-4}$$

Achieving a high *COP* value corresponds to decrease energy consumptions, while delivering the same amount of heat, hence this parameter must be maximized to guarantee high efficiencies.

Considering the ideal Carnot cycle working between the temperatures T_{eva} and T_{cond} and exploiting the first and second principles of thermodynamics, the expression for the ideal *COP* is obtained:

$$COP_{id} = \frac{T_{cond}}{T_{cond} - T_{eva}} \tag{3-5}$$

This equation reveals that the ideal COP of a heat pump is mainly influenced by the temperature lift, defined as the difference between the condensation and evaporation temperature. An increase in the temperature lift determines the decrease of the heat pump's performance.

3.3.1. Real life considerations

In a real heat pump, additional effects must be taken into account, such as pressure losses in the heat exchangers and fluid dynamic losses in the compressor, as well as electrical efficiency. Additionally, the refrigerant is usually found in a sub-cooled liquid state when leaving the compressor, whereas it may be in a superheated vapor condition as a result of evaporation, to ease compressor operation.

For these reasons, the COP exhibit real values which are much lower than the ideal one.

The relationship between ideal and real COP is given by the Carnot efficiency factor.

$$\eta_{carnot} = \frac{COP}{COP_{id}} \tag{3-6}$$

This value is normally in a range between 0.48 – 0.64, meaning that the energetic performance of a real heat pump is significantly penalized when taking into account real conditions [33].

When dealing with vapor compression heat pump integration industrial processes the general approach followed by pinch analysis first involves the calculation of the ideal COP, followed by the real one, making a hypothesis on Carnot efficiency. This methodology provides an estimate of heat pump's efficiency and is useful to perform initial techno-economic considerations.

The approach followed in this thesis is slightly different: instead of making a hypothesis on η_{carnot}, the compressor efficiency was assumed adding the advantage of simulating the behavior of the heat pump with different refrigerants. This aspect will be clarified in section 4.3.2

3.4. Hybrid absorption compression heat pump

The hybrid absorption compression heat pump (HACHP) is a combination of a vapor compression heat pump and an absorption heat pump. The scheme of this device is presented in Figure 3-10.

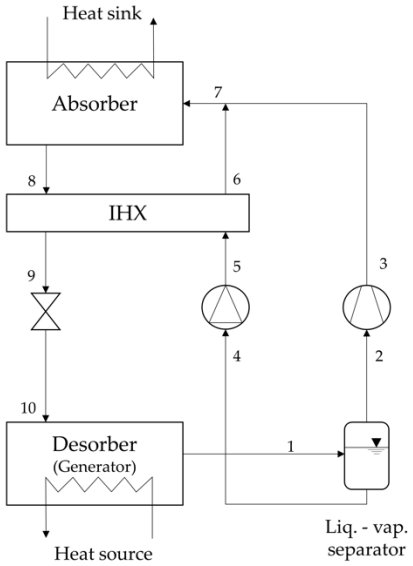

Figure 3-10: Schematic representation of a hybrid absorption compression heat pump

In this figure, one may recognize some typical components of vapor compression heat pumps, namely the two low- and high-pressure heat exchangers, compressor

and expansion valve. However, the topology is slightly changed, due to the different working principle, which is based on the Osenbruck cycle (Osenbruck, 1895) and it works with a zeotropic mixture, namely ammonia–water. As consequence of the choice of the working mixture and of the cycle design, a liquid vapor separator is needed to separate refrigerant vapor from the liquid solution and a solution pump is needed besides the compressor.

This layout allows to exploit the advantages of absorption and desorption processes, instead of simple condensation and evaporation, as a normal heat pump would do. Thus, in order to provide a full comprehension of the working principle of this technology, basic concepts about zeotropic mixture and absorption/desorption processes are now introduced.

3.4.1. Mixture properties

In Figure 3-11 the binary mixture ammonia–water is represented in a liquid vapor equilibrium for given pressure-temperature conditions

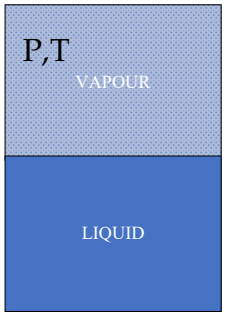

Figure 3-11: Binary mixture (ammonia-water) at thermodynamic equilibrium for given temperature–pressure conditions

At thermodynamic equilibrium conditions, the system is defined by four thermodynamic properties, namely P,T,X_L,X_G where X is the mass fraction of the refrigerant in the mixture, computed both for vapor and liquid phase.

According to Gibbs phase rule, the variance of the system is defined as:

$$IV = 2 + NC - NP = 2 \tag{3-7}$$

Where NC represents number of components, ammonia and water, and NP is the number of phases, again equal to two.

Therefore, the system is defined when two out of four intensive properties are known.

What is commonly done with this kind of system, is to define the mass fraction of liquid and vapor phase in terms of temperature and pressure. Translated in mathematical terms, this corresponds to:

$$X_L = X_L(P,T) \tag{3-8}$$

$$X_G = X_G(P,T) \tag{3-9}$$

Finally, fixing one of the two properties above, either *P* or *T*, the phase diagram for a binary mixture can be represented. Figure 3-12 shows the phase diagram for ammonia-water, with pressure fixed at 1 bar.

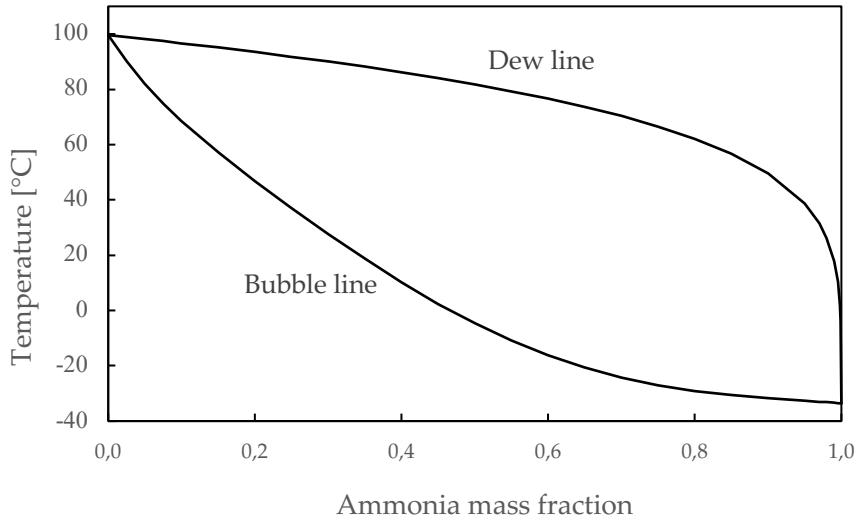

Figure 3-12: General representation of a phase diagram for ammonia-water at atmospheric pressure

On the X-axis, the most volatile component of the mixture (i.e. ammonia) is represented. Hence *X = 1* is the case of pure ammonia, while *X = 0* is the case of pure water.

The two lines in this graph represent the bubble and dew line. The former can be seen as the temperature at which the first bubble of vapor is formed. The latter represents the state at which the first drop of liquid appears.

Two things are immediately noticeable from Figure 3-12 which characterizes a mixture:

- When liquid and vapor phases coexist in equilibrium, the saturation temperature varies with mass fraction, even if the pressure is constant.

- The mixture exhibits a temperature glide during the phase transition, which becomes equal to zero only for pure substances (i.e. $X = 0$ or $X = 1$).

3.4.2. Desorption and absorption processes

A desorption process consists in the generation of vapor from the condensed phase of a mixture of two or more components. The vapor mainly contains one component, in contrast to evaporation, where all the components are assumed to vaporize [54]. The process is represented in Figure 3-13, supposing steady state and steady flow configuration:

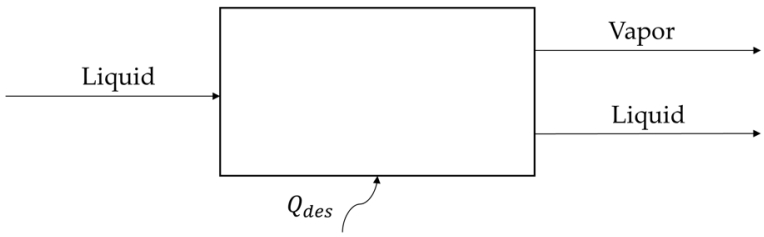

Figure 3-13: Schematic representation of a desorption process

Since this in an endothermic process, energy in the form of heat is required; in Figure 3-13 this is indicated as Q_{des}

The process can be visualized in the phase diagram in Figure 3-14, at a constant pressure of 8 bar, a realistic value for the operating conditions of the HACHP studied in this thesis (as will be discussed in the Results chapter).

The liquid inlet solution (1) is assumed to be in saturated conditions and is heated by an external source, entering the two-phase zone (1′). The two outlet phases are identifiable as the liquid phase 3 and the vapor phase 2, considered at the same temperature of 1′.

The vapor phase will be characterized by a higher mass fraction of ammonia, due to its higher vapor pressure. The liquid, instead, will be mainly composed of the less volatile component (water).

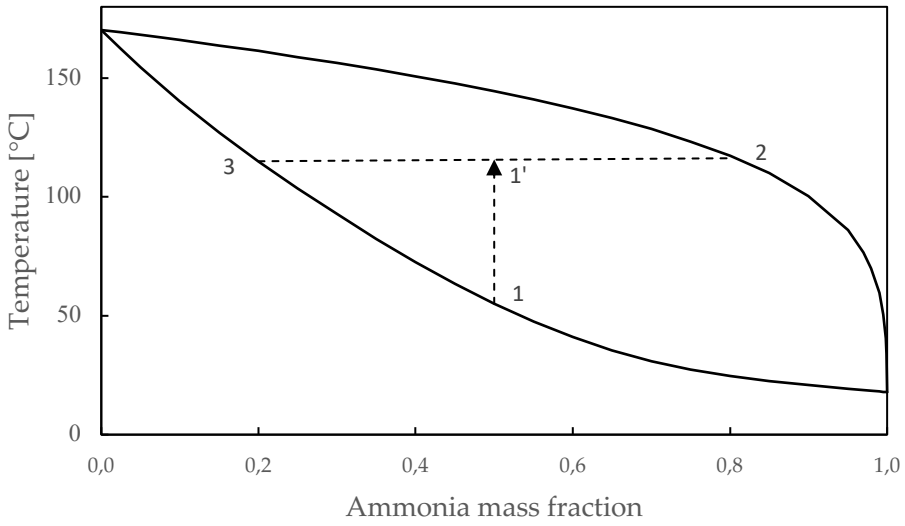

Figure 3-14: Simplified representation of a desorption process in the phase diagram at a constant pressure of 8 bar

On the other side, an absorption process describes the dilution of a vapor into an absorbent mixture (liquid), as represented in Figure 3-15. A condensed phase is already present at the inlet of the absorber [54]. This difference the process from a common condensation, in which only vapor phase is involved.

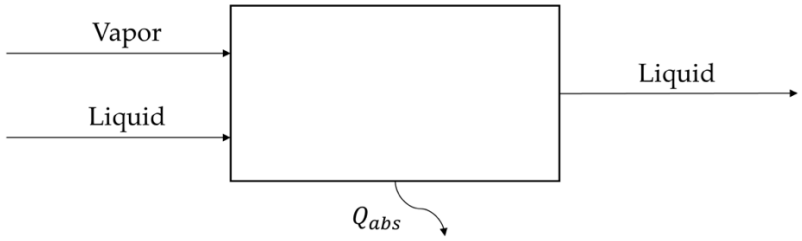

Figure 3-15: Schematic representation of an absorption process [54]

Again, the process is represented on the phase diagram in Figure 3-16; the considered pressure, in this case, is 30 bar as this is a representative value of the working conditions of the HACHP for this thesis project.

The absorption process is divided in two steps: first, the liquid solution (1) absorbs the vapor phase (2), which are assumed at the same temperature (saturated conditions), revealing the mixing state 3′.

The outlet condition from the absorber will be at same composition of 3′, but lower temperature, due to the exothermic nature of the process.

Due to the dilution process, the outlet mass fraction of the liquid is increased from 1 to 3 and it will be enriched by the more volatile component.

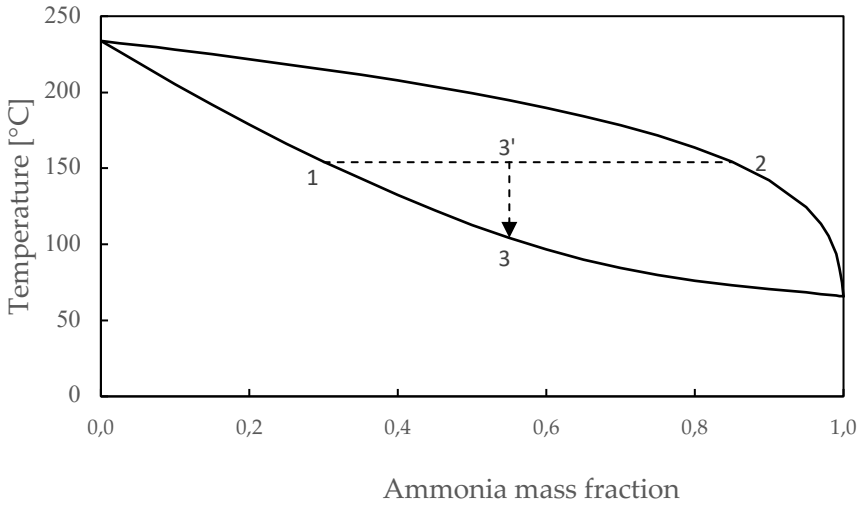

Figure 3-16: Simplified representation of an absorption process in the phase diagram at a constant pressure of 30 bar

3.4.3. Working principle & components design

The working principle of the HACHP is now briefly described, with reference to Figure 3-10.

In the desorber (often named generator) a rich solution (rich = rich in ammonia content) of ammonia-water is present (point 10, Figure 3-10). Heat is provided to the solution by an external source (normally in the form of residual heat) and this allows the desorption process to take place, which determines the evaporation of ammonia, due to its higher vapor pressure compared to water. Unlike in vapor compression cycles, the evaporation of the working fluid is not completed, thus, at the desorber outlet (point 1, Figure 3-10), ammonia vapor needs to be separated from a liquid solution of ammonia-water (the so called "poor"); the former is compressed to the high pressure, while the second, being liquid, is pumped through the solution pump.

At high pressure the liquid and vapor streams are reunited to perform the absorption process (point 7, Figure 3-10): the ammonia vapor is absorbed into the poor solution, releasing heat to an external source (the heat sink).

The outlet liquid solution leaving the absorber (point 8, Figure 3-10) represents the rich solution, as introduced previously.

Before reentering in the desorber, the rich solution passes through a heat exchanger, where it preheats the poor solution, and is then expanded to the low-pressure level.

The most common representation of this process is done in the Dühring plot (Figure 3-17), a pressure-temperature-concentration diagram. This is useful to represent saturated liquid states and visualize the solution cycle, i.e. strong and weak solution.

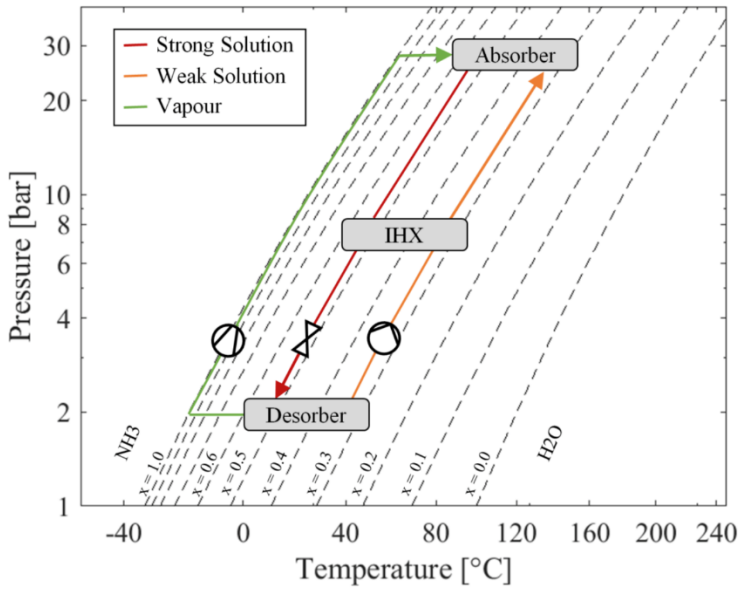

Figure 3-17: Absorption-compression heat pump cycle on the Dühring plot [15]

In the cycle presented above, only a single compressor is included. This leads to several challenges, such as high discharge temperature and pressure ratio, typical of ammonia compression, as illustrated in Section 3.2.3

Furthermore, liquid droplets may be present in the ammonia vapor, hence the compressor must be able to operate under such conditions. As discussed in [55], the best solutions in this case are positive displacement compressors, due to higher achievable pressure ratio and lower swept volumes. The most cited in literature are screw and reciprocating solutions, similarly to the compressors adopted in vapor compression heat pumps.

An alternative that is often explored considers a two-stage compression, with intercooling. This allows to reach higher sink temperatures and pressure level, avoiding problems, such as decomposition of the working fluid or carbonization of the lubricant, while adding a complexity degree to the configuration.

While vapor compression heat pumps typically use common heat exchanger types, the construction of the absorber may be more challenging, due to the

thermodynamic of the process: a good vapor–liquid mixing, in fact, must be achieved.

Both shell-and-tube and plate heat exchangers are possible, even if the tendency is moving towards vertical plate heat exchangers, since the plates can be pressed together with different shapes, increasing turbulence and area, while providing a better fluid distribution [56].

Heat transfer could take place through falling film and bubble absorption as recommended by [57], see Figure 3-18.

In the first option, the poor solution flows from the top of the heat exchanger, down to the bottom, during which it is in contact with the vertical plate. The refrigerant vapor occupies the free space and it is absorbed by the poor solution, releasing heat to the sink. For operation in bubble mode, instead, vapor is first absorbed by the poor solution at the bottom of the plate, while then flowing in counter current to the coolant.

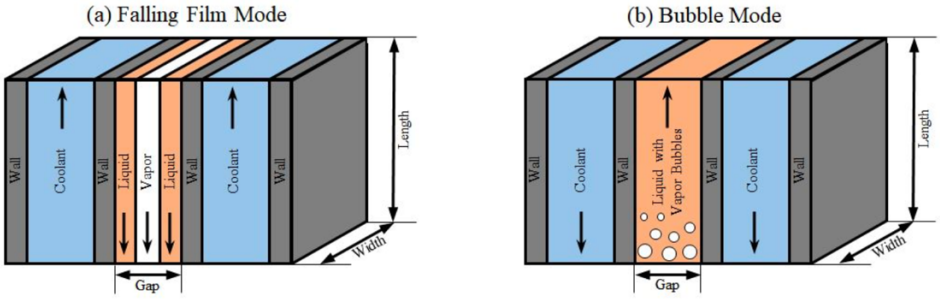

Figure 3-18: Comparison between falling film (a) and bubble (b) heat transfer mode [56]

The desorber, instead, is “easier” to build and normally is in the form of a flooded evaporator, due to the similarity of operating conditions.

3.4.4. Peculiarities of HACHP

A hybrid absorption-compression heat pump has different advantages compared to a common vapor compression system. The most cited one is the fact that ammonia-water is a zeotropic mixture, thus it exhibits a certain temperature glide during phase transition, as it can visualized in left image of Figure 3-19.

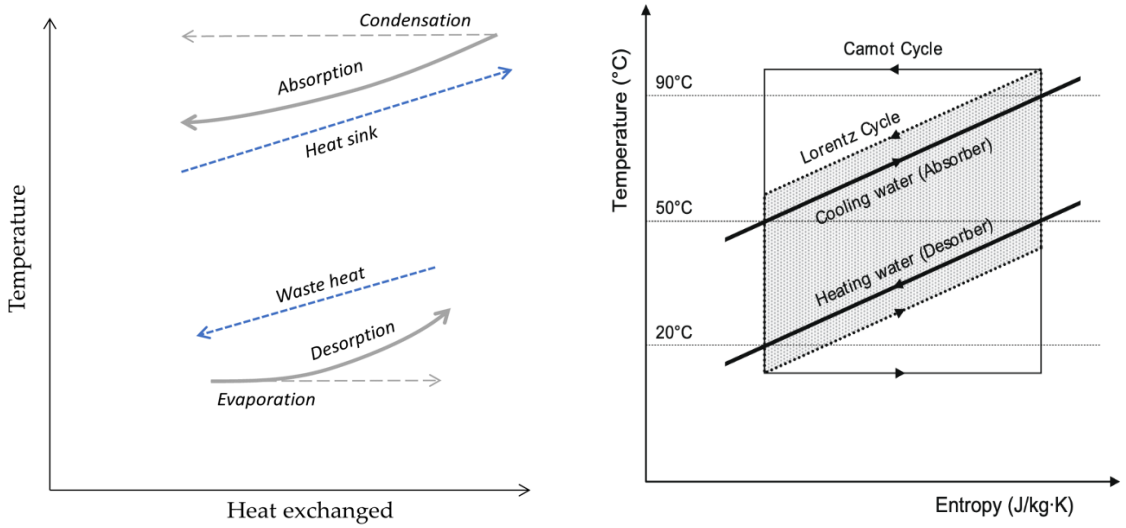

Figure 3-19: Comparison of hybrid and vapor compression heat pumps (left, own figure). Carnot and Lorentz cycle comparison (right,[58])

This reduces temperature difference with external source (lower irreversibility), which is of direct interest for residual heat recovery, typically characterized by large temperature glides [15].

The gliding profile recalls the Lorentz cycle, which has better performance compared to the well-known Carnot cycle with the same higher and lower temperatures (right image in Figure 3-19). The consequence is that COP is higher than that of conventional vapor compression system [59].

Another advantage is that the vapor pressure of ammonia and water is lower with respect to the one of the pure refrigerant: at the same working pressure, the hybrid heat pump can achieve higher supply temperature compared to a normal compression heat pump working with pure ammonia: the pressure reached in this case would be unacceptably high, as the vapor pressure curve of pure ammonia showed (Figure 3-8).

This makes this technology perfect for high temperature applications [60] and extends the range of temperature [59]. The reduction of vapor pressure also allows the design of the heat pumps using common refrigerant components [16] (compatible with ammonia properties).

As seen in the working principle, a separator is used at the desorber outlet to divide the liquid weak solution from the ammonia vapor. Therefore, it is possible to vary the composition of the working fluid by controlling the ammonia concentration in the weak solution: this controls the low-pressure gas density, hence, at constant

speed and volume flow of the compressor, the mass flow rate of the vapor is controlled. This represents a great advantage since the behavior of the heat pump could be adapted to eventual temperature fluctuations or heat duties [56].

The last advantage is related to the choice of the refrigerant blend used in the cycle, namely ammonia / water. There is an increased demand for refrigerants that are environmentally friendly, i.e. with a low global warning potential (GWP) and low ozone depletion potential (ODP). Ammonia is one of the most environmentally benign fluids, since both GWP and ODP values are negligible [61]. On the other hand, ammonia is toxic and flammable; however, as explained in Section 3.2.3, this can be handled by appropriate technology.

The challenges of the hybrid absorption heat pump are mainly in the compressor discharge temperature, which may determine different problems if high temperature are required.

Also, absorber and generator design are often challenging, since they must guarantee a good liquid – vapor mixing and separation, in order to achieve high heat transfer coefficient.

3.5. State of the art of high temperature heat pumps

As introduced before, in ref. [62] it is stated that at least 26 heat pumps with sink temperatures higher than 90 °C are currently available on the market. Different manufacturers are present and they will be now presented.

Viking heat Engine SA developed a heat pump named HeatBooster, which is able to produce heat at temperatures as high as 150 °C with a capacity of almost 200 kW, but further studies have been conducted to increase its capacity up to 1500 kW. This heat pump features three plate heat exchangers, namely evaporator, condenser and recuperator, which guarantees a certain degree of superheat at the compressor's inlet.

The compressor is a reciprocating piston type, which is fully controllable so to adjust the performance at a wide range of working conditions. The paramount refrigerant used is R1336mzz(Z), but it has also been successfully tested with R245fa.

The COP could reach a value of 7 at the lowest temperature lift (30 °C). [63]

The company Ochsner Energie Technik GmbH successfully built a heat pump that exploits residual heat in two different ranges (30 – 55 °C and 8 – 25 °C), upgrading it up to 130 °C.

They used a screw compressor and claim a capacity that could reach values of 1.5 MW by connecting several machines, with COP values ranging from 2.7 to 5.8

The tested refrigerant are R134a and R245fa [64]

The same refrigerants are used by other two benchmarked products, that are the Kobelco SGH 120 and SGH165: these two heat pumps are able to generate steam at temperatures of 120 and 165 °C, respectively, from process residual heat in the range 35 – 70 °C, by recompressing 120 °C steam to 165 °C. The compressor in this case is a twin screw type and COP values are around 2 to 3. These heat pumps are produced by Kobelco, which also propose the HEM-90A model, that delivers up to 90 °C hot water form ambient air, with capacities and COP respectively up to values of 230 kW and 3. [65]

Combitherm GmbH developed the series HWW, which includes two different models, depending on the selected working fluid, namely R245fa or R1234a. The first case, which represent their flagship model, exhibits a sink temperature as high as 120 °C with 252 kW heating capacity. The compressor is, again, a piston type [66]

Another example is the Unitop series by Friotherm AG. Their model Unitop 50 is able to reach very high capacity (up to 20 MW) using a two-stage turbo compressor, with a maximum sink temperature of 90 °C. Refrigerant, in this case, is R134a, but their small capacity model, Unitop 22, uses instead the more environmentally friendly R1234zeI.[67]

These are just some of the examples of the available models, but they represent the different possibilities that are currently available. Other companies that are pioneering developments in this field are Mayekawa, GEA refrigeration and Durr.

The alternatives that have been cited so far are vapor compression heat pumps and their difference is mainly in the compressor used and in the choice of the refrigerant.

Focusing on hybrid absorption compression systems, [56] evaluated 23 different experimental investigations, having a power output ranging from *1.4* to *4500 kW*. It was found that the most common cycle exploited is the single-stage one, accounting for 16 different publications from 1983.

The supply temperature reached by an absorption heat pump was demonstrated to be as high as 115 °C during a steam generation process, while temperature lift is in the range of 5.6 to 38.7 K. *COP* instead, was extremely variable, in a range between 2.1 to 11.3.

This technology is commercially available at industrial level and already in use in different plants. The only identified company that produces this kind of heat pumps

is Hybrid Energy AS [68] and their fleet includes three models (reported in Table 3-5) , which are characterized by different output power and sector of application. They claim that the COP could reach a value of 8, while the supply temperature ranges between 100 – 120 °C.

Table 3-5: HACHP fleet produced by Hybrid Energi AS [68]

Model	Capacity [MW]	T_{source}[°C]	T_{supply}[°C]	COP
GreenPAC – R	0.5 – 2	40 – 60	80 – 100	5 – 8
HyPAC – R	0.75 – 2	40 – 60	80 – 120	3.5 – 6
HyPAC – S	2 – 5	40 – 60	80 – 120	4 – 7

3.6. Heat pump integration in industrial processes

3.6.1. Heat pump working point through pinch analysis

Heat pumps exploits low temperature heat, upgrades it and releases it at higher temperature. Seen from a pinch analysis point of view, a heat pump is exploiting process excess heat to generate process hot utility. Rules have been defined for the correct placement of a heat pump with respect to the background process (i.e. the system composed by hot and cold streams together, as defined in section 2.3): this is crucial to provide real benefits to the system.

The implementation of a heat pump could be performed with three different strategies:

- Below the pinch point (see Figure 3-20 (a))
- Above the pinch point (see Figure 3-20 (b))
- Below to above the pinch point (Figure 3-21)

In Figure 3-20 the first two methods are represented:

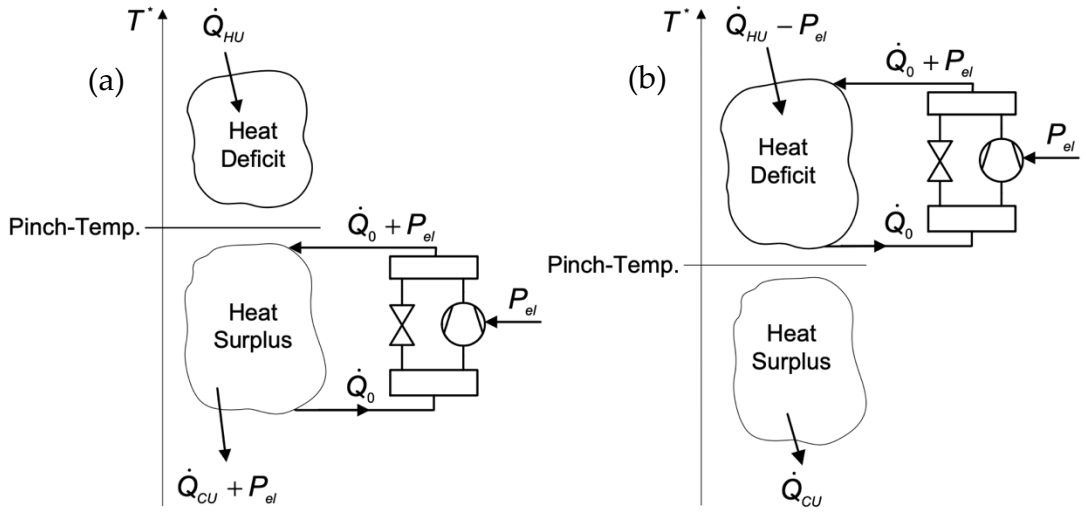

Figure 3-20: Heat pump positioning below the pinch point (a) and above the pinch point (b) [17]

As once can notice looking at the figure on the left, the heat pump exploits process heat ($\dot{Q}_0$) and electrical power (P_{el}) to generate additional hot utility ($\dot{Q}_0 + P_{el}$) below the pinch point. However, the process does not need hot utility below the pinch since this would be against the third rule of pinch analysis ("do not use hot utilities below the pinch").

The result is that the additional amount of heat introduced, equal to P_{el}, will be cascaded throughout the system and generate an additional requirement for cooling utility, that will be now equal to $\dot{Q}_{CU} + P_{el}$. The heat pump is recovering heat, consuming electrical energy to produce heat that will have to be cooled: it is easy to understand that this placement makes no sense.

The right image, instead, represents the case in which the heat pump is placed above the pinch point. In this case the device recovers process heat $\dot{Q}_0$ consuming P_{el}. The net effect is that of replacing a quantity of hot utility (equal to P_{el}) by electrical work (P_{el}), similarly to what happened in the "below the pinch point" case. Hence no benefits are achieved.

Therefore, the only correct placement of a heat pump is the one "from below to above the pinch point"(see Figure 3-21): in this way, in fact, part of the excess heat below the pinch is used as the heat source of the heat pump, which will eventually discharge high temperature heat above the pinch point, decreasing the amount of hot utility needed by the system: the beneficial effect is that both hot and cold utility duty decrease.

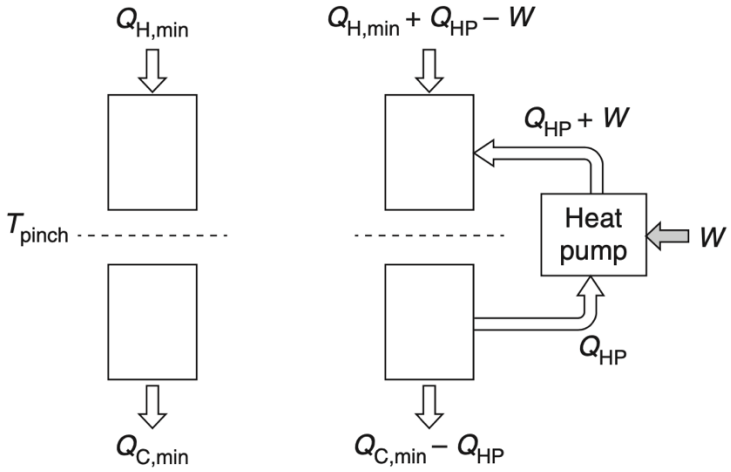

Figure 3-21: Correct placement of a heat pump [33]

3.6.2. Representation of heat pumps in the GCC

The operation of a conventional compression heat pump can be represented against the grand composite curve of the background process (Figure 3-22)

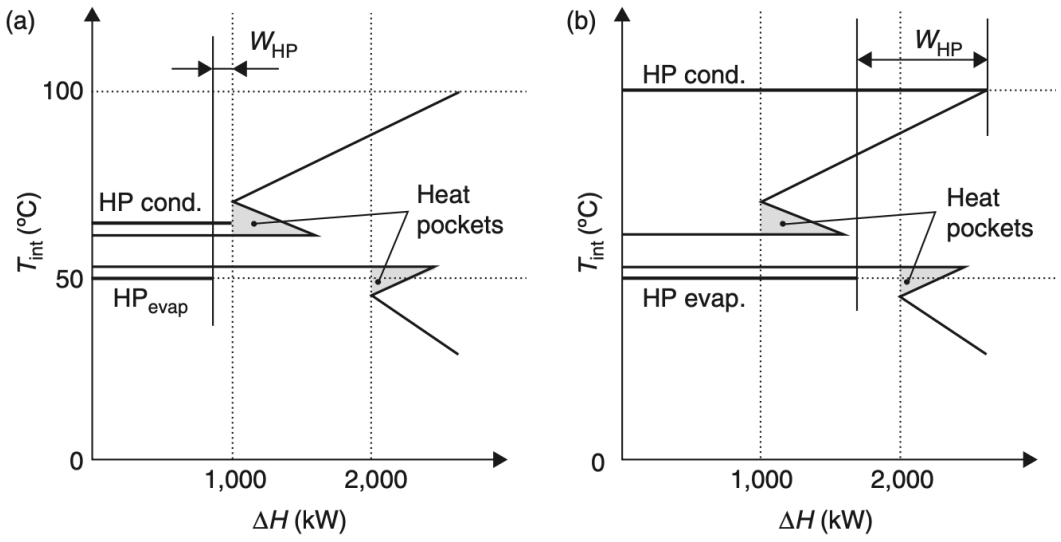

Figure 3-22: Heat pump representation in the GCC: max COP (a) and max heat delivery (b)[33]

The low temperature line represents the evaporator, which is driven by excess heat released from the background process, below the pinch point. The condenser, instead, is represented as the high temperature line, as it is discharging heat to the background process above the pinch point, decreasing the overall amount of hot utility needed. Both processes are represented at their shifted temperature

Figure 3-22 shows the two possible alternatives of implementing a heat pump: in case (a) the temperature lift with the background process is minimized, in order to achieve the maximum COP possible; the process, however, still has the necessity of external hot utility.

In case (b) the goal is to provide the whole amount of hot utility needed by the system, hence the COP of the device will be penalized due to higher temperature lift. However, the amount of heat that can be delivered is in most cases limited by the maximum output temperature that can be achieved by the heat pump.

Concerning the integration of a hybrid heat pump, evaporation and condensation are replaced by desorption and absorption processes that occur with a certain temperature glide. Therefore, they are represented in the GCC as sloping lines (Figure 3-23). Again, the low temperature line is representative of the desorber/generator, while the high temperature one represents the absorber.

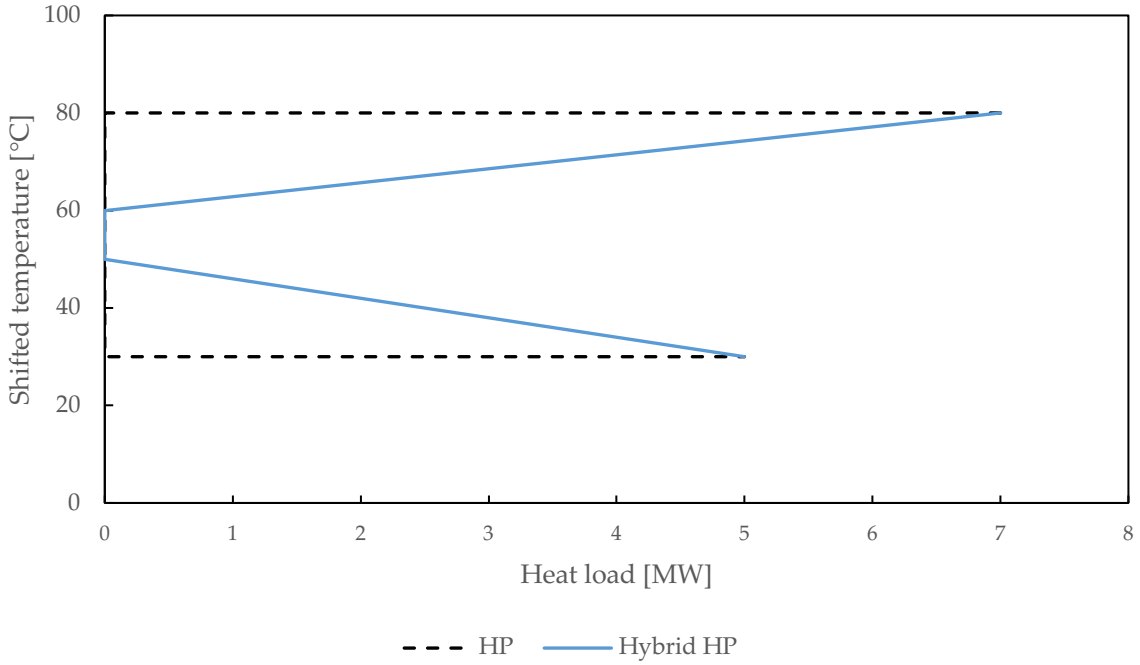

Figure 3-23: Comparison of hybrid and vapor compression heat pump, considering same heat duties

The high temperature of the absorber corresponds to the adiabatic mixing state of ammonia vapor and weak solution; this, in fact, is the temperature at which the solution begins the heat transfer process with the sink (state 3′ in Figure 3-16). The outlet temperature of the absorber, instead, corresponds to the one of the rich solution, which is generally found in the saturated liquid state.

Similarly, the inlet temperature of the generator corresponds to the one of the rich solution (after the throttling process), while the outlet temperature corresponds to the one of the liquid vapor mixture (state 1´ in Figure 3-14)

In this qualitative representation, is possible to denote how the temperature glide could be adapted to the background process, to minimize the temperature difference while providing the same temperature lift to the sink with a higher COP

3.6.3. Real life considerations: heat recovery loop

The GCC approach explained in section 3.6.1 provide a solution to the challenging task of heat pump integration in industrial processes.

However, the main drawback of this methodology is that the grand composite curve is represented as a single line, in which information about a multitude of heat sources and sinks are merged together.

In practice, matching a heat pump to such a system implies that the evaporator (generator) and condenser (absorber) are split in many streams, in order to perfectly match the background curve. This is unfeasible in real life design.

Two solutions are possible:

- Select a subset of streams to match the heat pump with, trying to respect the idea of transferring heat from below to above the pinch point. This is a straightforward approach, but limits the advantages of using the pinch analysis approach.

- Adoption of heat transfer loops (HTL) for heat recovery and heat supply, a solution often cited in literature ([69], [70], [71]), that transfer heat between the background process and the heat pump´s heat exchangers.

In this way, the heat transfer loops are subjected to stream splitting, integrating the heat as completely as possible into the process, minimizing the energy demand [69] and respecting real life constraints.

The downside of this methodology is that additional temperature driving forces (ΔT) are needed to transfer heat from the background process to the heat transfer loops and vice versa. Furthermore, there can be possible heat losses in the heat transfer loops and electricity is needed to drive the pumps necessary for fluid circulation in the loops.

The integration of the heat pump though external loops is shown in Figure 3-24, where the two ΔT contributions are highlighted

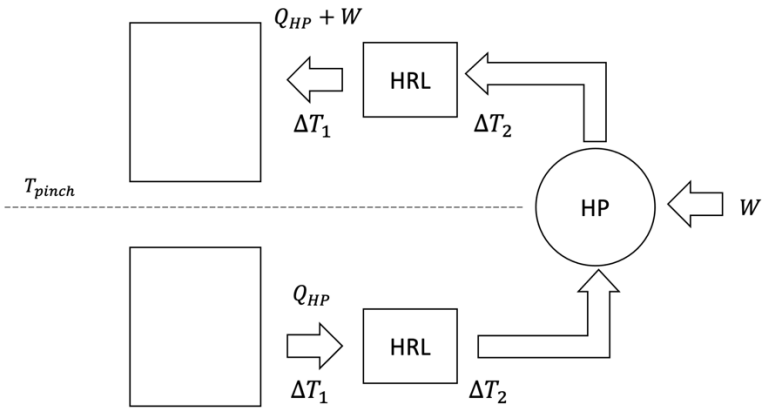

Figure 3-24: Heat pump integration in background process though heat recovery loops. Two different ΔT contributions are necessary for each loop

For the purpose of this thesis, the second approach was considered, in order to fully exploit the potential of pinch analysis. This aspect will be further discussed in paragraph 4.3

4 Method

The Renova WtE plant includes four separate systems for incineration of waste material, each one composed of a furnace, a boiler and a flue gas treatment unit.

Municipal waste is continuously combusted in the furnace, reaching a temperature of almost 1000 °C. The combustion heat is recovered to produce steam. The steam produced by the four furnace boilers is collected and supplied to a single back-pressure turbine, which drives a generator for electricity production. The heat released in the condenser at the turbine outlet supplies the district heating network. Additional heat is recovered from the flue gas treatment processes for each of the furnaces and it is supplied to the district heating system.

As presented in the Aim and scope section, this thesis focuses on flue gas treatment process *number 7*, due to data availability and synergies with previous work [20], understanding how CCS integration would affect the district heating supply and proposing different solutions for heat recovery implementation. Therefore, three different systems are considered in the investigation: boiler P7, CCS and district heating. The heat interaction of these systems is shown schematically in Figure 4-1.

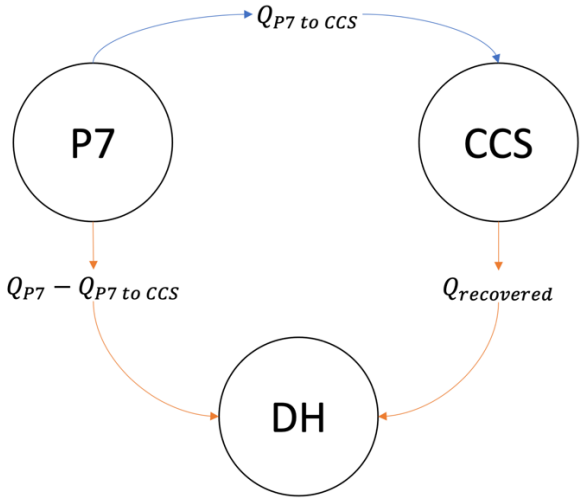

Figure 4-1: Heat interaction between process P7, CCS plant and district heating network (DH)

The heat supplied to district heating by process P7 , Q_{P7}, (including steam condensation and flue gas treatment process) is penalized by the fact that the reboiler of the capture plant is assumed to be supplied by low pressure steam bled from the turbine. This amount of heat is indicated as $Q_{P7\ to\ CCS}$ in Figure 4-1

At the same time, residual heat could be recovered from the CCS ($Q_{recovered}$ in Figure 4-1) and supplied to district heating, compensating for the loss derived by reboiler duty. Heat recovery is both in the form of direct heat recovery as well as heat pumping.

An overview of these systems will be presented in Section 4.1.

Given the complexity of the problem, pinch analysis, together with numerical modeling software, was exploited to find the best way possible of recovering heat, achieving the maximum energy savings (Sections 4.2 and 4.3)

A total of four different scenarios were analyzed, described in Section 4.3.1.2: these include direct heat recovery in combination with the hybrid absorption compression heat pump. The difference between each of the scenarios is in the working condition of the heat pump and thus in the recovered heat.

The hybrid absorption compression heat pump was then compared to a vapor compression heat pump: the comparison was carried out for the same amount of recovered heat. In this context, a preliminary thermodynamic analysis was necessary to select the working fluid of the vapor compression heat pump.

The heat pump implementation is discussed in Section 4.3 for both the hybrid and vapor compression topologies.

4.1. System specifications

4.1.1. Process P7: the reference case

Process P7 includes furnace and boiler P7, together with its own flue gas treatment process. Since the steam produced by this boiler is mixed with the steam produced by the other three boilers, thermal energy generation from the steam condensation unit and steam bleeds from the turbine were scaled proportionally to the steam supply from P7.

Table 4-1 reports data for boiler P7 which was used as a basis to estimate the fraction of total heat delivered to district heating water that can be allocated to P7.

Table 4-1: Boiler P7 data, [Renova]

Parameter	Value
Operating hours ($\frac{h}{year}$)	7920
Fuel mass flow rate ($\frac{ton}{h}$)	14
LHV ($\frac{MJ}{kg,moist}$)	10.5
Steam production ($\frac{ton}{h}$)	53
Flue gas thermal output*	0.28
Boiler efficiency (η_{BOIL})	0.85
Boiler thermal energy contribution ε_{BOIL}**	0.73

*The flue gas (FG) thermal output represents the amount of heat derived from the flue gas treatment process with respect to the total energy produced by the boiler

** ε_{BOIL} represents the faction of energy supplied to the water/steam flow in the boiler which contributes to the thermal load, hence not to the electricity generation.

The thermal energy generated by boiler P7 is calculated according to equation (4-1).

$$\dot{Q}_{P7,\text{thermal}} = \dot{m}_{\text{fuel},7} * LHV * \eta_{BOIL} * \varepsilon_{BOIL} = 25.34\ MW \quad (4\text{-}1)$$

This can be seen as the amount of steam derived from boiler P7 which condensates, providing thermal energy to the district heating network.

For the sake of comparison, if the same calculation is repeated for all of the boilers, the total thermal energy generated is equal to 132.11 MW, thus the contribution of boiler P7 can be estimated as:

$$\text{P7 thermal contribution} = \frac{Q_{P7,\text{thermal}}}{Q_{tot,\text{thermal}}} = 19.18\ \% \quad (4\text{-}2)$$

The flue gases from boiler P7 undergo and extensive clean-up process before being released to the atmosphere. Part of the heat release during these processes is exploited to preheat district heating water: this can be estimated using the flue gas thermal output:

$$\dot{Q}_{flue\ gas,P7} = m_{fuel,7} * LHV * \eta_{BOIL} * FG\ thermal\ output = 9.72\ MW \quad (4\text{-}3)$$

Part of the steam provided by the boilers is bled from the turbine and is used for internal processes. The thermal energy associated to this loss was provided by Renova estimations, appropriately scaled to P7

$$\dot{Q}_{bleed} = 2.4\ MW \tag{4-4}$$

Finally, the total heat delivered by the boiler P7 to the district heating system:

$$\dot{Q}_{P7\ to\ DH} = \dot{Q}_{P7,thermal} + \dot{Q}_{flue\ gas,P7} - \dot{Q}_{bleed} = 32.66\ MW \tag{4-5}$$

A simplified layout of process P7 is shown in Figure 4-2, together with the thermal energy generation and district heat supply. This system will be referred to as the reference case.

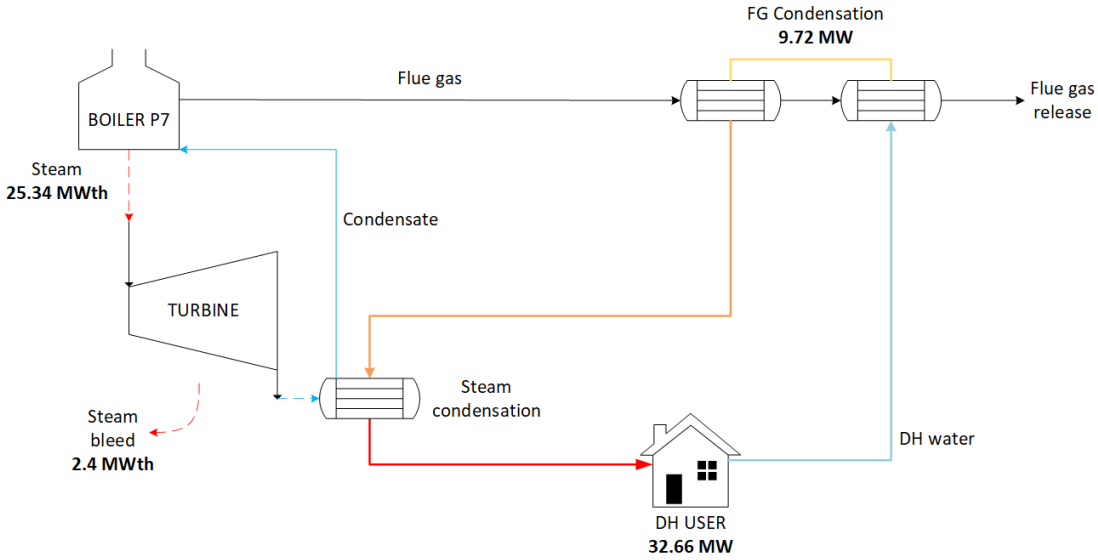

Figure 4-2: Simplified layout of boiler P7 process

NOTE: the turbine is common to all four plant boilers

4.1.2. Modeling of CO_2 capture and conditioning

The CO_2 capture and CO_2 conditioning processes were simulated in two separate steady-state Aspen PLUS V12 models. The processes were sized to match the amount of CO_2 that is present in the flue gas treatment of P7, with a CO_2 concentration equal to 10 % on a volumetric dry basis. The assumed location of the CO_2 capture plant is downstream of the flue gas condensation unit. Since P7 is only one of four boilers, the capture plant size is relatively small. Note, however, that the specific energy consumption (heating, cooling, power) per kg CO_2 captured would be the same if the CO_2 plant were to be scaled-up to capture CO_2 from all boilers

(assuming the gas specifications to be the same except for flow rate). Data regarding flue gas composition of boiler P7 are reported in Table 4-2 and were supplied by Renova and the work by J. Andersson [20]. The data were used to specify the industrial flue gas stream in the Aspen PLUS capture model.

Table 4-2: Flue gas data of the boiler and flue gas treatment systemP7 [Renova] [11].

Parameter	Unit	Value
CO_2 content	vol%(dry) / %m (wet)	10/13.95
O_2 content		9/9.13
N_2 conent		81/71.92
H_2O		0/5
Flowrate	Nm3/h (dry)	65000
Temperature	°C	35
Pressure	bara	1.01

A simplified representation of both processes is shown in Figure 4-3, where the CO_2 capture section is shown in black and the CO_2 conditioning section in orange. The capture model was developed in previous work using the simulation software Aspen PLUS V12 to rigorously model mass and heat transfer of CO_2 absorption into a 30 wt.% aqueous MEA solvent brought into contact with the CO_2-rich gas in columns with structured packing. Detailed kinetics and electrolyte chemistry are resolved as well. A detailed description can be found in [72].

The CO_2 conditioning model used, also constructed in Aspen PLUS V12, was based on the work of Deng et al. [31]

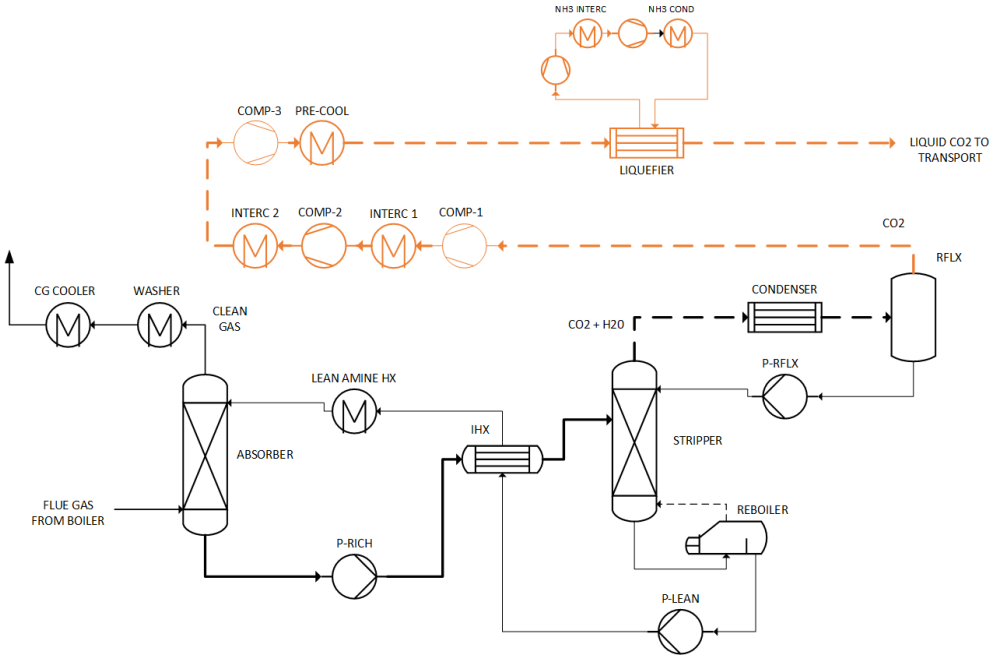

Figure 4-3: Aspen PLUS V12 model for capture (black) and conditioning (orange) section, simplified representation.

The capture section (represented in black in Figure 4-3) is modeled in the so-called standard configuration three structured packing columns [73]: an absorber, a washer and a stripper. Their diameter is calculated based on the flooding approach (gas load factor) [74] set to 80%. Important design data on these columns and other key units can be found in Table 4-3 and are based on common design assumptions for such processes, see [75] [76]. In the context of this work, it is important to highlight that the lean solvent temperature (absorber inlet), the washer cooler outlet, and the solvent makeup was set to 40 °C; the common range is 30-50°C. Note that the temperature of the CO_2-depleted gas exiting the capture section as effluent stream was set to 35 °C initially. This is the same temperature as the flue gas entering the CO_2 capture unit, thus, the same temperature that equipment downstream flue gas conditioning unit experiences in the reference case without CCS. Furthermore, the flowsheet model of the CO2 capture process was optimized towards lowest specific reboiler duty (MJ/kg CO2 captured). This procedure is often done, also experimentally [77] (u-curves), and is achieved by: 1.) choosing a lean CO_2 loading value (mol CO2/mol MEA) which is correlated to the reboiler temperature 2.) varying the solvent flow rate to reach a capture rate of 90% 3.) repeating the first two steps until a minimum specific reboiler duty is found for given lean loading. The identified lean loading of 0.21 gave a specific reboiler duty of 3.86 MJ/kg CO_2.

The liquefaction section model (represented in orange in Figure 4-3) consists of a three compression stages, with a knockout drum (not represented in Figure 4-3) and

intercoolers in between each compression step, in order to reach a pressure of 28 bara. The compressors' isentropic efficiency was set to 0.85. Before entering the liquefier, the CO_2 stream is precooled to 25 °C [31]. The liquefier itself is powered by an ammonia refrigeration cycle. The two-stage vapor compression cycle, characterized by the presence of one intercooler (in between the compressors) that operates between 9.4 and 1.4 bara (resulting in a COP of ~3.4), set by the liquefaction temperature, the cooling water temperature, and assumed temperature approaches in the ammonia evaporator (5 K) and condenser (5 K). The liquefied CO_2 is then flashed (this was found to be cost-optimal according to Deng el al. [31]) to reach the targeted pressure of 15 barg and temperature of -25 °C, which are the conditions for CO_2 ship transport specified by the Norwegian CCS demonstration project "Northern Lights" [30]. Key design parameters and assumptions for the CO_2 conditioning model are listed in Table 4-3

Table 4-3: Key assumptions and design parameters for the simulation of the CO2 capture and conditioning processes, adapted from [73] [72] [75] [76] [77]

Parameter	Unit	Value
CO_2 capture section		
Column diameter: flood approach	%	80
Column internals: structured packing	Koch FlexiPac 2X	
Lean solvent concentration (MEA in water)	wt.%	30
Lean loading	Mol CO_2/mol MEA	0.21
CO_2 capture rate	%	90
Absorber gas outlet pressure	bara	1.01
Absorber gas inlet tempeature	°C	40
Absorber lean solvent. inlet temperature	°C	40
Absorber packing height	m	20
Stripper outlet pressure [reboiler temperature ~120 °C]	bara	1.9
Stripper packing height	m	10
Stripper overhead condenser temperature	°C	20
Washer packing height	m	2
Lean -rich cross heat exchanger temperature approach	°C	10

CO2 conditioning section		
CO_2 delivery pressure	barg	15
Compressor stages	-	3
Intercooling temperature	°C	25
Refrigeration cycle fluid	Ammonia	
Refrigeration cycle compression stages	2	
NH_3 condensing temperature	°C	23
NH_3 condenser subcooling	°C	3
NH_3 evaporation temperature	°C	-26
NH_3 evaporator superheating	°C	5
General		
Isentropic efficiency (compressors/fans/pumps)	%	85
Mechanical efficiency	%	95

4.1.2.1. Simulation output

The main purpose of the CCS modeling was to obtain consistent data regarding the reboiler duty and the cooling duty of the different hot streams of the capture and conditioning sections. This data was then used to conduct the pinch analysis and evaluation of residual heat recovery possibilities, which are described in Section 4.2

The simulation results revealed that the energy needed to drive the capture plant reboiler, Q_{REB}, is equal to 12.3 MW

$$Q_{REB} = 12.3\ MW$$

This amount of heat is required at a constant temperature of 120 °C, and is likely to be supplied by steam bleeds from the turbine.

The hot streams in the capture process section are characterized in term of initial temperature (T_{start}), target temperature(T_{target}), thermal capacity (CP) and heat duty ($\dot{Q}$), see Table 4-4.

Table 4-4: Hot streams of CO_2 capture section

Name	T_{start}[℃]	T_{target}[℃]	$CP(\frac{kW}{K})$	$\dot{Q}(kW)$
Lean amine cooler	54	40	200.6	2808.4
CO_2 condenser-1	101.4	89.2	155.7	1900
CO_2 condenser-2	89.2	61.1	55.4	1556.7
CO_2 condenser-3	61.1	20	17.9	735.7
Clean gas cooling	61.1	35	262.5	6851.3

As can be noticed in Table 4-4, the *CO_2 condenser* is divided in three sections. This is due to the necessity to linearize the curved heat-temperature profile, which results from the simultaneous condensation of water and cooling of CO_2 (Figure 4-4).

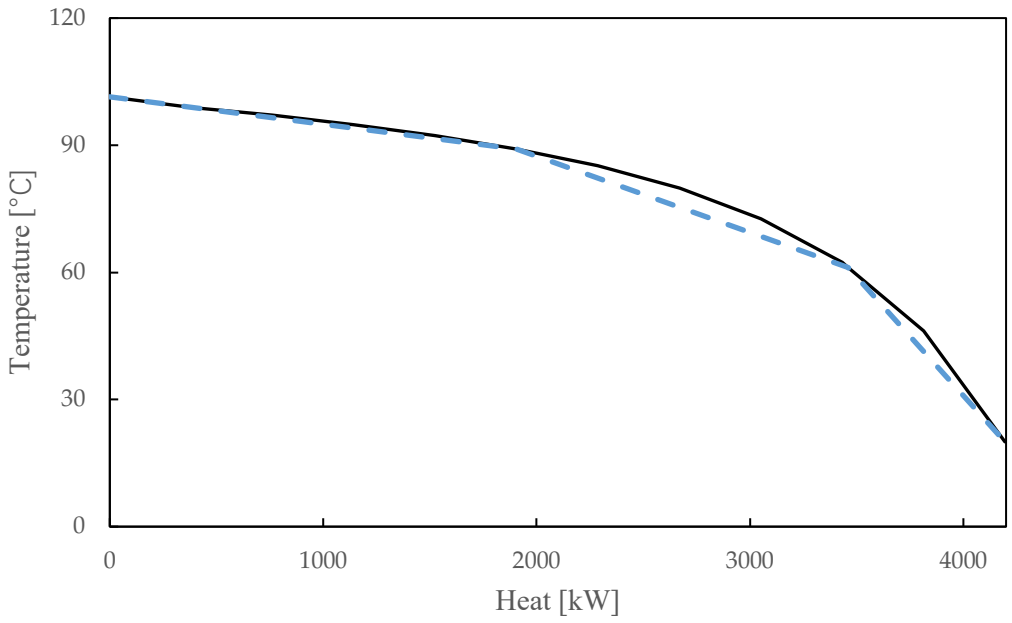

Figure 4-4: Heat–temperature profile of CO_2 condenser: the curved profile is caused by simultaneous condensation of water and CO_2 cooling. A blue dashed line represents the linearized profile

Since the water flow required to wash out the MEA from the clean gas was found to be really small, the heat in the related washer cooler was found to be negligible. This, however, results in a high energy content of the gas leaving the washer. This is an effluent stream, which is normally released in the atmosphere, but heat recovery from this stream could be beneficial to the system, therefore it was included the analysis.

Being an effluent stream, the target temperature of this stream can be selected freely so as to maximize the potential for heat recovery. However, in this case the temperature should not be lower than 35 °C, to ensure adequate flue gas buoyancy in the stack. The initial target temperature was set to 35 °C, to match the flue gas temperature after the flue gas condensation in the reference case, i.e. without CCS. In this way, it is assumed that the CCS process is placed after the flue gas condensation and produces a CO_2 depleted flue gas at the same temperature.

Data regarding the conditioning section are reported in Table 4-5

Table 4-5: Hot streams of conditioning section

Name	T_{start}[°C]	T_{target}[°C]	$CP(\frac{kW}{K})$	$\dot{Q}(kW)$
Intercooler	104	25	3.2	256
Intercooler 2	114	25	3.2	284.8
Precooler	69	25	3.7	162.8
NH_3 intercooler	69	25	2	88
NH_3 condenser-1	95	23	2.14	154
NH_3 condenser-2	23	20	384.6	1154

Note that the ammonia condenser hot stream was linearized to account for its phase change, dividing the heat-temperature profile in two sections.

What is immediately noticeable from Table 4-5 is that the thermal capacity and thus the heat content of the conditioning section is low compared to that of the capture section.

The only relevant stream in the conditioning section is the *NH_3 condenser-2* stream defined by the latent heat released by the ammonia phase change process. However, the temperature of this stream is too low for direct heat recovery or heat pumping.

The contribution of the conditioning section, excluding *NH_3 condenser-2*, compared to the one of the capture section can be defined as the ratio of total heat available from capture to total heat available from conditioning section, as defined in equation (4-6)

$$Conditioning\ share = \frac{Q_{conditioning}}{Q_{conditioning} + Q_{capture}} = 6.4\ \% \qquad (4\text{-}6)$$

For this reason, the conditioning section would barely contribute to heat recovery potential. Moreover, its influence on the composite curve is negligible: this is shown

in Figure 4-5 comparing the composite curve of the capture section to that of the conditioning section.

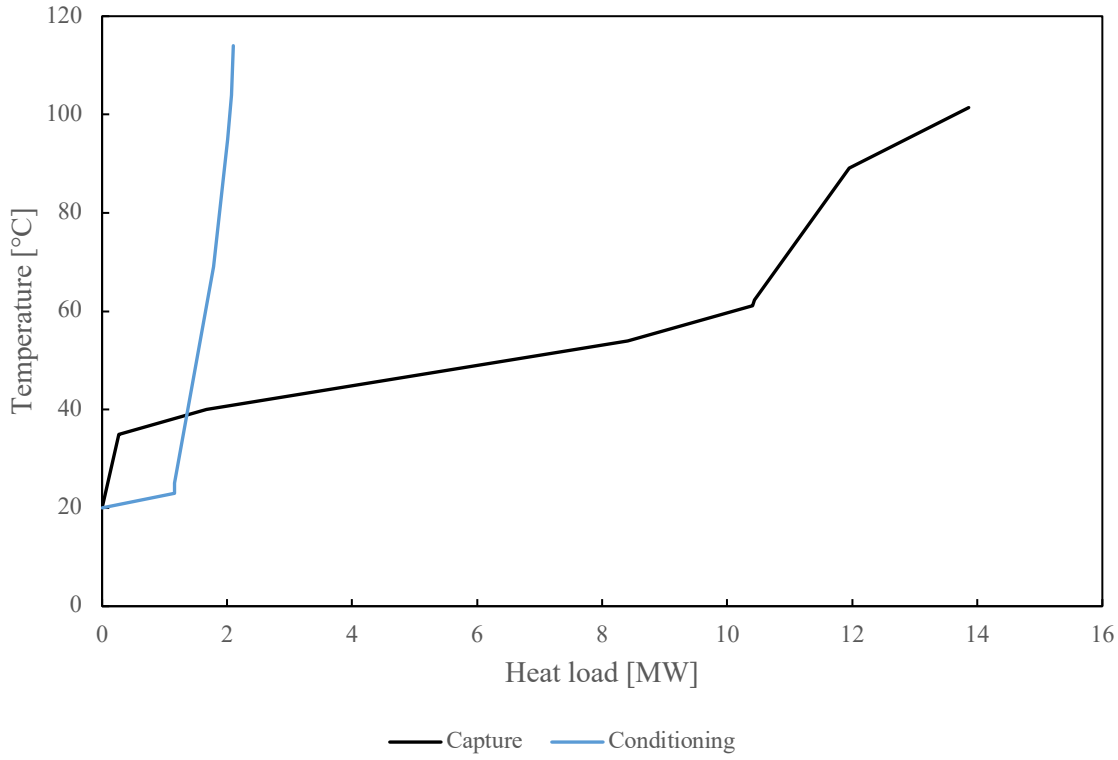

Figure 4-5: Hot composite curve for capture (black) and conditioning (blue) section

The conclusion is that it is not justified to include the conditioning section in the analysis, since it would simply add an extra degree of difficulty without any substantial benefits.

4.1.3. CCS integration in process P7

The integration of the carbon capture plant in process P7 implies that the flue gases, after the pollutant removal and heat exchange with district heating, are fed to the absorber of the capture section.

The loss of district heat delivery associated to the carbon capture integration is assumed to be equal to the heat needed to drive the reboiler Q_{REB}. This heat is assumed to be supplied by low pressure steam bled from the turbine, which only contributes to generate thermal energy.

Therefore, the district heat delivery after CCS integration ($Q_{DH@CCS}$) can be estimated starting from the heat originally delivered by boiler P7 to district heating, subtracting Q_{REB}, as shown in equation (4-7):

$$Q_{DH@CCS} = Q_{P7\ to\ DH} - Q_{REB} = 32.66 - 12.3 = 20.36\ \text{MW} \quad (4\text{-}7)$$

The aim of this thesis is to investigate whether this loss can be compensated (fully or partially) by heat recovery from the hot streams of the capture section.

The heat recovery network is considered to be separated from the reference case network described previously.

The simplified representation of the plant shown in Figure 4-2 is updated in Figure 4-6 to include the CCS plant, with a focus on heat recovery integration.

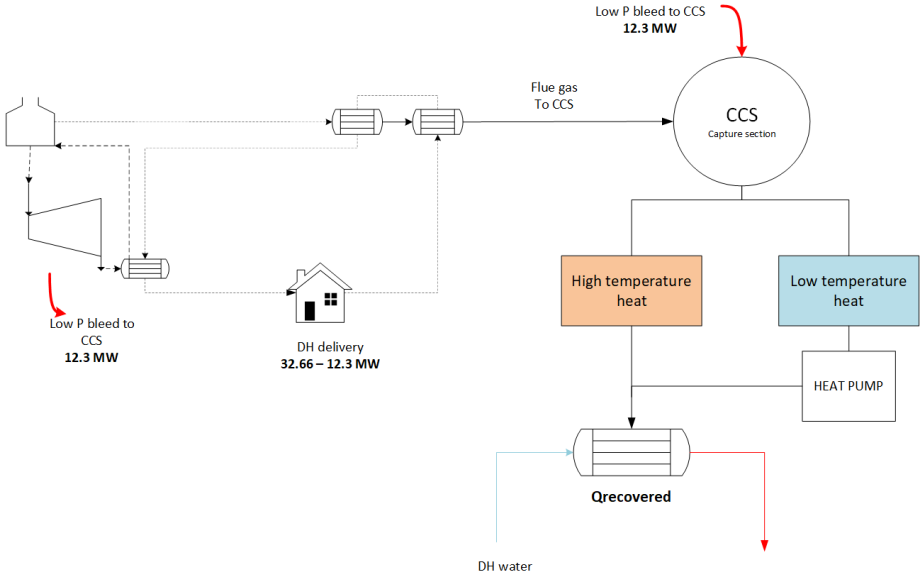

Figure 4-6: Integration of CCS plant in the original plant; distinction between high and low temperature heat derived from CCS capture section

Direct heat recovery, i.e. exploiting internal heat exchanger between CCS streams and district heating water, provides a straightforward solution to recover a significant amount of residual heat ("high temperature heat" in Figure 4-6). Direct heat recovery is limited by temperature constraints since the hot streams must be warmer than district heating water to allow for heat transfer. As a result, part of the residual heat available from the CCS plant is characterized by temperatures which are too low to perform direct recovery ("low temperature heat" in Figure 4-6). In this context, a heat pump would be able to raise the temperature of the "low temperature heat", turning it into "high temperature heat", eventually providing additional capacity that can be recovered by the district heating network.

4.1.3.1. District heating temperature

Data for district heating return and supply temperatures at Renova WtE plant were supplied by Renova for period January 2021 through 13th December 2021, see Figure 4-7.

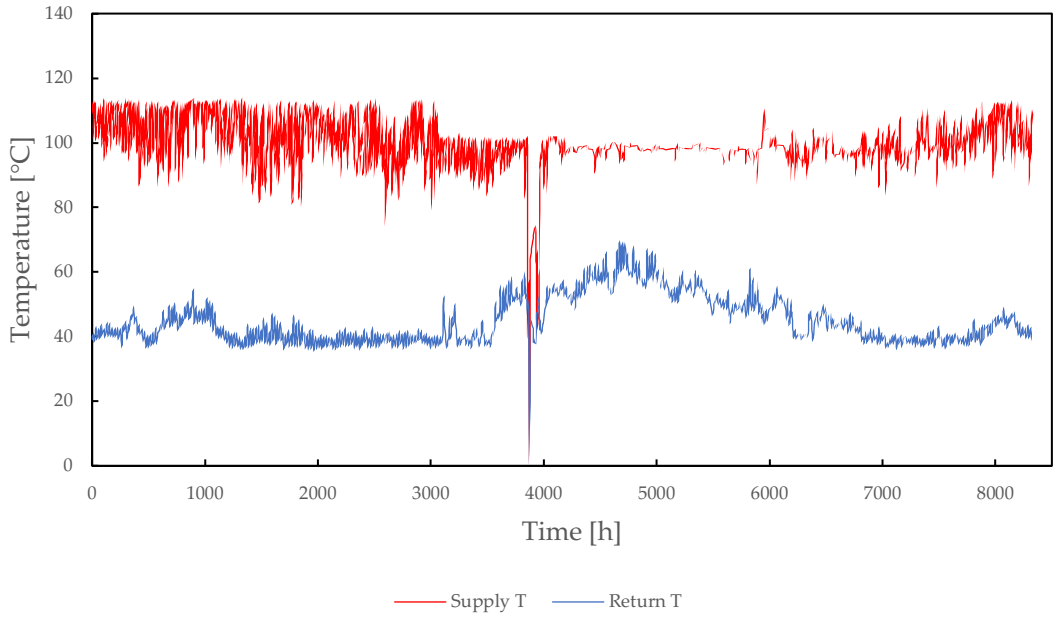

Figure 4-7: Supply and return temperature of district heating network at Renova WtE plant

Since the analysis is carried out considering steady state conditions, average temperature values for the winter/spring season were considered (i.e. February, March and April), in which the boilers operate at nominal load. The resulting average temperatures are shown in Table 4-6.

Table 4-6: Average supply and return temperature of district heating water at Renova WtE plant (February – April 2021)

T_{supply}[°C]	T_{return}[°C]
103	41

4.2. Heat recovery targeting using pinch analysis

Due to the complexity of the systems, pinch analysis was used to evaluate residual heat recovery opportunities.

The hot streams of the capture section were defined based on the simulations conducted in Aspen and they are listed in Table 4-4.

The hot composite curve is the black one shown in Figure 4-5

A single stream was introduced corresponding to the district heating water that must be heated from the return temperature to the supply one, defined in Table 4-6. The capacity of this stream is equal to the heat recovered from the capture section, resulting from a combination of direct heat recovery and heat pumping.

For the sake of simplicity, this will be referred to as total district heat recovery, defined in equation (4-8)

$$Q_{DH,rec} = Q_{direct} + Q_{heat\ pump} \tag{4-8}$$

$Q_{DH,rec}$ represents the variable of the problem since both Q_{direct} and $Q_{heat\ pump}$ are not known a priori. Therefore, both the cold composite curve and the grand composite curve (GCC) are variables.

Having to deal with heat recovery and heat pump integration, the grand composite curve represents the main support tool and thus the influence of $Q_{DH,rec}$ on the GCC is discussed in Section 4.2.1.

Recalling the basic theory of pinch analysis, the "background process" (BG process) of this case study is defined as the system composed by hot streams of the capture section, together with total district heat recovery.

A minimum ΔT_{min} of 5 °C between hot and cold streams was selected which is a reasonable value for gas-liquid heat exchanging, as this is the case for most of the heat exchangers in the study.

4.2.1. Influence of total district heat recovery on the GCC

As introduced in Section 2.3.3, the GCC is a graphical representation of the heat cascade of an energy process. Above the pinch point, the heat deficit is shown, together with hot utility needs, while below the pinch point heat excess and cold utility are represented.

Introducing a cold stream with a variable capacity, as done in this method with $Q_{DH,rec}$, causes the shape of the GCC to be variable and, as consequence, hot and cold utility, as well as the pinch point, are variable.

A higher capacity of the cold stream (i.e. a higher value of $Q_{DH,rec}$, case (b) in Figure 4-8) can be interpreted as an increase in the mass flow rate of the district heating

water, since supply and return temperature of this stream are fixed, as defined in section 4.1.3.1. The system is "requesting" more heat and is thus characterized by a higher heat deficit (i.e. higher hot utility demand above the pinch); at the same time, a decrease of the heat surplus is determined, leaving a lower amount of excess heat available below the pinch point.

On the contrary, a lower capacity of cold stream (i.e. a lower value of $Q_{DH,rec}$ and thus lower mass flow rate, case (a) in Figure 4-8) corresponds to lower heat deficit above the pinch point (lower hot utility needs), while it increases the heat availability below the pinch (higher cold utility requirement).

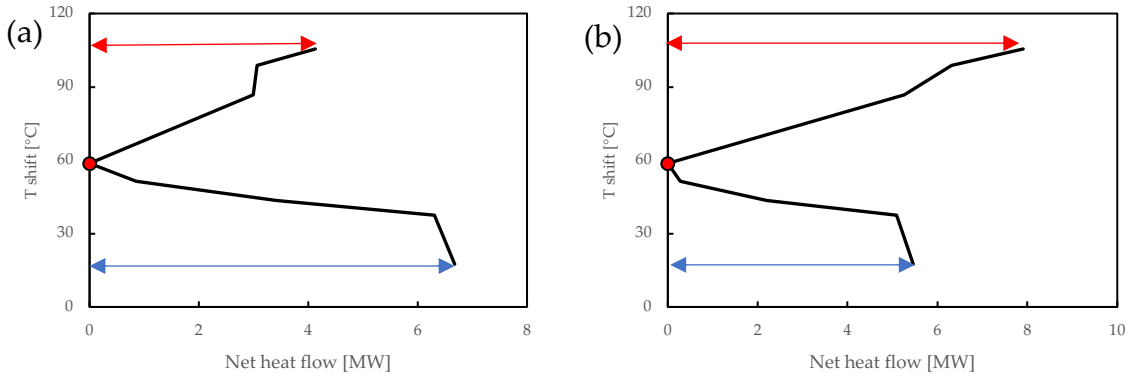

Figure 4-8: Influence of $Q_{DH,rec}$ in GCC shape: case (a) is for a low value of $Q_{DH,rec}$, while case (b) is for higher values of $Q_{DH,rec}$. The red line is a qualitative indication of hot utility needs, while the blue line represents the cold utility. The red marker highlights the pinch point

The pinch point of the stream system occurs at a shifted temperature of 58.6 °C, which corresponds to hot and cold streams temperature of:

$$T_{pinch,hot\ streams} = T_{pinch,shift} + \frac{\Delta T_{min}}{2} = 61.1\ °C \quad (4\text{-}9)$$

$$T_{pinch,cold\ streams} = T_{pinch,shift} - \frac{\Delta T_{min}}{2} = 56.1\ °C \quad (4\text{-}10)$$

The pinch temperature corresponds to the starting temperature of *clean gas cooling* stream and *CO_2 condenser-3* (see hot streams of capture section in Table 4-4). Due to the high capacity of clean gas cooling stream the pinch point temperature is barely influence by total district heat recovery, unless very high (or low) values are considered.

4.3. Process modeling: heat pump integration

Considering the relevant case study, the BG process is composed of:

- Three hot streams and one cold stream below the pinch point
- Two hot streams and one cold stream above the pinch point

Matching a heat pump to such a system implies that the evaporator (or generator) and condenser (absorber) are split in many streams, to perfectly match the background curve. As explained in 3.6.3 this is unfeasible in real life design and a heat recovery loop (HRL) must be considered.

The ΔT_{min} values for both heat exchange operations involving the heat transfer loop (BG process–HRL and HRL–heat pump) are assumed to be equal to 5°C; as suggested by the work of H.C. Becker [78]. These values are a good compromise between energy and investment cost. Heat losses in the heat recovery loop were neglected.

A hybrid absorption compression heat pump was selected as the most suitable technology to recover residual heat below the pinch point.

The heat pump was configured so that the amount of heat delivered by the absorber, Q_{ABS}, is equal to that of the hot utility requested by the background process, Q_{HU}, in order to completely satisfy the heat deficit of the system.

Q_{ABS} is strictly linked to the amount of heat recovered by the heat pump's generator, Q_{GEN}.

Q_{GEN} can be chosen arbitrarily and it corresponds to the amount of heat surplus below the pinch point (termed waste heat, Q_{WH}) recovered by the heat pump.

Heat input and heat output of the heat pump can be expressed according to equations (4-11) and (4-12).

$$Q_{ABS} = Q_{HU} \text{ determined by the GCC} \tag{4-11}$$

$$Q_{GEN} = Q_{WH}, \text{ arbitrarily chosen} \tag{4-12}$$

As will be discussed in 4.3.1.1, Q_{GEN} was in practice chosen according to the temperature level of the background process.

Recalling equation (4-8)

$$Q_{DH,rec} = Q_{direct} + Q_{heat\ pump} \tag{4-8}$$

The more heat is recovered below the pinch point by the heat pump (higher $Q_{GEN} = Q_{WH}$) the more can be delivered by the absorber (higher $Q_{ABS} = Q_{HU}$), and thus the higher will be the capacity of the recovered district heat stream (higher $Q_{DH,rec}$)

The system is therefore characterized by two variables: $Q_{DH,rec}$ and Q_{GEN}, linked by equation (4-8) and by the performance of the heat pump. In practice, these were found through an iterative procedure as will be described in Sections 4.3.1 and 4.3.2

Four scenarios are discussed, each corresponding to a different amount of Q_{GEN} and thus of $Q_{DH,rec}$

Furthermore, heat recovery using a vapor compression heat pump was also investigated and compared with the hybrid device: the comparison was carried out for the same amount of total district heat recovery $Q_{DH,rec}$. Due to the different working principle of the vapor compression device, a different iterative procedure was implemented (see 4.3.1 and 4.3.2)

4.3.1. HACHP model in STACY

The mathematical modeling of absorption cycles, such as absorption chillers or heat pumps, is complex. A model for simulation of steady-state operation of hybrid absorption compression heat pump cycles was developed in previous work in STACY [79], an innovative modeling tool developed by a group of researchers of Politecnico di Milano. Further information is available in Aprile et al [79].

Figure 4-9 shows the STACY model of the HACHP that was used in this project.

Detailed information regarding the modeling of the different components in STACY are reported in Appendix A.

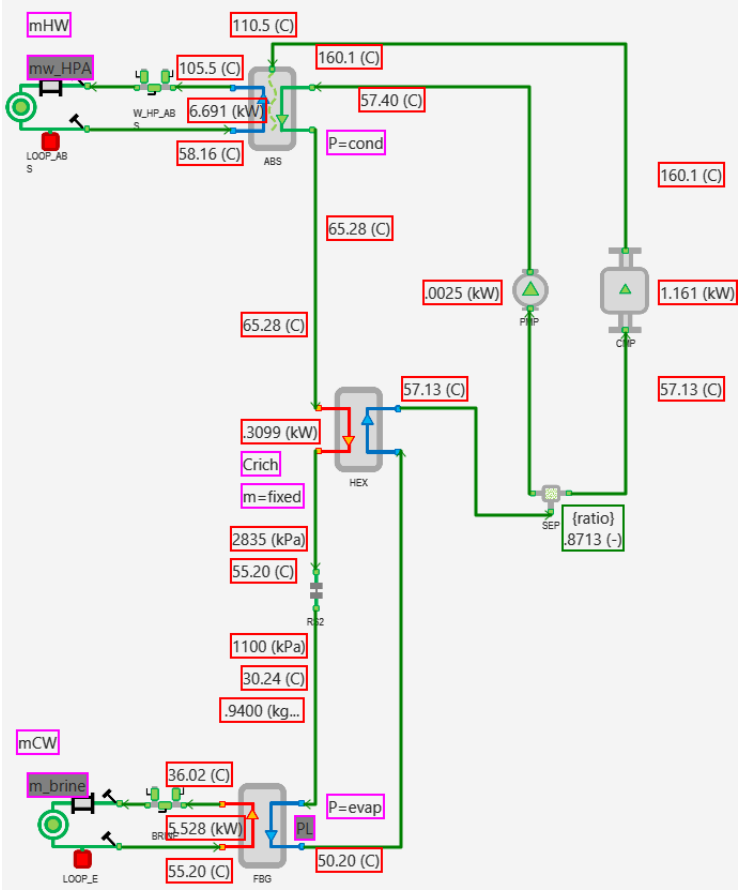

Figure 4-9: STACY model of the hybrid absorption compression heat pump

Both the generator (FBG in the bottom of Figure 4-9) and the absorber (ABS at the top of Figure 4-9) were modelled as counter current liquid/solution heat exchangers. The model considers a minimum temperature difference of 5 °C (valid for both heat exchangers) and a pressure drop of 20 kPa in the absorber; pressure drop in the generator is neglected.

The external heat transfer loops associated with both components (LOOP_E for the generator and LOOP_ABS for the absorber, see Figure 4-9) represent the two heat recovery loops used to match the heat pump to the background process, as discussed in Section 3.6.3.

The isentropic efficiency of compressors and pumps were set to 0.7, while the efficiency of the electric motors driving both the components have been set at 0.9.

To constrain the model and successfully execute the simulation, it is necessary to define four parameters:

- Temperature change (ΔT_{GEN}) of the generator´s external loop (LOOP_E), i.e. the difference between inlet and outlet temperature of this loop.

- Temperature change (ΔT_{ABS}) of absorber´s external loop (LOOP_ABS)
- Mass flow rate of the refrigerant (m_{ref})
- Rich solution concentration (C_{rich})

Absorber and generator´s pressure, instead, are constrained through two additional conditions:

- Absorber's outlet pressure is set to the bubble point pressure at the temperature $T_{\mathrm{ABS,out}} + \Delta T$, where ΔT was set 1 K and $T_{\mathrm{ABS,out}}$ is the temperature of the solution at the outlet of the absorber
- Generator outlet port pressure set to that of the bubble pressure at the temperature $T_{\mathrm{GEN,out}} - \Delta T$, where ΔT was set to 6 K and$T_{\mathrm{GEN,out}}$ is the temperature of the solution at the outlet of the generator

4.3.1.1. HACHP matching to BG process

The matching procedure is divided in four steps, so that it is more intuitive to understand:

- STEP 1 defines the background process and the grand composite curve
- STEP 2 defines the external loops temperature inlet and temperature change of the external loop itself
- STEP 3 provides an explanation of how mass flow rate of the refrigerant and the rich solution concentration were determined
- STEP 4 illustrates the iterative procedure

STEP 1: GCC definition

A value for $Q_{DH,rec}$ is selected.

The background process, composed of hot streams of the capture section and the district heating stream, is thus completely defined and the GCC can be derived, as well as the minimum hot and cold utilities (Q_{HU} and Q_{CU}).

Figure 4-10 provides an example of grand composite curve for a given value of $Q_{DH,rec}$.

STEP 2: external loops definition

The inlet and outlet temperature of two external heat transfer loops are defined after linearization of the heat–temperature profile in the GCC, if required.

Below the pinch point, a shifted temperature value is selected, indicated by T_{WH}, in order to specify a cut-off temperature for the heat pump based on the shape of the GCC (this aspect will be clarified at the end of the iterative procedure description).

From the GCC is possible to read the heat load corresponding to this temperature, defined as Q_{WH}. A point with coordinate (Q_{WH}; T_{WH}) can be defined on the GCC of the background process; Figure 4-10 shows an example of this point for a given value of T_{WH} and $Q_{DH,rec}$.

Above the pinch point, the heat pump must provide the overall amount of hot utility (Q_{HU}), as descripted in Section 4.3 The shifted temperature related to Q_{HU} is T_{HU}, corresponding to the highest temperature at which the heat pump must deliver heat. The point with coordinates (Q_{HU}; T_{HU}) is highlighted on the GCC of the background process in Figure 4-10.

Two heat–temperature profile are identified, one below (highlighted in red in Figure 4-10) and one above the pinch point (highlighted in blue in Figure 4-10)

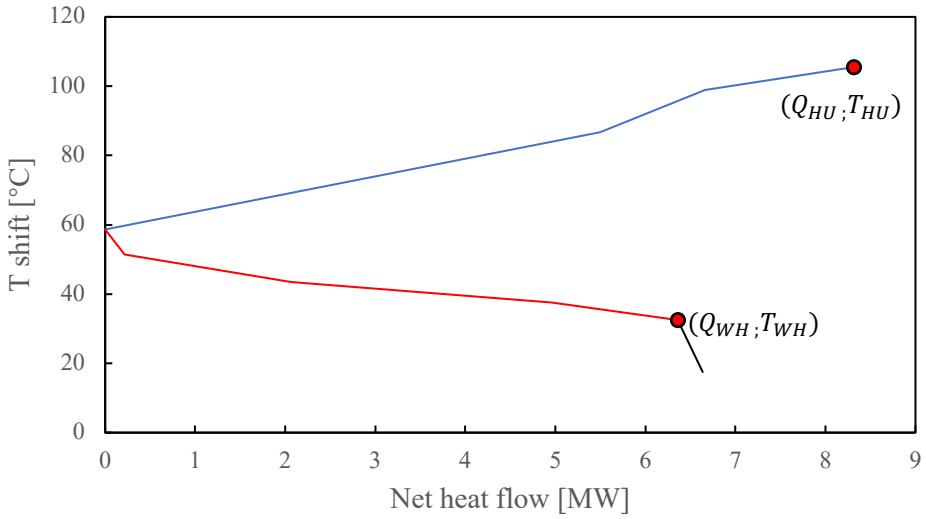

Figure 4-10: Waste heat and hot utility points above and below the pinch point. Distinction between heat–temperature profile above and below the pinch point (highlighted by a blue and a red line respectively)

The two heat–temperature profiles are separately linearized using the REGR LIN function implemented in Excel. A black dashed line shows the linearized profile in Figure 4-11.

These lines, however, are likely to cross the GCC of the background process, which implies an infeasible heat transfer between background process and heat recovery loop. Thus, the lines must be shifted until a compatible heat transfer with the background process is granted: a utility pinch point is found, highlighted by a yellow marker in Figure 4-11.

In this way, the linear profile which best fit the background process and allows for feasible heat transfer is found (dashed red and blue lines in)

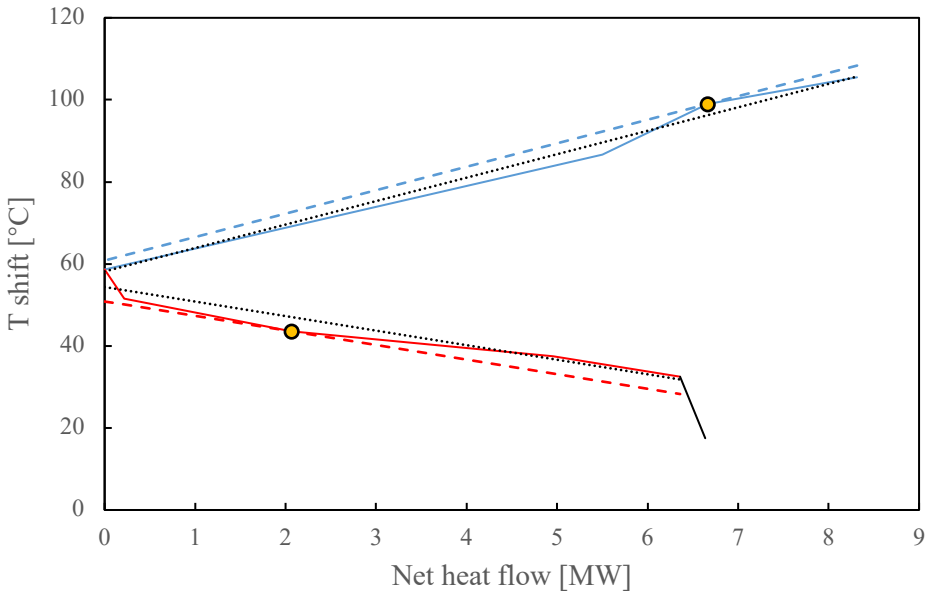

Figure 4-11: Heat -temperature profile linearization: the black dashed line are the results of the REGR_LIN function, which however crosses the GCC. The shifted line (blue above the pinch point and red below it) are representative of the external loops which best fit the BG process, allowing for feasible heat transfer

Inlet and outlet shifted temperature of the low heat recovery loop can then derived.

The HRL loop below the pinch point is a cold stream for the background process, thus the temperatures are shifted by $-\frac{\Delta T_{min}}{2}$ to find the real temperatures

The HRL above the pinch point, instead, is a hot stream for the background process, hence the temperatures are shifted by $+\frac{\Delta T_{min}}{2}$ to find the real temperatures.

Inlet and outlet temperature of external loops are input in STACY; the procedure now moves to the real modeling.

STEP 3: refrigerant mass flow rate and rich solution definition

The mass flow rate of the refrigerant is chosen so that the heat duty of the generator, calculated by STACY simulation (Q_{FBG}), matches the considered excess heat below the pinch point (Q_{WH}).

The rich solution concentration C_{rich} is varied between 0.65 and 0.95 $\frac{kg_{ammonia}}{kg_{rich\ solution}}$ performing a parametric analysis aiming at maximizing the COP.

The selection of $m_{ref}$and C_{rich}totally constrain the STACY model: the simulation with these boundary conditions determines the heat duty of the absorber.

STEP 4: iterative procedure

Two alternatives are possible, depending on the entity of the hot utility requested by the background process and heat delivered by the absorber

- $Q_{ABS} > Q_{HU}$: the heat pump is discharging more heat than is needed by the background process. This means that the total amount of district heat recovery, $Q_{DH,rec}$,could be increased.
- $Q_{ABS} < Q_{HU}$: the heat pump is not able to provide the overall amount of hot utility needed: the background process needs an external hot utility other than the heat pump, which is pointless. The amount of total district heat recovery, $Q_{DH,rec}$, must be decreased.

The procedure is iterative with $Q_{DH,rec}$, which is varied until the conditions $Q_{ABS} = Q_{HU}$ and $Q_{FBG} = Q_{WH}$ are satisfied.

Since the matching procedure is performed manually, the best methodology is to choose a shifted temperature value below the pinch point, T_{WH}, and keep it constant throughout the iterations: in this way, the streams involved in the heat exchange below the pinch point are always the same, while Q_{WH} will be varying at each iteration (since $Q_{DH,rec}$ is varying). This is the most general procedure possible.

The advantage of this approach is that is allows to define the working point of the heat pump based on the GCC shape, defining the region of the GCC to include in the analysis.

For example, as shown in Figure 4-10, a heat pump should not be matched to the tail of the GCC profile below the pinch point (highlighted in black) due to its steep profile, which will cause a detrimental heat pump´s performance. Therefore, choosing a proper shifted temperature value, it is possible to correctly match the heat pump, guaranteeing high performances.

4.3.1.2. Heat recovery scenarios

Four different scenarios were evaluated; these are classified depending on the chosen value of the shifted temperature below the pinch point T_{WH}; as said above, in fact, selecting a value of T_{WH} was found to be the most efficient approach, both from a computational and methodological point of view.

The parameters defining the scenarios are listed in Table 4-7:

Table 4-7: Analyzed scenario and correspondent shifted temperature

T_{WH}[°C]	ID
43.5	District heating starting temperature
39.7	Base case
37.5	Lean amine target temperature
32.5	Clean gas cooler target temperature

- The scenario at $T_{WH} = 43.5\ °C$ corresponds to the real starting temperature of district heating (equal to 41 °C, found by subtracting $\frac{\Delta T_{min}}{2}$ to T_{WH}, that is a shifted value). The hot streams involved are *CO_2 condenser-3*, *clean gas cooler* and partially the *lean amine cooler*. Their heat availability is limited by the fact that they are exchanging heat with the district heating stream in the whole interval considered (from pinch point temperature to $T_{WH} = 43.5\ °C$), thus this can be considered a sort of worst-case scenario for heat recovery since the heat processed by the heat pump is low and thus the hot utility that it can generate.
- The "base case" scenario, was found so that the total district heat recovery is equal to the heat required by the capture plant reboiler, namely:

$$Q_{DH,rec} = Q_{direct} + Q_{heat\ pump} = Q_{REB} \quad (4\text{-}13)$$

  In this way, the loss associated with the capture plant reboiler is exactly compensated and the total heat delivered by process P7 to district heating water can be "restored" to the reference case value.

- The scenario at $T_{WH} = 37.5\ °C$, instead, corresponds to the target temperature of the *lean amine cooler*, thus this stream will be completely exploited.
- The scenario at $T_{WH} = 32.5\ °C$ corresponds to the beginning of the steep profile of the GCC, which should not be included in heat pump integration. All the hot streams are completely exploited, apart from a small contribution of *CO_2-condenser3,* represented by the steep profile itself.

These points are qualitative highlighted in Figure 4-12, from the highest to the lowest shifted temperature. Note that, in each iteration $Q_{DH,rec}$is varying, thus the heat load corresponding to these points will also vary in each iteration.

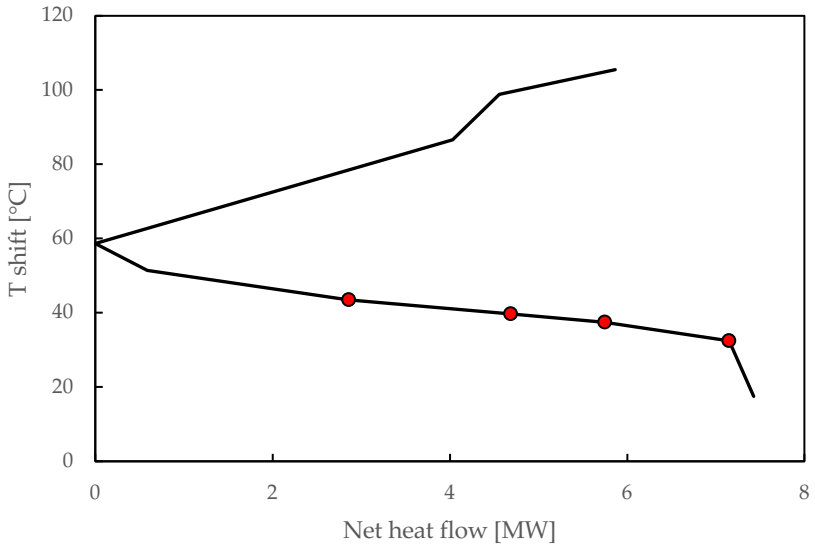

Figure 4-12: T_{WH} highlighted on the GCC for a given value of $Q_{DH,rec}$; consider that, since $Q_{DH,rec}$ is varying at each iteration, the heat load of this point varies throughout the iteration, as descripted above.

4.3.2. VCHP model in MATLAB

The hybrid heat pump was compared to a standard vapor compression heat pump (VCHP). Given VCHP cannot be simulated in STACY due to some fluid missing data, a thermodynamic model for a single stage vapor compression heat pump was developed in MATLAB: this allows to characterize the thermodynamic stages of the heat pump´s cycle in term of pressure, temperature, enthalpy and entropy. Thermodynamic properties were calculated using the library available in *Coolprop* [80].

The model requires the definition of condensation and evaporation temperatures in saturation condition and some assumptions, reported in Table 4-8.

Table 4-8: Assumption for the single stage vapor compression heat pump model in MATLAB

Parameter	Value
η_{is} compressor	0.7
Superheating (K) [51]	10
Subcooling (K) [51]	5
ΔP (kPa)	-

Detailed information for this model is reported in Appendix B.

4.3.2.1. VCHP matching procedure

Since the MATLAB model is only based on thermodynamics, it was not possible to include external loops in the calculations. Thus the approach followed for the matching of the heat pump to the background process is based on the approach presented in the literature [70, 71], which however computes COP based on an assumed value of the Carnot COP efficiency factor. The methodology followed this thesis, instead, assumes a value compressor isentropic efficiency and is able consider different working fluids exploiting the model built in MATLAB.

The comparison between the VCHP and HACHP was carried out for the same amount of total district heat recovery ($Q_{DH,rec}$), found with matching procedure of the HACHP, described in 4.3.1.1. Since $Q_{DH,rec}$ is known, the hot utility is also known Q_{HU} as well as the condenser duty (Q_{cond}), since this must be set equal to Q_{HU}, according to equation (4-14)

$$Q_{cond} = Q_{HU} \tag{4-14}$$

Condensation temperature (at saturation condition) is calculated accounting for the ΔT between background process–HRL ($\Delta T_{cond,1} = 5$ °C) and the one between HRL-heat pump ($\Delta T_{cond,2} = 5$ °C). The temperature difference between the heat pump and the background process is therefore equal to:

$$\Delta T_{BG-COND} = \Delta T_{cond,1} + \Delta T_{cond,2} = 10\ °C \tag{4-15}$$

Considering T_{HU} as the maximum temperature reached by the GCC (see Figure 4-10),

$$T_{cond} = (T_{HU} - \frac{\Delta T_{min}}{2}) + \Delta T_{BG-COND} = 113\ °C \tag{4-16}$$

Where the contribution $\frac{\Delta T_{min}}{2}$ is subtracted to consider the real cold stream temperature

The evaporator heat duty is found through an iterative procedure, whose purpose is to guarantee a temperature difference with the background process equal to 10 °C (ΔT_{BG-EVA}), while being compatible with the heat delivered by the condenser, equation (4-14).

ΔT_{BG-EVA} accounts for the temperature differences between background process–HRL ($\Delta T_{eva,1} = 5$ °C) and the one between HRL- heat pump ($\Delta T_{eva,2} = 5$ °C).

$$\Delta T_{BG-EVA} = \Delta T_{eva,1} + \Delta T_{eva,2} = 10\ °C \tag{4-17}$$

The iterative procedure exploits both the GCC and the MATLAB model; the inputs are T_{eva}, T_{cond} and the assumptions listed in Table 4-7. A stepwise procedure of the procedure is shown in Table 4-9 and a detailed description is then provided.

Table 4-9: Iterative procedure for the VCHP matching to the BG process

Input: T_{eva}, T_{cond}, parameters listed in Table 4-8	
1:	**Calculate** $m_{ref} = \frac{Q_{COND}}{h_2 - h_{3,sub}}$
2:	**Calculate** $Q_{eva} = m_{ref} * (h_{1,sh} - h_4)$
3:	**Define** $T_{eva,shift} = T_{eva} + 2.5\ °C$
4:	**Define** $P = (Q_{eva};\ T_{eva,shift})$
5	**Define** Q = $(Q_{eva};\ T_{GCC@Qeva})$
6	**Calculate** ΔT as the vertical distance P to Q
7:	**if**
	$\Delta T < 5\ °C$ → decrease T_{eva}
	$\Delta T > 5\ °C$ → increase T_{eva}
	Iteration ends when $\Delta T = 5\ °C$

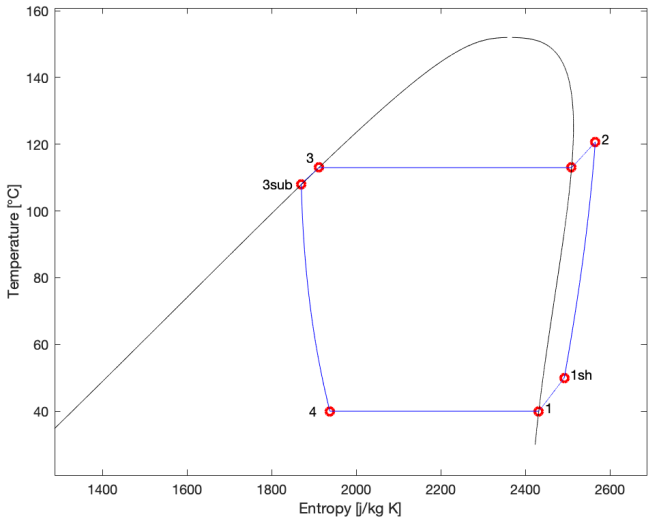

Figure 4-13: reference for Table 4-9: thermodynamic stages of the heat pump in the T - s diagram

The MATLAB model calculates the thermodynamic properties of the refrigerant in the different stages of the vapor compression cycle; those properties are used to compute the following steps:

1. The mass flow rate of the refrigerant that guarantees a delivered heat equal to Q_{cond} (step 1 in Table 4-9) is found.
2. The associated evaporator heat duty ($Q_{eva,}$) is derived. Since evaporation and condensation temperature are defined, together with heat duties of condenser and evaporator, the GCC of the heat pump is completely characterized.
3. Calculate the shifted evaporation temperature
4. P is defined as the point with coordinates (Q_{eva}; $T_{eva,shift}$), see Figure 4-14
5. Q is the point on the GCC correspondent to Q_{eva}: Q = (Q_{eva}; $T_{GCC@Qeva}$), see Figure 4-14

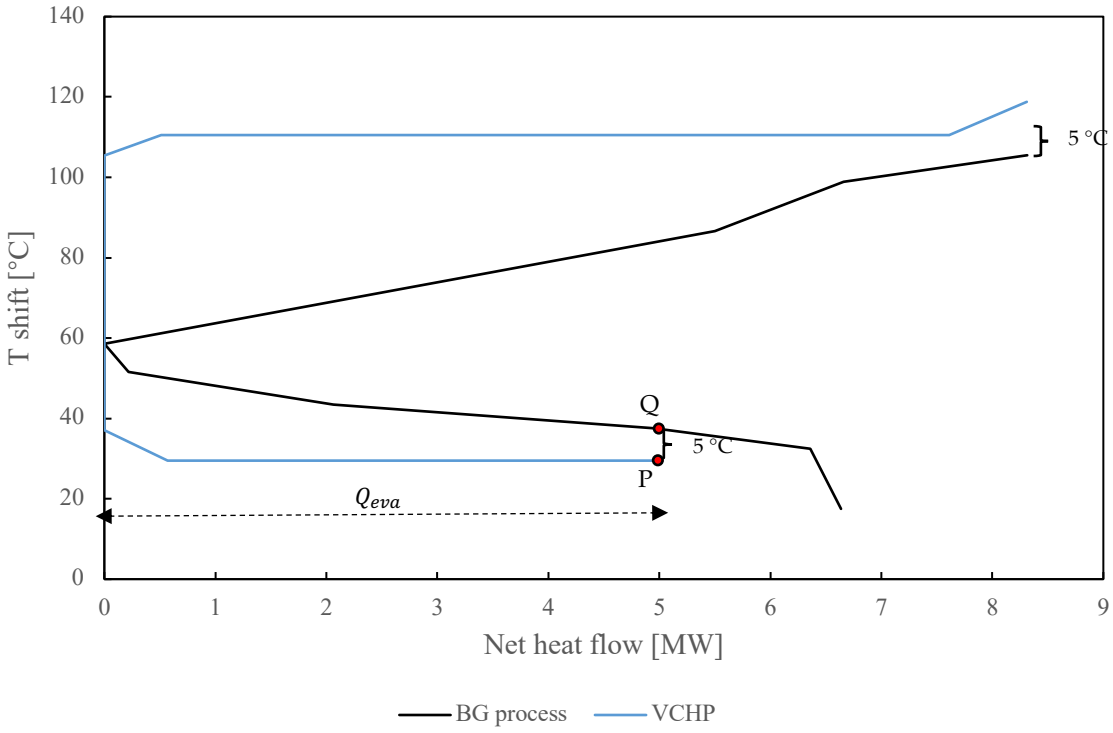

Figure 4-14: Definition of points P and Q on the GCC: their temperature difference must be equal to 5 ℃

6. The temperature difference (i.e. vertical distance on the GCC, simply defined as ΔT in Table 4-9) that must be granted between these two points is equal to 5 ℃, so to allow for feasible heat transfer while having minimum driving forces; the logic behind 5 ℃ is that the HRL and the heat pump are both cold streams from the point of view of the background process

This point can be clarified considering that the real evaporation temperature, T_{eva}, must guarantee a temperature difference of 10 °C (equal to ΔT_{BG-EVA}), from the real temperature of the background process. The latter is found as the hot streams temperature read on the GCC ($T_{GCC@Qeva}$), shifted by a contribution of $+\frac{\Delta T_{eva,1}}{2}$, which takes into account the heat exchanging between background process-HRL. See equation (4-18).

Since the evaporator is a cold stream for the HRL, the shifted evaporation temperature ($T_{eva,shift}$) is equal to the real evaporation temperature shifted by $+\frac{\Delta T_{eva,2}}{2}$; equation (4-19) clarifies that the vertical distance between $T_{eva,shift}$ and $T_{GCC@Qeva}$ is only equal to 5 °C.

$$T_{eva} = (T_{GCC@Qeva} + \frac{\Delta T_{eva,1}}{2}) - \Delta T_{BG-EVA} \quad (4\text{-}18)$$

$$T_{eva,shift} = T_{eva} + \frac{\Delta T_{eva,2}}{2} = T_{GCC@Qeva} - 5\ ℃ \quad (4\text{-}19)$$

7. T_{eva} is iteratively changed until the distance between P and Q is exactly equal to 5 ℃.

4.3.2.2. Thermodynamic analysis

A preliminary thermodynamic analysis was carried out to choose the candidate refrigerant of the VHCP. Three different alternatives were compared, namely R1234ze(Z), R1233zd(E) and R600, since they were found to be the best solutions in this temperature range, considering also the limits exhibited by the other refrigerants, as discussed in Section 3.2.

The purpose of this analysis was to compare the compressor´s discharge temperature and pressure, the volumetric heat capacity(*see definition of VHC in equation (4-23) & (4-24) at the end of section 4.3.3) and the COP, varying the evaporation temperature in a suitable temperature range. From the GCC, it was tentatively found that the VCHP evaporation temperature would have been included in the temperature range $30 - 40$ ℃ for each fluid; this was then confirmed by the matching procedure. Thus, three evaporation temperature level were selected: 30, 35 and 40 ℃. The condensation temperature was fixed, as defined by equation (4-16)

Temperature and pressures exhibited by the different refrigerants were found to be quite similar and well below the limits presented in Section 3.2. Hence, they do not represent an issue for the working of the compressor or the lubricant oil.

These parameters are presented in Figure 4-15.

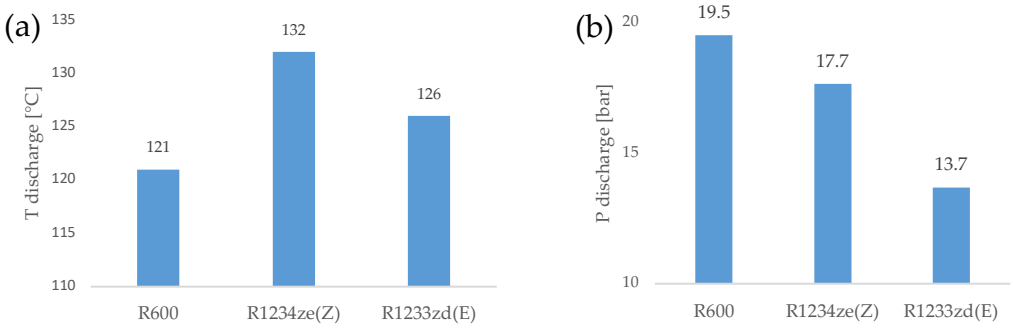

Figure 4-15: Compressor´s discharge temperature (a) and compressor´s discharge pressure (b) for the selected refrigerants. These parameters are provided in output by the MATLAB model

Since the COP values were also found to be very similar for the different refrigerants and evaporation temperature considered (see Figure 4-16) the parameter of focus is the volumetric heat capacity, which exhibited the highest value for R600 (Figure 4-16 (b)). Moreover, this refrigerant is often cited in literature, as it is characterized by a wide range of operations and it is indicated as one of the most promising alternatives for the immediate future [50]. Thus, it was selected to carry out the comparison.

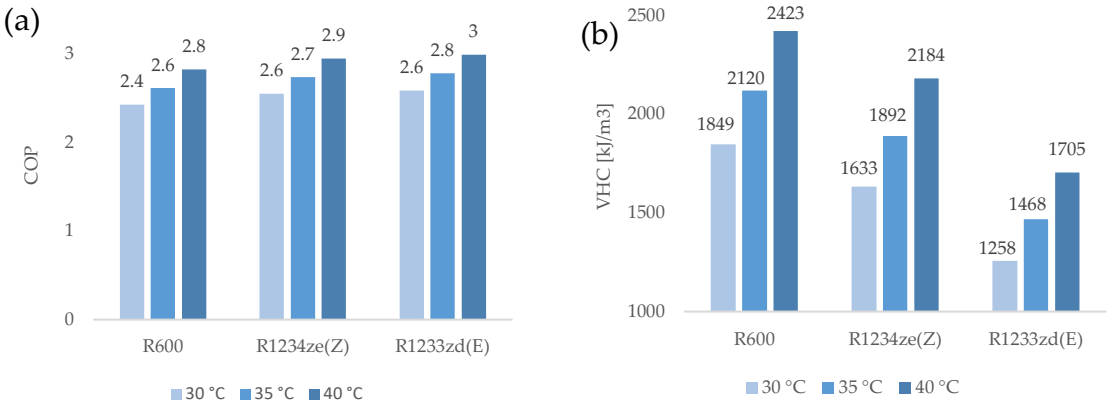

Figure 4-16: COP (a) and VHC (b) values for the selected refrigerants and evaporation temperature considered.

4.3.3. Performance indicators

The comparison between the HACHP and VCHP mainly focused on technical parameters, such as heat input, COP, electrical power consumption and the

working point of the compressor, characterized in term of discharge pressure and temperature, pressure ratio and volumetric heat capacity.

A simple economic analysis was also carried out, comparing the operational expenses of the two models. The hypothesis for this were an interest rate (*int*) of 10 % and an inflation rate of 2 % (*infl*), kept constant over a lifetime period of 20 years (n). The electricity price was also varied, between 40 to 130 €/MWh, a range that is compatible with the average electricity price of Sweden in 2021 [81].

Assuming that the HACHP has a higher investment cost (due to higher number and more critical components), but lower operational expenses, due to the savings in electrical power consumption ($\Delta P_{el} = P_{el,VCHP} - P_{el,HACHP} > 0$), the purpose of the economic analysis was to identify the total cost of investment of the HACHP for which it becomes more profitable than the VCHP.

This was calculated as the acceptable increase in total investment cost (ΔTIC), that corresponds to the decrease in operational expenses ($\Delta OPEX$), taking into account an annualization factor (for a single year, calculated as $\frac{1}{1+int-inlf}$)

Considering n years, 7920 operational hours per year (equal to the one of boiler P7), and *"price"* as the general electricity price, ΔTIC is calculated as follows:

$$\Delta TIC = \Delta OPEX * \sum \frac{1}{(1 + int - infl)^n} \quad (4\text{-}20)$$

$$\text{where } \Delta OPEX = \Delta P_{el} * 7920 * price \quad (4\text{-}21)$$

The total investment cost of the vapor compression heat pump ($CAPEX_{VCHP}$) is estimated as the product of the investment cost (specific to the thermal power output) and the thermal power output of the heat pump (i.e. capacity of the condenser)

$$CAPEX_{VCHP} = Specific\ inv.cost * thermal\ power\ output \quad (4\text{-}22)$$

Taking as reference a study performed by the RELAB Group [82] (not yet published at the time of writing this thesis) a specific cost of investment of the VCHP of 500 €/kW was considered.

*the volumetric heat capacity is define as the generated heat capacity per volume of processed refrigerant and it is measure in $[\frac{J}{m^3}]$.

Although the thermodynamic meaning is the same, this parameter was calculated in two slightly different ways, adapting to the working principle of the considered device and the parameters supplied by the modeling procedure (MATLAB and STACY).

$$VHC_{VCHP} = \rho_{suc} * (h_2 - h_{3,sub}) \quad (4\text{-}23)$$

$$VHC_{HACHP} = \frac{Q_{abs}}{m_{rich\ sol}} * \rho_{suc} \quad (4\text{-}24)$$

Where ρ_{suc} is the density of the refrigerant at the compressor´s suction port.

5 Results

The GCC analysis shows that, although hot streams of capture section are characterized by a significant amount of heat availability, direct heat recovery to district heating water is not feasible for the following reasons:

- Heat availability is mostly related to low temperature (below 61.1 °C) since most of the heat derives from the *lean amine cooler* and the *clean gas cooler*. For higher temperature, *CO2 condenser – 1* and *CO2 condenser – 2* are available, but their thermal capacity is low and, thus, the heat available is relatively low.
- Linked to the previous point, most of the heat is introduced below the pinch point, acting as an excess for the system.
- Supply temperature of district heating (103 °C) is higher than the highest temperature of the hot streams (101.4 °C). Considering that a temperature difference of 5 °C is required between hot and cold streams, district heating target temperature could be reached only with an external hot utility.

The maximum amount of district heat recovery that could be provided by direct heat recovery only ($Q_{direct\ only}$) is equal to

$$Q_{DH} = Q_{direct\ only} = 4.73\ MW$$

Additionally, hot utility equal to 568 kW is necessary to reach the targeted 103 °C, as for the composite curves for direct heat recovery only shown in Figure 5-1.

This explains the importance of including a heat pump in the system, which allows for an increase in the direct heat recovery, while taking care of the hot utility demand.

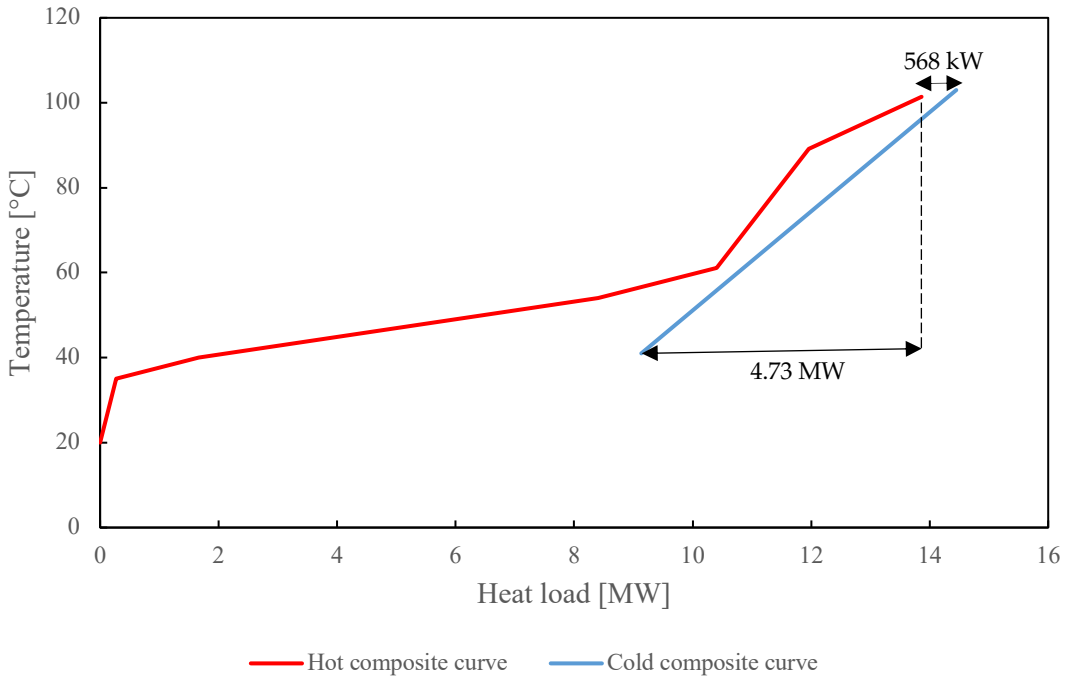

Figure 5-1: Composite curve in case of direct heat recovery only: district heating could successfully recover only 4.73 MW. Hot utility of 568 kW is needed to reach the targeted temperature

5.1. HACHP integration

The hybrid absorption heat pump integration is represented against the background process in the GCC graphs shown in Figure 5-2.

The different scenarios are identified by the shifted temperature, as illustrated in 4.3.1.2.

The characteristic glide reported by absorption and desorption processes is clearly represented in Figure 5-2, where the refrigerant heat temperature profile is highlighted in red.

Thanks to the gliding characteristic, the temperature differences with the background process are low, allowing for higher efficiency to be reached.

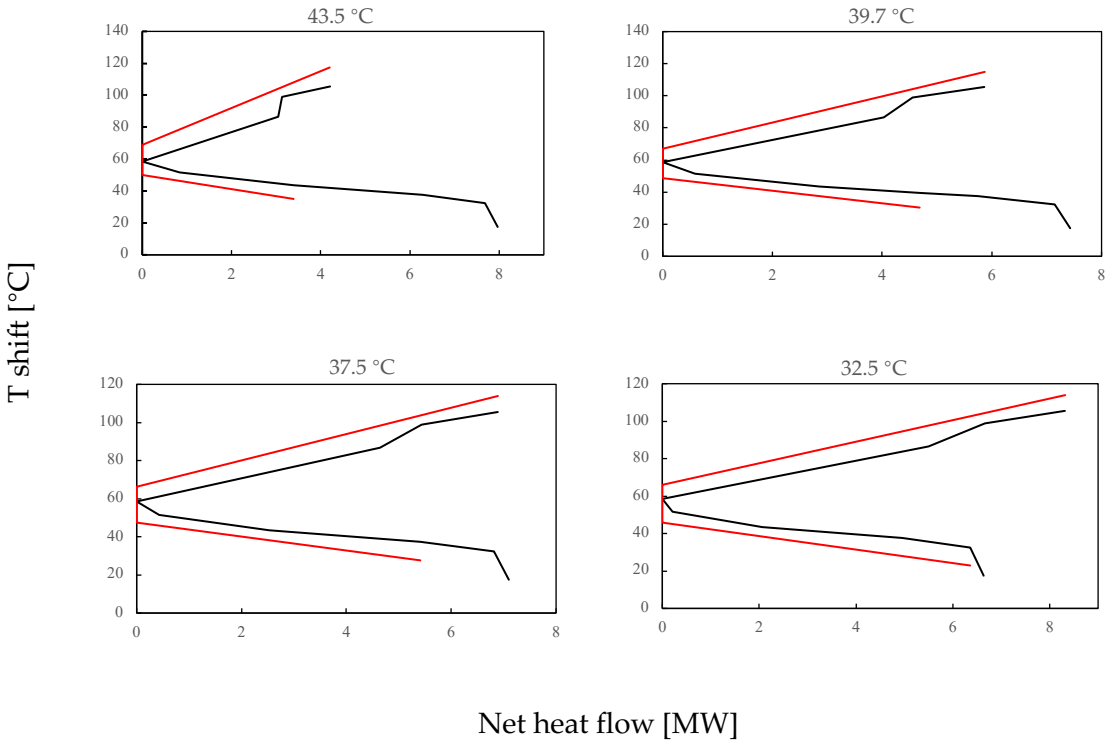

Figure 5-2: HACHP (red curve) integration in the background process (black), divided in the different scenarios, identified by the shifted temperature

In Figure 5-2 two effects are recognizable among the different scenarios:

- Increase in the capacity of the heat pump when the shifted temperature is decreased;
- Consequent increase in the total district heat recovery.

Regarding heat pump's capacity, Figure 5-2 clearly highlights that the lower the temperature level considered, the more heat can be used in the heat pump´s generator, identified by the red line below the pinch point.

As a consequence, the heat delivered by the absorber also increases, identified by the red line above the pinch point.

Generator and absorber duty are shown in Figure 5-3 in the four different scenarios: the grey column represents the heat duty of the generator, while the blue one the absorber´s heat duty.

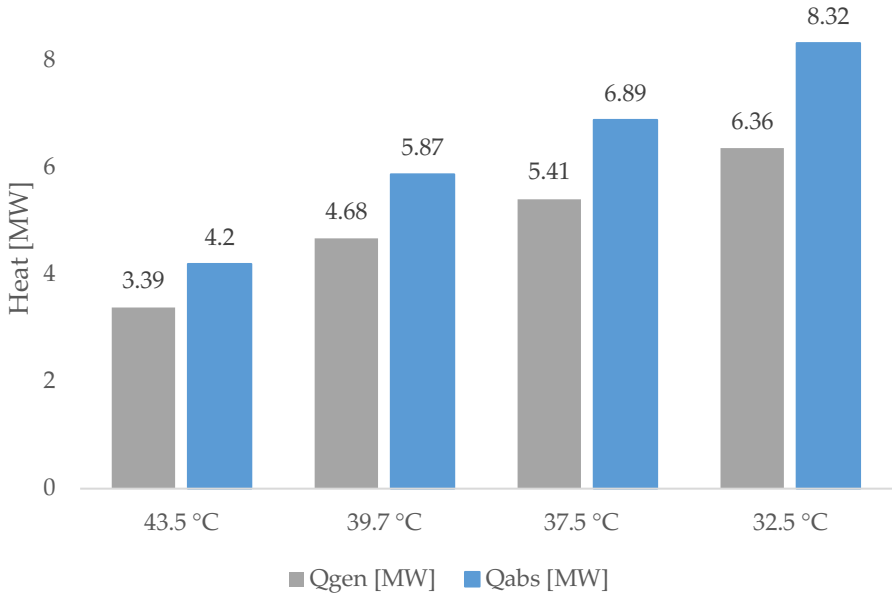

Figure 5-3: Generator (grey) and absorber (blue) heat duty in the different scenarios

The increase in the district heat recovery is, instead, testified by the shape of the GCC of the background process (black curve in Figure 5-2): the higher the district heat recovery, the lower the heat surplus below the pinch with an increase in the hot utility needs.

The scenario at 32.5 °C is the one that provides the highest district heat total recovery, equal to 15.54 MW; and all residual heat available below the pinch point is completely exploited by the heat pump. This can be considered as the physical limit for total district heat recovery from the capture section hot streams.

The scenario at 37.5 °C is fully exploiting the potential of the *lean amine cooler*, but only partially the one of the *clean gas cooler*, hence the total district heat recovery that is possible to achieve decrease to 13.65 MW.

The base case scenario is found so that the total district heat recovery is exactly equal to 12.3 MW, to perfectly compensate for district heat recovery loss associate to the reboiler of the capture section.

The scenario at 43.5 °C is highly penalized by the low amount of residual heat that the heat pump is exploiting and thus the total district heat recovery achievable is equal to 10.1 MW.

The total district heat recovery divided in the different scenarios are summarized in Table 5-1

Table 5-1: Total district heat recovery in the different scenario

Scenario	$Q_{DH,rec}$ [MW]
43.5 °C	10.1
39.7 °C (base case)	12.3
37.5 °C	13.65
32.5 °C	15.54

(note: to ease the presentation, $Q_{DH,rec}$ will be approximated to one decimal place from now on)

Direct heat recovery also benefits from the integration of the heat pump. The reason for this can be explained by examining the shape of the GCC in Figure 5-2: the higher the value of $Q_{DH,rec}$, the lower the heat surplus of the background process, meaning that the hot streams are more and more exploited.

A comparison between heat pump contribution and direct heat recovery is shown in Figure 5-4: for higher shifted temperature scenario (i.e. low values of total district heat recovery), internal heat exchanging (grey bar in Figure 5-4) is contributing more than the heat pump (absorber duty, highlighted with a blue bar in Figure 5-4).

In the lower shifted temperature scenario (i.e. higher $Q_{DH,rec}$), the amount of residual heat exploited by the heat pump increases, and thus its contribution to district heat recovery: this relation is linear and in the scenario at 37.5 °C and 32.5 ° C the internal heat exchanging contributes less than the heat pump:

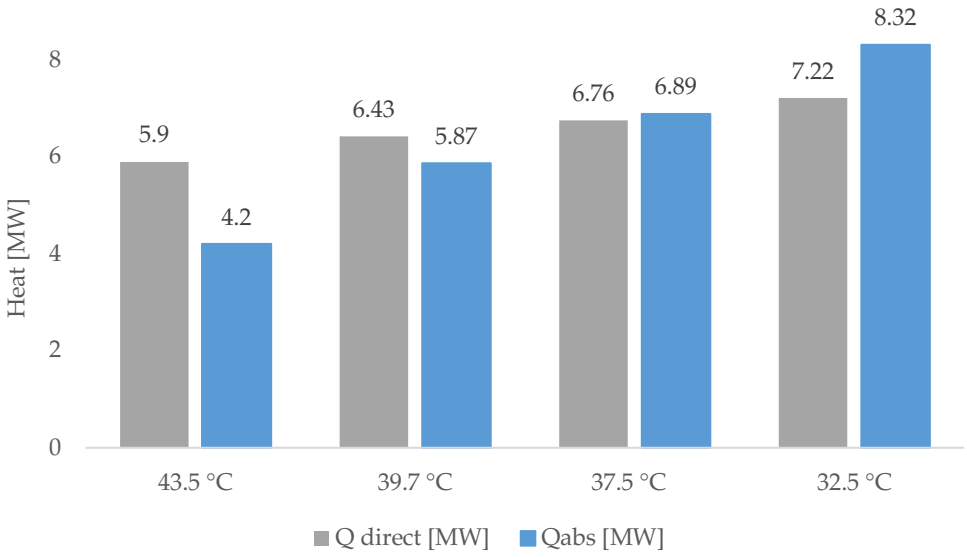

Figure 5-4: Comparison between direct heat recovery (grey) and heat pump contribution (absorber duty, in blue) in the different scenario

The price to be paid for larger district heating recovery is that the heat pump COP decreases: Table 5-2 shows that the COP ranges from a value of 5.3 to 4.2. This is determined by the fact the in the lower shifted temperature scenario, the generator´s external heat transfer loop is characterized by lower inlet temperature and higher temperature difference on the loop itself.

The concentration of the rich solution which guarantees the maximum COP value also varies, from 0.95 for the 43.5 °C scenario to 0.86 for the 32.5 °C scenario (Table 5-2). This was found to be primarily determined by the higher temperature difference on the generator's external loop. The higher is this temperature difference, the higher is the glide required to the solution in the generator to match the temperature profile in the external loop. The heat pump "counteracts" the higher glide by lowering the rich solution concentration at which the COP is maximum (i.e. the optimal configuration is found for a lower ammonia mass fraction).

Table 5-2: COP and rich solution concentration (C_{rich}) in the different scenario

Scenario	$\boldsymbol{COP}$	$\boldsymbol{C_{rich}}$
43.5 °C	5.3	0.95
39.7 °C	4.9	0.92
37.5 °C	4.6	0.9
32.5 °C	4.2	0.86

Another consideration is related to the shape of the GCC: Figure 5-2 shows that for low shifted temperature scenario (higher total district heat recovery) the background process (black curve) tends to flatten above the pinch point, becoming more "linear".

This is beneficial for the heat pump integration: the refrigerant profile is able to better match the background process exhibiting lower temperature differences with the background process itself. This behavior is fully captured by simulation in STACY: the model provides a lower adiabatic mixing temperature at the absorber´s inlet, as well as lower outlet temperature. Furthermore, the entropy generation on the component due to heat transfer was found to decrease for "more linear" profile. This partially compensates for the COP decrease that is associated with the high district heat recovery scenario.

The flattening of the background process profile also results in a lower compressor discharge pressure, which is included in a range of 33–28 bar for the various scenarios. The flatter the background process profile above the pinch point, the

lower the temperature requirements of the external loop, meaning that the high pressure of the cycle can be lowered.

On the other hand, the compressor's discharge temperature and pressure ratio are higher for the low shifted temperature scenario due to higher pressure ratio.

Discharge pressure and temperature, as well as pressure ratio (β_{compr}), are reported in Table 5-3.

Table 5-3: Discharge pressure, discharge temperature and compression ration of the HACHP in the different scenario

Scenario	$P_{disch}[bar]$	T_{disch}[°C]	β_{compr}
43.5 °C	33.1	172.4	2.8
39.7 °C	30.8	180	3.1
37.5 °C	29.7	187	3.3
32.5 °C	28.1	202	3.8

Finally, the volumetric heat capacity is favored in the higher shifted temperature scenario due to higher pressure and temperature at compressor´s suction port, as reported in Figure 5-5.

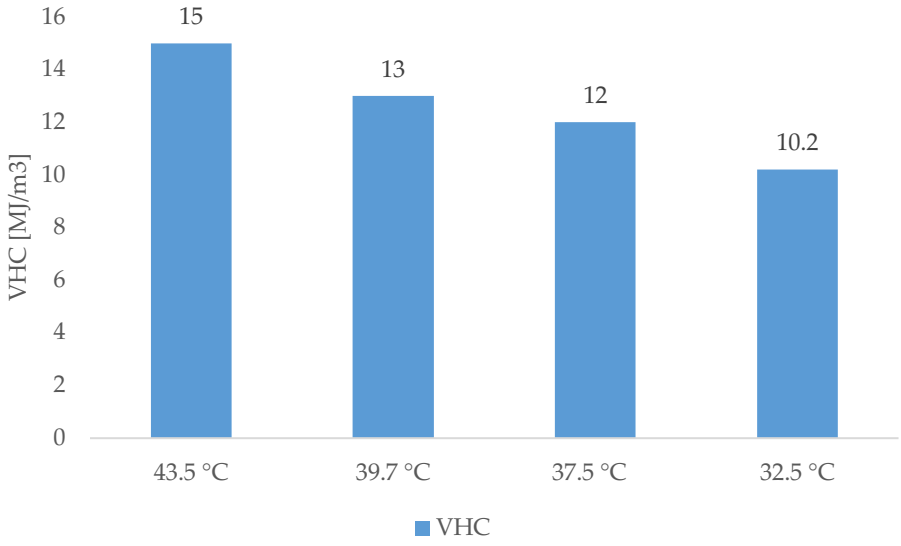

Figure 5-5: Volumetric heat capacity of the HACHP compressor´s in the different scenarios

5.2. VCHP integration & comparison with HACHP

The vapor compression heat pump integration is represented against the background process in the GCC graphs in Figure 5-6

As explained in 4.3.2 the comparison was carried out for the same amount of total district heat recovery $Q_{DH,rec}$; the background process profile (black curve in Figure 5-6) is therefore equal to that of Figure 5-2.

For this reason, the scenarios shown in Figure 5-6 are identified by $Q_{DH,rec}$ rather then the shifted temperature classification.

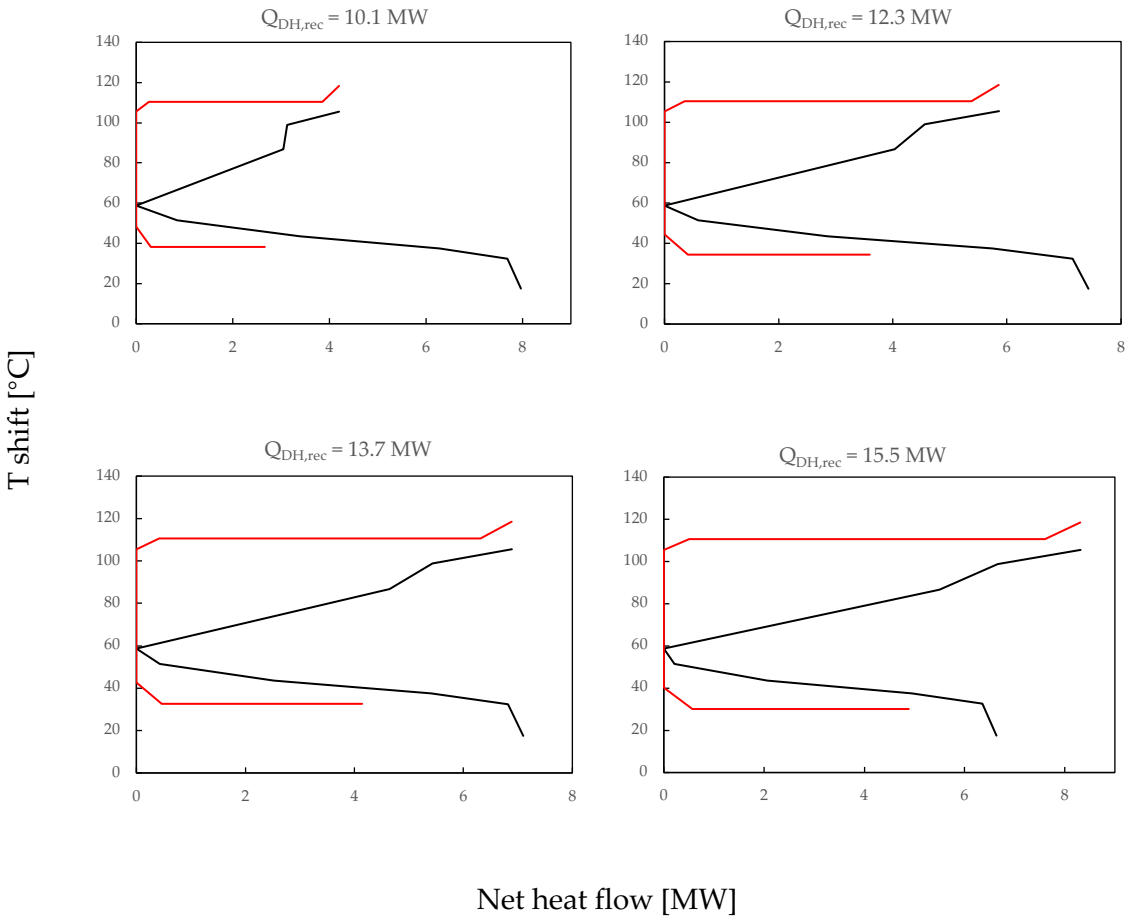

Figure 5-6: VCHP (red curve) integration represented against the background process (black curve): the scenarios are identified by the total amount of district heat recovery

What is immediately noticeable from Figure 5-6 is that the VCHP is characterized by higher temperature differences with the background process compared to that of the HACHP (Figure 5-2) , since evaporation and condensation occurs at constant

temperature and pressure, excluding the small contribution of superheating and subcooling.

Also, for the same amount of heat output, the vapor compression heat pump has a lower evaporator duty compared to that of the HACHP.

This determines a higher cooling utility demand of the background process, which is shown in Figure 5-7. The blue column represents the cooling demand of the background process in case a vapor compression heat pump is implemented, while the grey bar is the cooling utility demand of the system in case the hybrid model is used.

Note: in the cooling demand calculation, the cooling duty of the clean gases has not been considered, since this is an effluent stream, as clarified in Section 4.1.2.

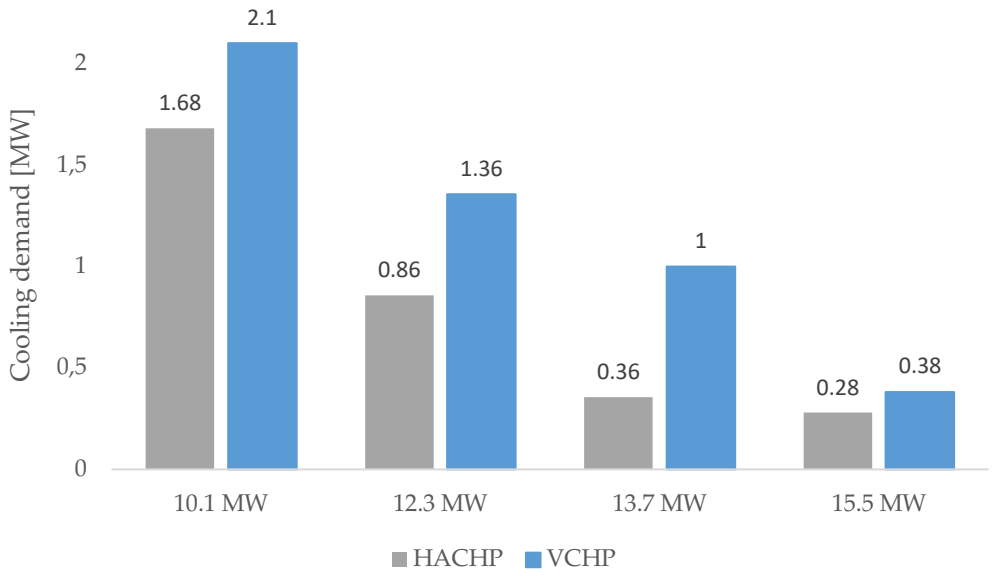

Figure 5-7: Cooling duty demand of the background process in the different scenario. Comparison between HACHP (grey) and VCHP (blue)

The lower evaporator duty is caused by the fact that the COP of the VCHP is much lower compared to that of the HACHP.

This implies that, considering the same amount of heat output, the vapor compression device will be characterized by higher electrical consumption and thus lower heat input.

The COP values of the VCHP are found to be almost the half of that of the HACHP in each of the considered scenario, as shown in Table 5-4

Table 5-4: COP of VCHP compared to that of HACHP in the different scenario

Scenario	VCHP	HACHP
10.1 MW	2.7	5.3
12.3 MW	2.5	4.9
13.7 MW	2.5	4.6
15.5 MW	2.4	4.2

The compressor of the HACHP is characterized by higher volumetric heat capacity (VHC): as shown in Figure 5-8 (a), in fact, the VHC is around 6 times higher compared to that of R600; this is related to higher specific heat of absorption process, compared to condensation, as well as to the fact the low pressure level of the cycle is higher compared to that of a VCHP (thanks to ammonia thermodynamic properties, as shown by pressure-temperature curve of Figure 3-8). Moreover, the equilibrium state at the outlet of the evaporator is found for higher temperature, thanks to the glide. The glide also determines higher outlet temperature from the generator (evaporator) thus the pressure ratio of the HACHP is lower compared to that of the VCHP (around the half, as shown in Figure 5-8 (b)).

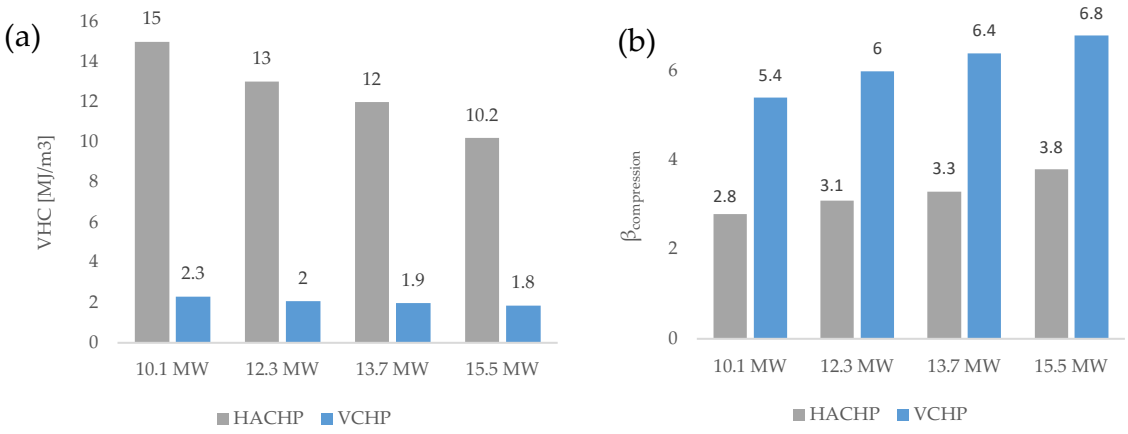

Figure 5-8: Volumetric heat capacity (a) and pressure ratio (b) comparison between the HACHP (grey) and VCHP (blue)

The only advantages of the VCHP are the compressor´s discharge pressure and temperature, which are considerably lower that than of the HACHP. This is, again, related to the thermodynamic properties of ammonia and represent a practical issue to be addressed when designing the HACHP.

R600 showed a constant discharge pressure of 19.5 bar in the different scenarios that were considered, with a discharge temperature varying between 120 to 122 °C, being slightly influenced by the different evaporation temperatures.

Both these values of pressure and temperature are considerably lower compared to the one reached by the HACHP, reported in Table 5-3.

5.2.1. Economics

Table 5-4 showed that the COP of the HACHP is much higher compared to that of the VCHP. The direct consequence is that, for the same amount of heat output, the vapor compression model is characterized by higher electricity usage.

As anticipated for the COP values, the VCHP is characterized by power consumption which are almost the double of that of the HACHP. The absolute values for the two models are presented in Figure 5-9

The scenario at 15.5 MW of total district heat recovery is the one that showed the highest absolute difference between the two models, equal to 1.45 MW, even if in relative terms the COP under this condition are closer.

The two intermediate scenario, base case and 13.7 MW, showed about same absolute difference (~1.1–1.2 MW)

Finally, the 10.1 MW scenario is the most favorable for the VCHP since it consumes "only" 0.74 MW more than the HACHP, even if in relative terms this means almost doubling the electricity consumption.

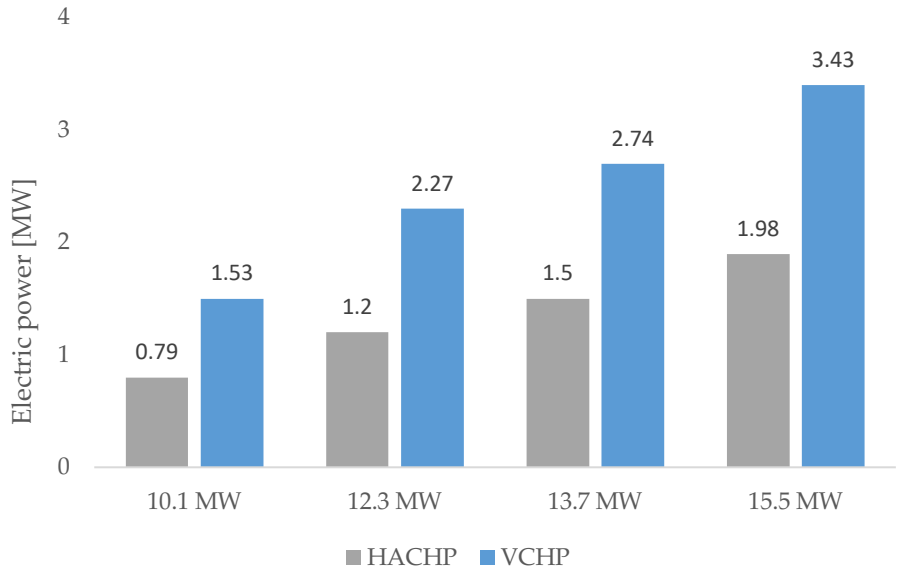

Figure 5-9: Electrical consumption of the HACHP compared to that of the VCHP

Higher electrical consumption determines higher operational costs (OPEX) that make the VCHP a less attractive investment, especially looking over the operating life of the heat pump.

The total investment cost difference between the HACHP and the VCHP (*delta TIC*) is reported in Figure 5-10, for the base case scenario, as a function of electricity price and techno-economic lifetime.

This has to be interpreted as the difference in the investment cost between the two technologies that justifies the installation of the hybrid heat pump versus the vapor compression model: in very informal terms, if the HACHP investment cost is lower than the *delta TIC* value exhibited in Figure 5-10, the implementation of the heat pump is advised.

As shown in Figure 5-10, the higher the average electricity price and lifetime considered, the more attractive the installation of the HACHP becomes, because of operational cost savings.

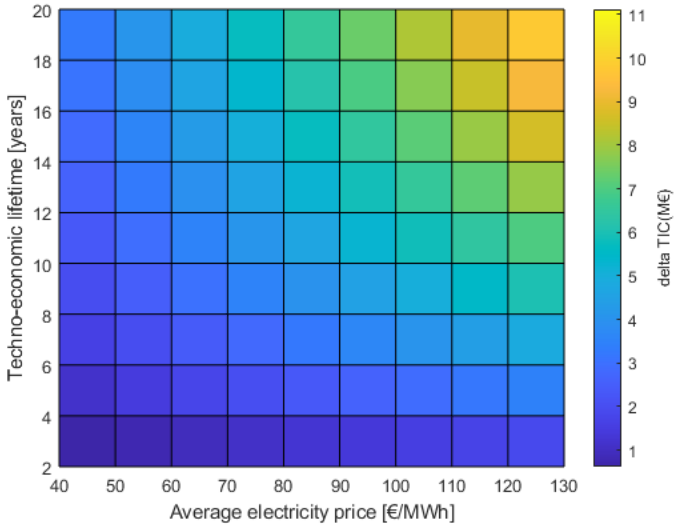

Figure 5-10: Differential total investment cost (delta TIC, measured in million €) reported as a function of techno economic lifetime and average electricity price.

In the worst-case scenario for the HACHP, which is found for the lowest electricity price (40 €/MWh) and lifetime (2 years), the difference in investment cost which justifies the installation of the HACHP is equal to 0.62 M€. The total cost of investment for the vapor compression heat pump in the base case scenario is equal to 2.94 M€ (derived as illustrated in section 4.3.3); thus, in these boundary conditions, the maximum acceptable investment cost of the HACHP which makes it convenient over the VCHP is equal to 3.56 M€. Translated in percentage terms,

the investment cost of HACHP could be around 21 % higher than the one of the VCHP.

Considering that:

- Lifetime of heat pumps and the average electricity price are likely to be higher than the values considered just above
- The higher cost of HACHP, compared to VCHP, is primarily related to the cost of the additional components required by the former (i.e. separator, internal heat exchanger and pump), which is likely to be lower than the 21 % of the total investment cost of the VCHP (equal to 0.62 M€)

The HACHP is considered an attractive investment compared to the VCHP, since its additional investment cost can be relatively rapidly recovered due to the savings in operational expenses.

5.3. Condiderations on Sävenäs plant

The overall analysis provided on heat recovery possibilities from the carbon capture plant are now summarized, with a focus on the consequences and possibilities for Sävenäs WtE plant.

Currently, process P7 at Sävenäs plant provides 32.66 MW to the district heating network: part of this capacity derives from steam condensation, part instead is recovered from the treatment of the flue gases. This was identified as the reference case in Section 4.1.1 (prior to CCS integration).

A carbon capture and storage plant with a CO_2 capture rate of 90 %. implemented on P7 will result in a 12.3 MW loss in the original district heat delivery, caused by the reboiler needs, which will be supplied by steam bleeds from the turbine. Allocating this loss to P7, the new district heat supply from P7 will be equal to 20.36 MW, causing a loss equal to the 37.7 % of the original district heat supply. This case is identified generally as "CCS only" (see Figure 5-11).

Heat recovery possibilities from the carbon capture process were identified in this work, which are divided in direct heat recovery only, or direct heat recovery and heat pump in combination.

If only direct heat recovery is considered ("DR only" in Figure 5-11), the maximum amount of heat that is possible to recover to district heating water is equal to 4.73 MW, partially compensating for the loss associated to the reboiler. In this case, however, hot utility of 568 kW must be provided to reach the targeted temperature

of 103 °C of district heating water. The inclusion of a heat pump is therefore highly recommendable.

The HACHP has been demonstrated to be a suitable candidate in this application: its advantages over the vapor compression model have been largely demonstrated, both from a technical and economic point of view.

Discarding the CO_2 conditioning section, due to the low amount of heat availability, a HACHP integrated in the capture section of the CCS plant would be able to deliver up to 8.32 MW of heat to district heating water, in addition to increasing the direct heat recovery to a maximum of 7.22 MW. Direct heat recovery and heat pumping under these conditions would be able to achieve 15.54 MW of total district heat recovery, compensating for the reboiler loss and even increasing the capacity of the original district heating network. Compared to the reference case, in fact, this scenario achieves a district heat capacity that is 9.9% higher than the original one.

If instead a lower heat pump capacity is considered, the heat recovery would also decrease.

Figure 5-11 provides an overview of the loss/gain in the district heat delivery in the different scenario, compared to the reference case.

Note: the value for the base case is equal to 0 % since this case was found so to perfectly compensate for the loss associated to the reboiler

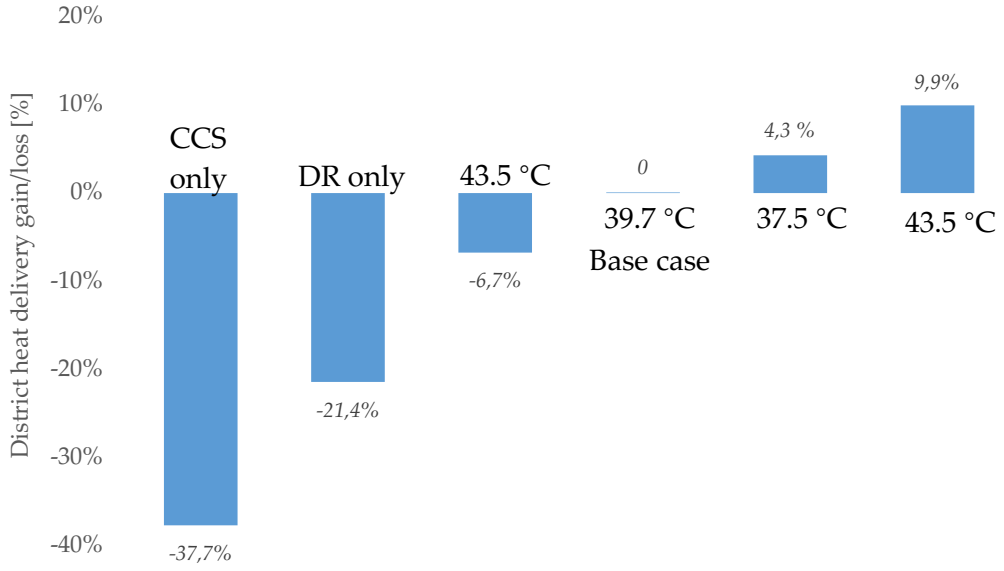

Figure 5-11: Percentage increase (or decrease) in district heating supply in the different scenarios, compared to the situation prior CCS integration

Including the CCS plant and a heat pump in process P7 will cause additional operational expenses compared to the reference case one.

Regarding the capture section, electricity expenses are related to the flue gas fan and pumps, with a total consumption of 322 kW.

The conditioning section, instead, is characterized by higher consumptions, due to the CO_2 compression and the liquefaction section, that also includes two different compressors. Electrical consumption reaches a value of 965 kW.

The heat pump, instead, is characterized by electrical consumptions which increase as more heat is delivered to the district heating water, as presented in section 5.2.1.

Hence, while considering a higher capacity heat pump allows to increase district heat capacity, it must be taken into account that the operational expenses will increase.

A summary for power consumption associated to each scenario is given in Figure 5-12.

Note: the pump's electrical expenses of the direct heat recovery only case have been neglected

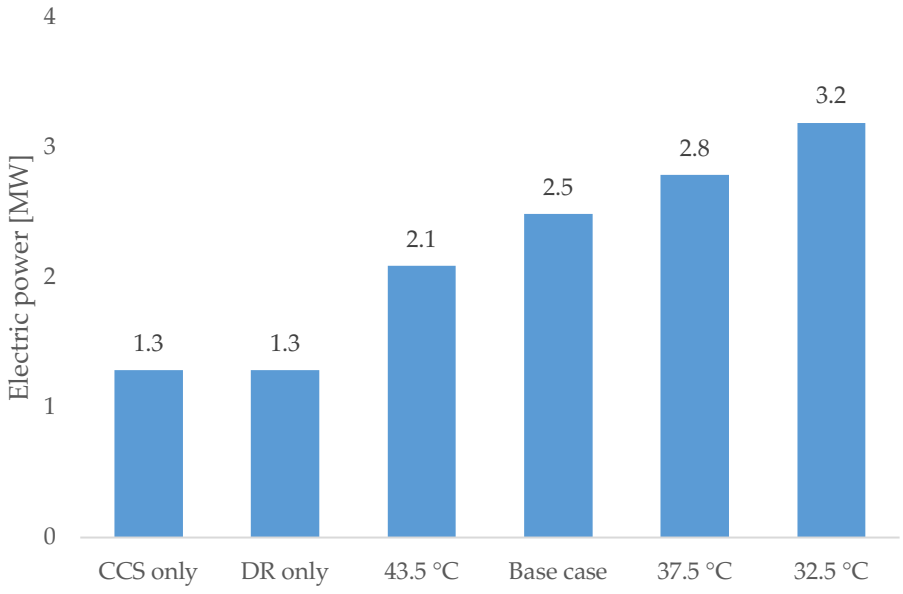

Figure 5-12: Electric power consumption associated to CCS plant and heat pump in the different analyzed scenario

Even though the price for cooling utility is normally low, it is nevertheless important to highlight the different cooling duties associated with each scenario.

The heat pump integration would decrease the cooling utility demand of the capture section, exploiting part of the heat availability of this section. Conditioning section cooling duty, instead, is not exploited and thus has to be completely cooled by external utilities.

The cooling demand of the clean gases is not considered, since this is an effluent stream, as clarified in Section 4.1.2.

The cooling demand of the capture and conditioning section in the different scenario is presented in Figure 5-13: it is clearly visible how, for higher heat pump capacity, the cooling demand is decreasing.

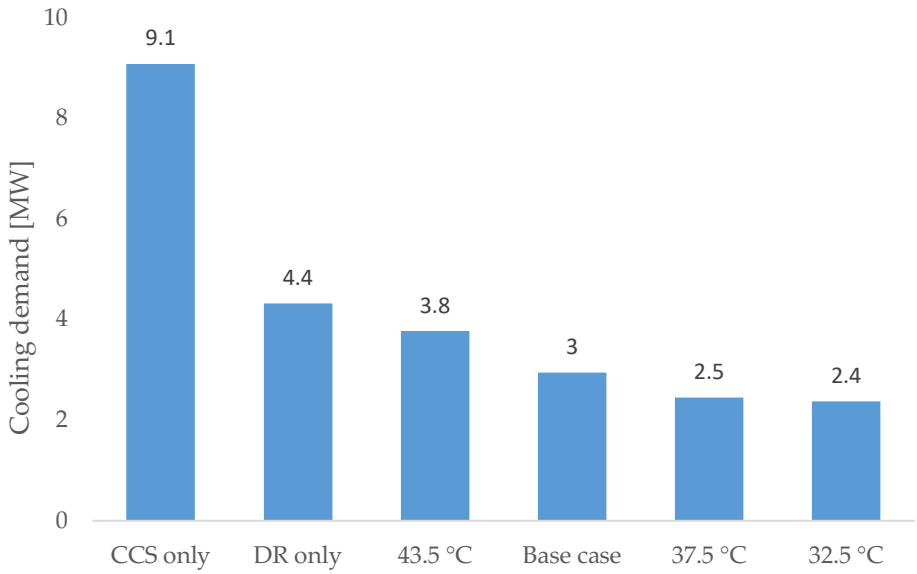

Figure 5-13: Cooling demand of the CCS plant (capture + conditioning section) in the different scenario

5.3.1. Draft about a real design

The real design of a heat exchanging network was not the main purpose of this study, however, some considerations are provided for the base case scenario.

The basic theory of pinch analysis divides the heat exchanging design network at the pinch and separately matches hot and cold streams in the two regions (above and below the pinch point) so to achieve the minimum energy requirement configuration [32].

A simplified draft of the real interaction between the different streams in the base case scenario is presented in Figure 5-14.

The name of the streams have been simplified in *COND-1*, *COND-2* and *COND-3* for the various linearized stream of the CO_2 condenser, while *LA* and *GC cooler* are representative of the *lean amine cooler* and of the *clean gases cooler*.

DH stands for *district heating*

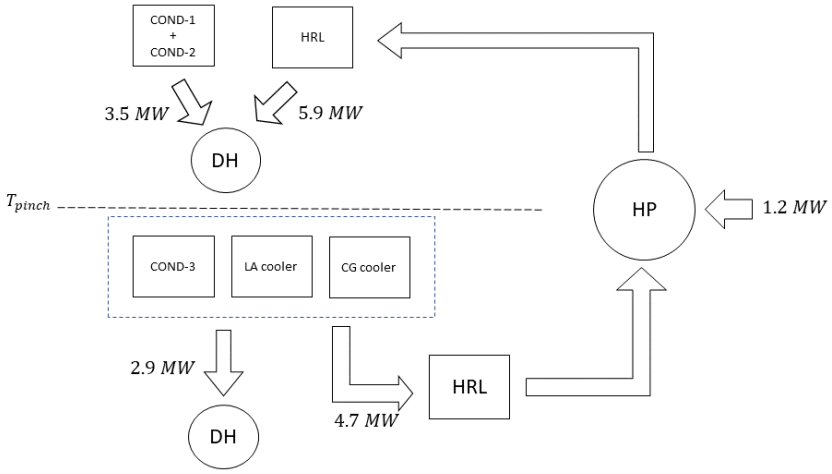

Figure 5-14: Simplified representation of heat exchanging among the different streams in the base case scenario.

Above the pinch point

- *COND-1* and *COND-2* could be directly exploited by direct heat recovery until a temperature of 61.1 °C, providing 3.5 MW to supply part of DH request.
- The remaining duty above the pinch point (5.9 MW) would be satisfied by the heat pump through the *HRL*, which is able to heat the district heating stream up to the target temperature, also taking care of the capacity of district heating water that has not been heated by *COND-1* and *COND-2*

The configuration above the pinch point can be easily achieved with low number of stream splits, only related to the district heating stream.

Below the pinch point

- *COND-3* is characterized by a pronouncedly non-linear heat-temperature profile, which is testified by the low thermal capacity of the relevant stream. The matching with the heat recovery loop may become problematic, although in principle one cannot exclude multiple stream splitting.
- The three streams involved below the pinch supply the district heating stream with a capacity of around 2.9 MW, while the HRL linked to the heat pump requires 4.7 MW

The configuration below the pinch point is more problematic, since 3 hot streams must be matched with two cold streams, meaning that multiple splitting are necessary to achieve the maximum energy savings configuration.

In order to simplify the problem, COND-3 could be excluded from the stream matching since its heat content is low

The working point of the heat pump would be barely influenced compared to the one already found (descripted in the Results chapter) due to the “poor” influence COND-3 has on the background process and thus on the GCC shape.

The same reasoning can be applied to the other case scenario. Also, one must consider that the heat pump capacity, and thus the total district heat recovery are both variables: an optimum configuration is likely to be found. This should be a compromise between the targeted amount of heat recovery and technological complexity of installation.

6 Conclusions

This thesis investigated residual heat recovery possibilities from a carbon capture and storage (CCS) plant integrated in a waste-to-energy (WtE) plant.

Boiler nr. 7 of Sävenäs WtE plant was selected as a suitable case study. Sävenäs WtE plant is a waste-fueled combined heat and power plant located in Sävenäs (Gothenburg, Sweden), which is run by Renova, the waste management company of the city.

The CO_2 capture and CO_2 conditioning processes were simulated in two separate steady-state Aspen PLUS V12 models and they were sized to match the amount of CO_2 that is present in the flue gas treatment of boiler nr. 7. The capture rate of the plant was set to 90%.

The simulation revealed that such a plant requires 12.3 MW of heat to drive the solvent regeneration in the reboiler. Since this heat demand is likely to be supplied by low pressure steam bled from the turbine, a loss equal to 37.7 % in district heating supply is determined, compared to the reference case (i.e. prior CCS integration).

Process integration methods (i.e. pinch analysis) were used to evaluate direct heat recovery possibility: the analysis revealed that a maximum of 5.3 MW can be recovered, including 568 kW that must be provided through an external hot utility. The district heating supply loss would be partially compensating, decreasing to 21.4 % compared to that of the reference case.

Including a heat pump is highly suggested, as this could increase the total district heat supply to a maximum of 35.8 MW, 9.9 % higher than in the reference case.

A hybrid absorption compression heat pump was compared to a vapor compression heat pump for this application. The former was demonstrated to be the best solution: apart from the compressor discharge pressure and temperature, in fact, the device performed better in any of the analyzed technical indicators. Also, an analysis on operational expenses revealed that hybrid model is a more attractive investment compared to the VCHP as the investment cost difference between the two devices could be rapidly repaid.

Lastly, some suggestion and thoughts about a real design following pinch analysis rules was provided.

6.1. Future work

The future work, taking off where this thesis has ended, could focus on a real heat exchanging network design.

Some guidelines were provided in 5.3.1, however, a real network design was not deeply investigated, as it lied outside the scope of the thesis.

The method developed for the integration of the hybrid absorption heat pump, in fact, could be extended to find a compromise between heat recovery and "real-life" feasibility of implementation, finding the working point of the heat pump (in term of temperature and capacity) which is able to satisfy both these constrains.

Also, the choice of the minimum temperature difference ΔT_{min} as well as district heating supply and return temperatures could be further investigated, so to evaluate their influence on heat recovery and heat pump working conditions.

Bibliography

[1] "Heating – Analysis," *IEA*. https://www.iea.org/reports/heating (accessed Feb. 15, 2022).

[2] "Integrating low temperature renewables in district energy systems," IRENA, 2019.

[3] "Il teleriscaldamento in Italia," AIRU, Legambiente, Italy, 2012.

[4] "Net Zero by 2050," *IEA*. https://www.iea.org/reports/net-zero-by-2050 (accessed Feb. 15, 2022).

[5] "District heating," *IEA*. https://www.iea.org/reports/district-heating

[6] S Frederiksen and S. Werner, *District heating and cooling*. Lund, Sweden, 2013.

[7] Euroheat, "District Energy explained." https://www.euroheat.org/knowledge-hub/district-energy-explained.html (accessed Feb. 15, 2022).

[8] J. Collins, "The hystory of district heating," 1959.

[9] O. US EPA, "What Is CHP?," Aug. 19, 2015. https://www.epa.gov/chp/what-chp (accessed Feb. 15, 2022).

[10] V. Ignell and E. Johansson, "Local Infrastructures for CCS clusters: a case study of two CHP Plants in gothenburg," Chalmers University of technology, Gothenburg, Sweden, 2021.

[11] "Waste to energy (WTE) systems for district heating | Elsevier Enhanced Reader." https://reader.elsevier.com/reader/sd/pii/B9780857090119500089?token=584D58F385BF08D254154F6F59810CD975D4B1A91C3BDA245AD864E3CAF409E5BEB655D309E2470CFE3446958668EB74&originRegion=eu-west-1&originCreation=20220227174428 (accessed Feb. 27, 2022).

[12] "Understanding the carbon impacts of Waste to Energy Incineration," *Zero Waste Europe*, Mar. 18, 2020. https://zerowasteeurope.eu/2020/03/understanding-the-carbon-impacts-of-waste-to-energy/ (accessed Feb. 27, 2022).

[13] "The barriers to waste heat recovery and how to overcome them," EUROHEAT & POWER, Jun. 2020.

[14] H. Fang, "Key issues and solutions in a district heating system using low-grade industrial waste heat," 2015.

[15] J. K. Jensen, W. B. Markussen, L. Reinholdt, and B. Elmegaard, "On the development of high temperature ammonia–water hybrid absorption–compression heat pumps," *Int. J. Refrig.*, vol. 58, pp. 79–89, Oct. 2015, doi: 10.1016/j.ijrefrig.2015.06.006.

[16] J. K. Jensen, T. Ommen, W. B. Markussen, L. Reinholdt, and B. Elmegaard, "Technical and economic working domains of industrial heat pumps: Part 2 – Ammonia-water hybrid absorption-compression heat pumps," *Int. J. Refrig.*, vol. 55, pp. 183–200, Jul. 2015, doi: 10.1016/j.ijrefrig.2015.02.011.

[17] D. Olsen, Y. Abdelouadoud, P. Liem, and B. Wellig, "The Role of Pinch Analysis for Industrial ORC Integration," *Energy Procedia*, vol. 129, pp. 74–81, Sep. 2017, doi: 10.1016/j.egypro.2017.09.193.

[18] "Pinch analysis," *Wikipedia*. May 25, 2021. Accessed: Feb. 27, 2022. [Online]. Available: https://en.wikipedia.org/w/index.php?title=Pinch_analysis&oldid=1025137884

[19] M. Bendig, F. Maréchal, and D. Favrat, "Defining 'Waste Heat' for industrial processes," *Appl. Therm. Eng.*, vol. 61, no. 1, pp. 134–142, Oct. 2013, doi: 10.1016/j.applthermaleng.2013.03.020.

[20] J. Andersson, "An investigation of carbon capture technologies for Sävenäs waste-to-energy plant," Luleå University of Technology, Luleå, Sweden, 2020.

[21] "Renova - Efficient waste recovery | Greengothenburg." https://www.greengothenburg.se/reference-objects/111 (accessed Feb. 04, 2022).

[22] "From waste to clean energy: Sävenäs Waste-to-Energy Plant, Gothenburg," Renova AB, 2012. [Online]. Available: https://www.renova.se/globalassets/from-waste_to_clean_energy3

[23] "The Paris Agreement | UNFCCC." https://unfccc.int/process-and-meetings/the-paris-agreement/the-paris-agreement (accessed Jan. 26, 2022).

[24] "A new era for CCUS – CCUS in Clean Energy Transitions – Analysis," *IEA*. https://www.iea.org/reports/ccus-in-clean-energy-transitions/a-new-era-for-ccus (accessed Feb. 04, 2022).

[25] D. Y. C. Leung, G. Caramanna, and M. M. Maroto-Valer, "An overview of current status of carbon dioxide capture and storage technologies," *Renew. Sustain. Energy Rev.*, vol. 39, pp. 426–443, Nov. 2014, doi: 10.1016/j.rser.2014.07.093.

[26] J. Gibbins and H. Chalmers, "Carbon capture and storage," *Energy Policy*, vol. 36, no. 12, pp. 4317–4322, Dec. 2008, doi: 10.1016/j.enpol.2008.09.058.

[27] M. Bui *et al.*, "Carbon capture and storage (CCS): the way forward," *Energy Environ. Sci.*, vol. 11, no. 5, pp. 1062–1176, 2018, doi: 10.1039/C7EE02342A.

[28] Å. Eliasson and E. Fahrman, "Utilization of Industrial Excess Heat for CO2 Capture: effects on capture process design and district heating supply," Chalmers University of technology, Gothenburg, Sweden, 2020.

[29] P. Johsonn and J. Kjarstad, "Avskiljning, transport och lagring av koldioxid i Sverige. Behov av forskning och demonstration," Chalmers University of technology, Gothenburg, Sweden, 2019.

[30] "Nothern lights project - Who we are," *Northern Lights*. https://northernlightsccs.com/who-we-are/ (accessed Feb. 04, 2022).

[31] H. Deng, S. Roussanaly, and G. Skaugen, "Techno-economic analyses of CO2 liquefaction: Impact of product pressure and impurities," *Int. J. Refrig.*, vol. 103, pp. 301–315, Jul. 2019, doi: 10.1016/j.ijrefrig.2019.04.011.

[32] I. C. Kemp, *Pinch Analysis and Process Integration*, Second Edition. Elsevier, 2007.

[33] S. Harvey and E. Svensson, "Industrial energy systems; Course Compendium." Chalmers University of Technology, 2021.

[34] "19.1: Spontaneous Processes," *Chemistry LibreTexts*, Nov. 20, 2014. https://chem.libretexts.org/Bookshelves/General_Chemistry/Map%3A_Chemistry_-_The_Central_Science_(Brown_et_al.)/19%3A_Chemical_Thermodynamics/19.1%3A_Spontaneous_Processes (accessed Feb. 23, 2022).

[35] P. Nellissen and S. Wolf, "Heat pumps in non-domestic applications in Europe: Potential for an energy revolution." https://docplayer.net/41987374-Heat-pumps-in-non-domestic-applications-in-europe-potential-for-an-energy-revolution.html (accessed Jan. 29, 2022).

[36] D. Mikielewicz and J. Wajs, "Performance of the very high-temperature heat pump with low GWP working fluids," *Energy*, vol. 182, pp. 460–470, Sep. 2019, doi: 10.1016/j.energy.2019.05.203.

[37] C. Arpagaus, F. Bless, M. Uhlmann, J. Schiffmann, and S. S. Bertsch, "High temperature heat pumps: Market overview, state of the art, research status, refrigerants, and application potentials," *Energy*, vol. 152, pp. 985–1010, Jun. 2018, doi: 10.1016/j.energy.2018.03.166.

[38] C. Arpagaus, F. Bless, M. Uhlmann, and J. Schiffmann, "High Temperature Heat Pumps: Market Overview,State of the Art, Research Status, Refrigerants,

and Application Potentials," 2018, doi: https://docs.lib.purdue.edu/iracc?utm_source=docs.lib.purdue.edu%2Firacc%2F1876&utm_medium=PDF&utm_campaign=PDFCoverPages.

[39] C. Mateu-Royo, J. Navarro-Esbrí, A. Mota-Babiloni, M. Amat-Albuixech, and F. Molés, "Theoretical evaluation of different high-temperature heat pump configurations for low-grade waste heat recovery," *Int. J. Refrig.*, vol. 90, pp. 229–237, Jun. 2018, doi: 10.1016/j.ijrefrig.2018.04.017.

[40] O. Bamigbetan, T. M. Eikevik, P. Nekså, M. Bantle, and C. Schlemminger, "Experimental investigation of a prototype R-600 compressor for high temperature heat pump," *Energy*, vol. 169, pp. 730–738, Feb. 2019, doi: 10.1016/j.energy.2018.12.020.

[41] D. Roskosch, V. Venzik, and B. Atakan, "Thermodynamic model for reciprocating compressors with the focus on fluid dependent efficiencies," *Int. J. Refrig.*, vol. 84, pp. 104–116, Dec. 2017, doi: 10.1016/j.ijrefrig.2017.08.011.

[42] O. Bamigbetan, T. M. Eikevik, P. Nekså, and M. Bantle, "Review of vapour compression heat pumps for high temperature heating using natural working fluids," *Int. J. Refrig.*, vol. 80, pp. 197–211, Aug. 2017, doi: 10.1016/j.ijrefrig.2017.04.021.

[43] M. Eriksson and G. Oskar, "Modelling and simulation of heat pump systems for hybrid and electrical vehicles," Linkoping University, 2018.

[44] I. Dincer and M. Kanoglu, "Refrigeration Systems and Applications, Second Edition," p. 484.

[45] J. S. Brown, C. Zilio, and A. Cavallini, "The fluorinated olefin R-1234ze(Z) as a high-temperature heat pumping refrigerant," *Int. J. Refrig.*, vol. 32, no. 6, pp. 1412–1422, Sep. 2009, doi: 10.1016/j.ijrefrig.2009.03.002.

[46] "Kyoto Protocol to the United Nations Framework Convention on Climate Change," *Rev. Eur. Community Int. Environ. Law*, vol. 7, no. 2, pp. 214–217, 1998, doi: 10.1111/1467-9388.00150.

[47] "In short about R1234ze," *KTH*. https://www.energy.kth.se/applied-thermodynamics/key-research-areas/heating-systems/low-gwp-news/kort-om-r1234ze-1.561807 (accessed Feb. 02, 2022).

[48] "R1336mzz-Z - new generation nonflammable low GWP refrigerant," *KTH*. https://www.energy.kth.se/applied-thermodynamics/key-research-areas/heating-systems/low-gwp-news/r1336mzz-z-ett-nytt-hogtemperaturkoldmedium-med-bra-egenskaper-1.501202 (accessed Feb. 03, 2022).

[49] K. Kontomaris, "A NON-FLAMMABLE, ZERO-ODP, LOW GWP WORKING FLUID FOR HIGH TEMPERATURE HEAT PUMPS: DR-148," *HPT - Heat Pump. Technol.*, Accessed: Feb. 02, 2022. [Online]. Available: https://heatpumpingtechnologies.org/publications/a-non-flammable-zero-odp-low-gwp-working-fluid-for-high-temperature-heat-pumps-dr-148/

[50] O. Bamigbetan, T. M. Eikevik, P. Nekså, M. Bantle, and C. Schlemminger, "Theoretical analysis of suitable fluids for high temperature heat pumps up to 125 °C heat delivery," *Int. J. Refrig.*, vol. 92, pp. 185–195, Aug. 2018, doi: 10.1016/j.ijrefrig.2018.05.017.

[51] H. Moisi and R. Rieberer, "Refrigerant Selection and Cycle Development for a High Temperature Vapor Compression Heat Pump," p. 10, 2017.

[52] S. Fukuda, C. Kondou, N. Takata, and S. Koyama, "Low GWP refrigerants R1234ze(E) and R1234ze(Z) for high temperature heat pumps," *Int. J. Refrig.*, vol. 40, pp. 161–173, Apr. 2014, doi: 10.1016/j.ijrefrig.2013.10.014.

[53] "Periodic Reporting for period 1 - TEES (A high-efficiency energy storage system that captures energy generated from renewable sources, waste energy from industry, and solar radiation, in a compressed fluid and heat pump hybrid system.) | H2020 | CORDIS | European Commission." Accessed: Feb. 02, 2022. [Online]. Available: https://cordis.europa.eu/project/id/729070/reporting/it

[54] K. E. Herold, R. Radermacher, and S. A. Klein, *Absorption chillers and heat pumps*, Second Edition. CRC Press, 2016.

[55] D. Zaytsev and C. A. I. Ferreira, "Screw Compressor For Ammonia-Water Heat Pump Lubricated By The Process Mixture," p. 9.

[56] M. U. Ahrens *et al.*, "Identification of Existing Challenges and Future Trends for the Utilization of Ammonia-Water Absorption–Compression Heat Pumps at High Temperature Operation," *Appl. Sci.*, vol. 11, no. 10, Art. no. 10, Jan. 2021, doi: 10.3390/app11104635.

[57] Y. Tae Kang, A. Akisawa, and T. Kashiwagi, "Analytical investigation of two different absorption modes: falling film and bubble types," *Int. J. Refrig.*, vol. 23, no. 6, pp. 430–443, Sep. 2000, doi: 10.1016/S0140-7007(99)00075-4.

[58] J. Kim *et al.*, "Experimental study of operating characteristics of compression/absorption high-temperature hybrid heat pump using waste heat," *Renew. Energy*, vol. 54, pp. 13–19, Jun. 2013, doi: 10.1016/j.renene.2012.09.032.

[59] M. Kim, Y. J. Baik, S. R. Park, K. C. Chang, and H. S. Ra, "Design of a high temperature production heat pump system using geothermal water at moderate temperature," *Curr. Appl. Phys.*, vol. 10, no. 2, Supplement, pp. S117–S122, Mar. 2010, doi: 10.1016/j.cap.2009.11.015.

[60] O. Brunin, M. Feidt, and B. Hivet, "Comparison of the working domains of some compression heat pumps and a compression-absorption heat pump," *Int. J. Refrig.*, vol. 20, no. 5, pp. 308–318, Aug. 1997, doi: 10.1016/S0140-7007(97)00025-X.

[61] "GWP of different refrigerants." UNEP.

[62] C. Arpagaus and S. Bertsch, "Experimental comparison of R1224yd(Z) and R1233zd(E) in a high temperature heat pump," p. 12, 2020.

[63] M. Nilsson, H. N. Rislå, and K. Kontomaris, "Measured performance of a novel high temperature heat pump with HFO-1336 mzz (Z) as the working fluid," 2017, Accessed: Feb. 02, 2022. [Online]. Available: https://www.semanticscholar.org/paper/Measured-performance-of-a-novel-high-temperature-(-Nilsson-Risl%C3%A5/9556df3042579994b0fa5fd7d05a8d079f9e7f8b

[64] "High Capacity Heat pumps - OCHSNER." [Online]. Available: http://www.ohps.co.uk/brochures/OHPS_Heatpumps_High_Capacity.pdf

[65] C. Watanabe, "Pioneering industrial heat pump technology in Japan," 2013, [Online]. Available: https://www.hptcj.or.jp/Portals/0/ahpnw/3rdmeeting/HPTCJ%20-%20Pioneering%20Industrial%20Heat%20Pump%20Technology%20in%20Japan%20rev1_130902.pdf

[66] https://www.dualmeta.io, "High Temperature Heat Pumps - Combitherm." https://combitherm-6w51aiwbz-dualmeta.vercel.app/produkte-und-loesungen/hochtemperaturwaermepumpen/ (accessed Feb. 02, 2022).

[67] "Friotherm - Unitop." https://www.friotherm.com/products/unitop/ (accessed Feb. 02, 2022).

[68] "Technology overview – Hybrid Energy." https://www.hybridenergy.no/tech-overview/ (accessed Feb. 02, 2022).

[69] Florian Schlosser, C. Arpagaus, and T. Walmsley, "Heat Pump Integration by Pinch Analysis for Industrial Applications: A Review," 2019, [Online]. Available: https://www.aidic.it/cet/19/76/002.pdf

[70] J. A. Stampfli, M. J. Atkins, D. G. Olsen, B. Wellig, M. R. W. Walmsley, and J. R. Neale, "Industrial Heat Pump Integration in Non-Continuous Processes

Using Thermal Energy Storages as Utility – A Graphical Approach," *Chem. Eng. Trans.*, vol. 70, pp. 901–906, Aug. 2018, doi: 10.3303/CET1870151.

[71] D. Olsen, Y. Abdelouadoud, P. Liem, S. Hoffmann, and B. Wellig, "Integration of Heat Pumps in Industrial Processes with Pinch Analysis," p. 11, 2017.

[72] S. Ó. Garðarsdóttir, F. Normann, K. Andersson, and F. Johnsson, "Postcombustion CO2 Capture Using Monoethanolamine and Ammonia Solvents: The Influence of CO2 Concentration on Technical Performance," *Ind. Eng. Chem. Res.*, vol. 54, no. 2, pp. 681–690, Jan. 2015, doi: 10.1021/ie503852m.

[73] M. Biermann, F. Normann, F. Johnsson, and R. Skagestad, "Partial Carbon Capture by Absorption Cycle for Reduced Specific Capture Cost," *Ind. Eng. Chem. Res.*, vol. 57, no. 45, pp. 15411–15422, Nov. 2018, doi: 10.1021/acs.iecr.8b02074.

[74] "Packing Hydraulics Calculations - Separation Technologies." http://seperationtechnology.com/packing-hydraulics/ (accessed Feb. 22, 2022).

[75] S. Ó. Garðarsdóttir, F. Normann, R. Skagestad, and F. Johnsson, "Investment costs and CO2 reduction potential of carbon capture from industrial plants – A Swedish case study," *Int. J. Greenh. Gas Control*, vol. 76, pp. 111–124, Sep. 2018, doi: 10.1016/j.ijggc.2018.06.022.

[76] L. Faramarzi *et al.*, "Results from MEA Testing at the CO2 Technology Centre Mongstad: Verification of Baseline Results in 2015," *Energy Procedia*, vol. 114, pp. 1128–1145, Jul. 2017, doi: 10.1016/j.egypro.2017.03.1271.

[77] E. Gjernes *et al.*, "Results from 30 wt% MEA Performance Testing at the CO2 Technology Centre Mongstad," *Energy Procedia*, vol. 114, pp. 1146–1157, Jul. 2017, doi: 10.1016/j.egypro.2017.03.1276.

[78] H. C. Becker, "Methodology and Thermo-Economic Optimization for Integration of Industrial Heat Pumps," 2012.

[79] M. Aprile, T. Toppi, S. Garone, and M. Motta, "STACY–A mathematical modelling framework for steady-state simulation of absorption cycles," *Int. J. Refrig.*, vol. 88, pp. 129–140, Apr. 2018, doi: 10.1016/j.ijrefrig.2017.12.019.

[80] I. H. Bell, J. Wronski, S. Quoilin, and V. Lemort, "Pure and Pseudo-pure Fluid Thermophysical Property Evaluation and the Open-Source Thermophysical Property Library CoolProp," *Ind. Eng. Chem. Res.*, vol. 53, no. 6, pp. 2498–2508, Feb. 2014, doi: 10.1021/ie4033999.

[81] "See hourly day-ahead prices." https://www.nordpoolgroup.com/en/Market-data1/Dayahead/Area-Prices/ALL1/Hourly/ (accessed Apr. 11, 2022).

[82] “RELAB | RENEWABLE HEATING AND COOLING LAB.” https://www.relab.polimi.it/it/ (accessed Apr. 11, 2022).

A Appendix A

A.1. HACHP components modeling in STACY

Absorber

The absorber is modelled as concurrent liquid–vapor flow. This is characterized by five ports, represented in the figure down below.

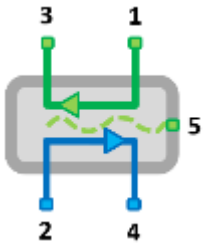

Figure A-1: Absorber model in STACY

Two and four represent the coolant inlet and outlet respectively (the external loop in the purpose of this thesis). Port 5 represents the refrigerant vapor that is absorbed by the poor solution inlet (port 1) so as to generate the rich solution (port 3).

The absorber is modeled thought the minimum ΔT mode, in which the flow arrangement is supposed to be counterflow. The parameters that are needed to solve the problem are UA, the overall heat transfer coefficient, ΔT_{MIN}, the minimum temperature difference at the pinch point, ε, the heat exchanger effectiveness and ΔP_{sol}, which is the pressure drop on the solution side.

During the absorption process, the refrigerant vapor is absorbed by the poor solution while releasing heat to the external source. This is a complex heat and mass transfer process, which is mathematically modeled dividing the process in two steps: adiabatic mixing between refrigerant vapor (port 5) and poor solution (port 1), which introduces the *mixing state 15,* followed by heat exchanging with the coolant.

The equations for the adiabatic mixing are:

- $m_{15} = m_1 + m_5$, overall mass balance

- $C_{15} = \frac{m_1 C_1 + m_5 C_5}{m_{15}}$, refrigerant mass balance
- $h_{15} = \frac{m_1 h_1 + m_5 h_5}{m_{15}}$, enthalpy balance

The rich solution outlet (port 3) is characterized by another set of equation:

- $m_3 = m_{15}$, overall mass balance
- $h_3 = h_{15} - \frac{Q_{ex}}{m_{15}}$, energy balance on the solution side
- $P_3 = P_1 - \Delta P_{sol}$, outlet pressure considering the given pressure drop

Lastly, a set of equation for the coolant must be assigned:

- $m_4 = m_2$, overall mass balance
- $C_4 = C_2$, mass species balance
- $h_4 = h_2 + \frac{Q_{ex}}{m_2}$, energy balance on the coolant side

Generator

The generator is modeled as counter current liquid/liquid heat exchanger which is characterized by four ports. Port 1 and 2 refers to stream 1 inlet and outlet, while port 2 and 4 correspond to the other stream (stream 2) involved in the heat exchanging process.

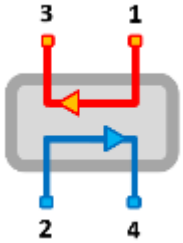

Figure A-2: Generator model in STACY

The generator is model with the minimum ΔT approach, supposing counterflow flow arrangement. The parameters required by this model are $UA, \Delta T_{min}$ and ε.

Two simple equations are used to model the generator, which are related to the enthalpy balance of the two streams. These are:

- $h_3 = h_1 - \frac{Q_{ex}}{m1}$, enthalpy balance on the outlet fluid
- $h_4 = h_2 + \frac{Q_{ex}}{m2}$, enthalpy balance on the refrigerant

The same equations and considerations are also valid for the internal heat exchanger, which is also modeled as counter current liquid/liquid heat exchanger

Compressor

The compressor is characterized by an inlet and outlet port, respectively port 1 and port 2, which represent the fluid at its inlet and outlet condition

Figure A-3: Compressor model in STACY

The compressor is modeled using the isentropic efficiency approach, η_{is},which is the only parameter needed to solve the equations. These are in the form of:

- $m_1 = m_2$, overall mass balance
- $C_1 = C_2$, mass species balance
- $h_2 = h_1 + \frac{h_{2s} - h_1}{\eta_{is}}$, enthalpy balance considering isentropic efficiency, where the state 2s is characterized by the pressure of the discharge section and entropy of inlet condition
- $W_{in} = m_1 * (h_2 - h_1)$, energy balance, where W_{in} is the power input to the compressor

Pump

Similarly to the compressor, the pump is characterized by two ports, respresentative of fluid inlet and outlet condition.

Figure A-4: Pump model in STACY

The model exploits the pump overall efficiency η.

The equations are then quite straightforward:

- $m_1 = m_2$, overall mass balance
- $C_1 = C_2$, mass species balance

- $L_p = \frac{m1*(P_2 - P_1)}{\rho_1}\frac{1}{\eta}$, energy balance to find the specific work duty. ρ_1 is simply the density of the fluid at the inlet condition (port 1)
- $h_2 = h_1 + L_p$ enthalpy balance

Restrictor (valve)

Figure A-5: Restrictor (valve) model in STACY

The valve is characterized by two ports (fluid inlet and outlet) and the isenthalpic model is exploited, hence no input parameters are required.

Three equations are necessary:

- $m_1 = m_2$, overall mass balance
- $C_1 = C_2$, mass species balance
- $h_2 = h_1$, isenthalpic condition

Separator

The separator is characterized by 3 ports: fluid inlet (port 1), vapor outlet (port 2) and liquid outlet (port 3).

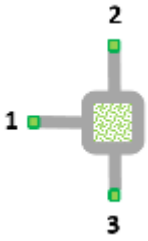

Figure A-6: Separator model in STACY

The only input parameter required is the fraction of vapor carried over in the liquid, which is indicated by f_{bub}. The equations that model this component are the following:

Pressure losses are considered to be negligible, hence:

- $P_3 = P_1$, liquid side
- $P_2 = P_1$, vapor side

Mass and enthalpy balance, vapor side (*1G* denotes the saturated gas state at the inlet conditions)

- $m_2 = (1 - f_{bub}) * m_{1G}$, overall mass balance
- $C_2 = C_{1G}$, mass species balance
- $h_2 = h_{1G}$, enthalpy balance

Mass and enthalpy balance, liquid side (*1L* denotes the saturated liquid state at the inlet condition)

- $m_3 = f_{bub} * m_{1G} + m_{1L}$, mass balance
- $C_3 = \frac{m_{1L}C_{1L} + m_{1G}C_{1G}f_{bub}}{m_3}$, mass species balance
- $h_3 = \frac{m_{1L}h_{1L} + f_{bub}m_{1G}*h_{1G}}{m_3}$, enthalpy balance

B Appendix B

B.1. VCHP model in MATLAB

A thermodynamic model was built in MATLAB for a single stage vapor compression heat pump.

The model requires as input evaporation and condensation temperature in saturation condition (T_{eva} and T_{cond}), compressor isentropic efficiency (η_{is}), superheating degree at evaporator´s outlet and subcooling degree at condenser´s outlet (ΔT_{SH} and ΔT_{SUB}) and the definition of the refrigerant fluid, selecting the one available in the library of *Coolprop* [80]

Pressure losses in the heat exchangers are neglected.

The reference points are shown in the following graph, provided by the simulation in MATLAB

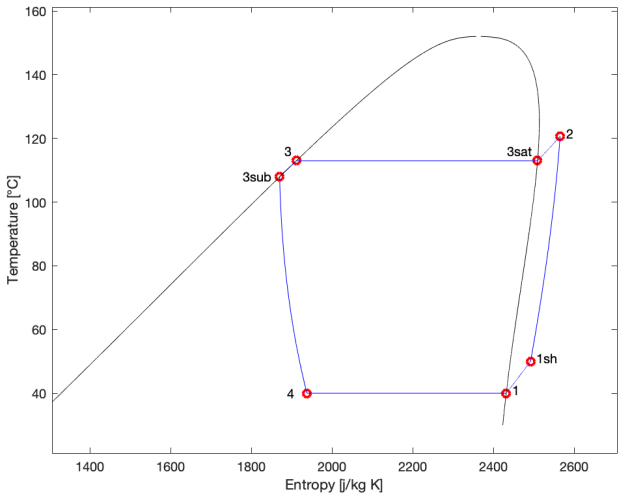

Figure B-1: reference stages of the VCHP model in the temperature-entropy diagram. The figure is an output from the model itself

The following equation were implemented to characterize these points in term of temperature (T), pressure (P), enthalpy (h) and entropy (s).

Q indicates the title of the refrigerant

State 1

$$T_1 = T_{eva}$$

$$P_1 = P_{sat}@T_1$$

$$h_1 = \mathrm{h}(P_1, Q = 1)$$

$$s_1 = \mathrm{s}(P_1, Q = 1)$$

State 1SH

$$T_{1.SH} = T_1 + \Delta T_{SH}$$

$$P_{1,SH} = P_1$$

$$h_{1,SH} = \mathrm{h}(P_{1,SH}, T_{1,SH})$$

$$s_{1,SH} = \mathrm{s}(P_{1,SH}, T_{1,SH})$$

State 2

$$T_2 = T(P_2, h_2)$$

$P_2 = P_3$, see definition of P_3 in state 3 characterization

$$h_{2s} = \mathrm{h}(P_2, s_{1,SH})$$

$$h_2 = h_1 + \frac{h_{2s} - h_{1,SH}}{\eta_{is}}$$

$$s_2 = \mathrm{s}(P_2, h_2)$$

State 3

$$T_3 = T_{cond}$$

$$P_3 = P_{sat}@T_3$$

$$h_3 = \mathrm{h}(P_3, Q = 0)$$

$$s_3 = \mathrm{s}(P_3, Q = 0)$$

State 3$_{sat}$

$$T_{3,sat} = T_3$$

$$P_{3,sat} = P_3$$

$$h_{3,sat} = \mathrm{h}(P_{3,sat}, Q = 1)$$

$$s_3 = \mathrm{s}(P_{3,sat}, Q = 1)$$

State 3$_{SUB}$

$$T_{3,SUB} = T_3 - \Delta T_{SUB}$$

$$P_{3,SUB} = P_3$$

$$h_3 = \mathrm{h}(P_{3,SUB}, T_{3,SUB})$$

$$s_3 = \mathrm{s}(P_{3,SUB}, T_{3,SUB})$$

State 4

$$T_4 = T_1$$

$$P_4 = P_1$$

$$h_4 = h_{3,SUB}$$

$$s_4 = \mathrm{s}(P_1, h_4)$$

List of Figures

List of Tables